SANDIA REPORT

SAND97-1494 • UC-411
Unlimited Release
Printed June 1997

Trace Water Vapor Determination in Nitrogen and Corrosive Gases Using Infrared Spectroscopy

L. H. Espinoza, T. M. Niemczyk, B. R. Stallard, M. J. Garcia

Prepared by
Sandia National Laboratories
Albuquerque, New Mexico 87185 and Livermore, California 94550

Sandia is a multiprogram laboratory operated by Sandia Corporation, a Lockheed Martin Company, for the United States Department of Energy under Contract DE-AC04-94AL85000.

Sandia National Laboratories

Issued by Sandia National Laboratories, operated for the United States Department of Energy by Sandia Corporation.

Available to DOE and DOE contractors from
Office of Scientific and Technical Information
PO Box 62
Oak Ridge, TN 37831

Prices available from (615) 576-8401, FTS 626-8401

Available to the public from
National Technical Information Service
US Department of Commerce
5285 Port Royal Rd
Springfield, VA 22161

NTIS price codes
Printed copy: A08
Microfiche copy: A01

SAND97-1494
Unlimited Release
Printed June 1997

Distribution
Category UC-411

Trace Water Vapor Determination In Nitrogen and Corrosive Gases Using Infrared Spectroscopy

L. H. Espinoza and T. M. Niemczyk
Department of Chemistry
University of New Mexico
Albuquerque, NM 87106

B. R. Stallard
Optics and Exploratory Technologies

M. J. Garcia
Surface and Sensor-Controlled Processes Department

Sandia National Laboratories
P.O. Box 5800
Albuquerque, NM 87185

ABSTRACT

The generation of particles in gas handling systems as a result of corrosion is a major concern in the microelectronics industry. The corrosion can be caused by the presence of trace quantities of water in corrosive gases such as HCl or HBr. Presently there are several commercial instruments that are capable of detecting trace water vapor with detection limits as low as 50 ppb in N_2. However, none of these commercially available instruments are compatible with corrosive gases. FTIR spectroscopy has been shown to be a method that can be made compatible with corrosive gases and is capable of detecting low ppb levels of water vapor. Furthermore, the use of chemometric multivariate calibration has been shown to improve detection limits compared to conventional calibration methods that employ peak heights or areas. In this report, the application of FTIR spectroscopy combined with classical least squares multivariate calibration to detect trace H_2O in N_2, HCl, and HBr is discussed.

Chapter 2 discusses the gas handling system and instrumentation required to handle corrosive gases. This system is used for the generation of samples used in the development of the infrared method.

The calculation of an absorbance spectrum relies on the measurement of a blank sample, called the background spectrum. In the case of the determination of gas phase water vapor, the acquisition of a blank sample is almost impossible, because of the difficulty of completely removing water vapor from the optical path of the FTIR system. A method of generating a background spectrum useful to the measurements discussed in this report, as well as in other application areas such as gas phase environmental monitoring, is discussed in Chapter 3.

A Nicolet model 800 FTIR system was initially used to establish the optimal conditions required to perform a H_2O vapor calibration in N_2 and estimate detection limits for this technique. The key problems identified were obtaining an adequate purge and establishing equilibrium in the cell. Experimental results obtained with that system are presented in Chapter 4. Those results made it possible to optimize the design options for the construction of a dedicate system for low ppb water vapor determination. These designs options are discussed in chapter 5.

An FTIR prototype accessory was built in collaboration with Axiom Analytical Inc. In addition, a commercially available evacuable FTIR system was obtained from Midac Corp. for evaluation. Test results obtained with both systems are discussed in chapter 6. Experiments dealing with the interaction between H_2O-HCl and potential improvements to the detection system are discussed in Chapter 7.

In conclusion, the detection limit of FTIR spectroscopy combined with classical least squares multivariate calibration is about 20 ppb using a one meter path length cell and a one minute collection time. Longer collection times or a longer pathlength cell can give greater sensitivity. Both options cause the speed of the measurement to be negatively impacted. The increase in the measurement time with longer data collection times is obvious. The use of longer pathlength cells requires longer equilibration times. Thus, the user can trade off speed for sensitivity depending on individual situations.

TABLE OF CONTENTS

LIST OF FIGURES

LIST OF TABLES

Intentionally Left Blank

CHAPTER 1

INTRODUCTION

1.1 RESEARCH OBJECTIVE

The objective of the research described in this dissertation is to develop an infrared spectrometer system that can be used as an in-line monitor for trace water vapor determination in corrosive gases. There are no commercial instruments available today that are compatible with corrosive gas samples.

The demand for high purity process materials, especially gases, has increased significantly over the past decade in the semiconductor industry. These gases are used during the manufacture of integrated circuits, mainly for wafer oxidation, chemical vapor deposition, sputtering, resist stripping, wafer etching, ion implantation, and wafer cleaning. Gas purity is specified by the assay number, with typical values ranging from 99.99 to 99.9999 percent, depending on the gas and the requirements of the process.[1]

Etching thin films is a very common process in the microelectronics industry. Film types commonly etched include silicon dioxide, polysilicon, aluminium, silicon nitride or selicide.[2] Polysilicon etching requires combinations of fluorine- and chlorine-based chemical gases, such as hydrogen chloride. The presence of contaminants in the etching gases such as water, can cause corrosion of the gas distribution system.[3] Anhydrous hydrogen chloride is converted to hydrochloric acid in the presence of water. Corrosion of the gas handling system leads to the production of particles that can be transported by the high purity gas streams to the wafer. The presence of particles impact device yields, or can even cause a process line failure. In either case, a corroded gas handling system must be replaced. A moisture contamination level as low as 1 ppm-v in a gas such as HCl is sufficient to cause these problems.[4] Therefore it is imperative that gases be delivered to the process site free of contaminants.

In order to achieve very high levels of purity, the semiconductor industry is working to update chemical purity standards, improving the technology in chemical filtration, employing new chemical manufacturing methods (e.g., point of use generation), and cleaning up chemical distribution and reprocessing systems.[5] The demands for starting materials of increased purity have created a need for analytical instrumentation which improved detection limits.

A number of analytical techniques have been employed to determine trace water in semiconductor gases. These methods include the chilled mirror hygrometer,[6-7] the electrolytic hygrometer,[6-7] quartz crystal oscillator,[6] capacitive (aluminium oxide and silicon oxide) hygrometers,[6] and the Atmospheric Pressure Ionization Mass Spectrometer (APIMS).[7-9]

The most widely accepted technique for determining trace water in inert gases is the chilled mirror hygrometer.[10] The chilled mirror hygrometer indicates the temperature (called saturation or dew point temperature), at which the moisture

vapor in a gas is saturated and in equilibrium with liquid moisture on the surface of a cooled mirror. When the sample gas flows into the gas chamber in the hygrometer, the sample gas passes over the surface of a mirror. The mirror is cooled, and the temperature at which the water vapor condenses into dew and clouds the mirror is the dew point temperature, which is electrically measured and related to the H_2O concentration in the gas. The main drawback of this technique is that the measurement is impractical for production applications, because the time required to establish equilibrium. Chilled mirror hygrometers are also expensive and relatively bulky for plant use.[6]

The electrolytic hygrometer consists of a hollow tube cell with two spiral wire electrodes, that are coated with a hygroscopic film such as phosphorous pentoxide (P_2O_5). When the gas sample flows through the cell at a fixed flow rate, moisture is adsorbed into the film, and is then electrolyzed into hydrogen and oxygen. The electrolytic cell hygrometer measures the current required to electrolyze the moisture that is proportional to its mass by Faraday's law. It is a reliable technique for trace water determination in inert gases above 50 ppb, but its time response is slow and its sensitivity is lost after prolonged use in a dry environment.[6]

A quartz crystal oscillator hygrometer measures the moisture content of a gas by measuring the change in vibrational frequency of a quartz crystal, coated with a hygroscopic resin like P_2O_5, when it is alternately exposed to the sample and a dry reference gas (a high efficiency dryer/filter is used when the gas is passed through the reference). The increase in mass caused by adsorbed moisture on the P_2O_5 film translates to a decrease oscillation frequency, which is related to the moisture content of the gas stream. Its suitability for use in corrosive gases has not been fully evaluated.[6]

Aluminium oxide and silicon oxide are porous materials, where their dielectric constant varies with the amount of water adsorbed. A capacitive sensor consists of one of these materials between two electrodes. The major disadvantages of these sensors are that they can suffer from hysteresis, instability, and drift in calibration.[6]

APIMS is a reliable technique that offers the lowest detection limit for the measurement of sub-ppb to ppt water levels. Its extraordinary sensitivity is due to the preferential ionization of impurities. APIMS utilizes a corona discharge to ionize some fraction of the matrix gas at atmospheric pressure. The preferential ionization of impurities results from collision between ionized matrix gas molecules and the impurities. Moisture is easily ionized and together with other ions is accelerated through regions of decreasing pressure into a quadrupole mass spectrometer. The ion currents for each mass/charge ratio are then separately detected. APIMS is considered a reliable laboratory technique for low level H_2O determination, but impractical for in-line analysis in the microelectronics industry.[7-9]

None of these methods are suitable for the measurement of trace water vapor in corrosive gases. All these methods require the sample to be in contact with a transducer, something not required by optical methods. Therefore by using spectroscopy techniques with corrosion resistant material parts to handle the corrosive samples provide a convenient method for the determination of trace water vapor in these difficult samples.

The use of Fourier transform infrared (FTIR) spectroscopy has been investigated to determine trace water vapor concentrations in HCl gas. Samples were generated using permeation tubes and nitrogen as diluent gas.[11-14] However, minimum detectability was estimated to be 30-100 ppb using 5 minutes scanning time at 2 cm^{-1} resolution, an 8-10 m pathlength gas cell, and Mercury-Cadmium-Telluride, HgCdTe (MCT) or Indium Antimonide (InSb) detectors. However, it must be noted that those determinations were achieved by using just one isolated frequency (1653 cm^{-1} or 3854 cm^{-1}) in the calibration. Nevertheless, FTIR spectroscopy has been shown to be a technique that can be successfully used for trace water detection in corrosive gases. In order to develop a FTIR system for in-line analysis in the semiconductor industry instrumental parameters and data analysis capabilities must be optimized to achieve optimal performance.

The use of multivariate calibration methods (Chemometrics Data Analysis Methods), coupled with FTIR Spectroscopy, has been shown to provide improved quantitative results compared with traditional peak-height measurements in the determination of dopant elements of borophosphosilicate glass (BPSG) films on Si wafers for the microelectronics industry.[15] The present work will demonstrate that infrared absorption spectroscopy together with classical least squares (CLS) multivariate calibration is capable of determining trace water vapor in corrosive gases with lower detection limits than achieved with the univariate methods. A product of this research will be an infrared system capable of being used as an in-line monitor in a production environment in the semiconductor industry.

A number of other optical techniques are currently being investigated for this application. In Tunable Diode Laser Spectroscopy (TDLS) the water 1456.888 cm^{-1} infrared absorption line is generated using a Pb-salt laser source. H_2O detectability of 0.4 ppb in N_2 and 4 ppb in HCl has been demonstrated.[16] Applying diode laser absorption spectroscopy to trace analysis with wavelength modulation spectroscopy in the near-IR region has also been applied to trace analysis.[17-19] Their approach is to generate the 7200 cm^{-1} (1.393 μm) H_2O absorption frequency using a InGaAs/InP laser. A Herriot cell design,[20] that is more appropriate for laser spectroscopy, is employed. The expected detection limits are in the sub-ppb range.[21] Part per trillion detection limits have been claimed by proponent of intracavity laser absorption spectroscopy. The high sensitivity derives from the fact that absorbing species are placed in the cavity of the laser, where an effective pathlength of kilometers can be achieved.[22-23] A similar concept is applied in a new technique called cavity ring-down spectroscopy, where the sample gas is placed in the laser cavity. The cavity consists of two high reflectance mirrors. Laser pulses are directed to the cavity where mirror reflectance of up to 99.99% ensures that the photons stay trapped in the cavity for microseconds, bouncing back and forth thousands of times. The intensity of the leaked light decreases exponentially (due to the reflectance of the mirror is less than 100 %), and the time it takes to decay to 1/e of the initial intensity is known as the "ringdown" time. The absorbance is measured indirectly through the relationship of absorbance to the time of photon decay in the cavity.[24-26] However, this technique has not yet been applied to trace water determination in corrosive gases.

1.2 THEORETICAL BACKGROUND

1.2.1 FTIR Spectroscopy for trace gas analysis

The Michelson interferometer is the basis of a FTIR spectrometer. A detailed explanation of how an FTIR spectrometer works has been given elsewhere.[27-29] There are two advantages of FTIR spectrometers when compared to dispersive spectrometers. First, FTIR spectroscopy is a multiplexing technique, where all optical frequencies from the source are observed simultaneously (Fellget's advantage). Thus, there is a signal-to-noise ratio (SNR) gain because the signal at each frequency is measured for the entire scan time. The second advantage of FTIR instruments is that it is a high-throughput technique because it does not require the use of slits as a dispersive instrument does (Jacquinot's advantage). This throughput advantage of FTIR spectrometers over dispersive spectrometers makes FTIR instruments more suitable for quantitative trace gas analysis. The improved throughput and Fellget's advantage result in an SNR gain, when compared to a conventional infrared spectrometer, of a factor of 10 to 40.

FTIR spectroscopy has been applied to the study of air pollutants and environmental samples for many years. Generally long pathlength absorption cells are used to achieve sub-ppm sensitivity for a variety of compounds. The sensitivity also depends on parameters as the inherent absorption strength of the bands being observed, and instrumental factors such as resolution, measurement time, source brightness, detector noise, and spectrometer throughput .

To determine trace amounts of analyte, according to Beer's law, the absorbance is directly proportional to the absorptivity of the analyte, its concentration and the pathlength of the cell:

$$A = \varepsilon\, b\, C \qquad .....(1.1)$$

where A = absorbance

ε = absorptivity in units of length^{-1} concentration^{-1} (e.g., $m^{-1}\, M^{-1}$)

l = pathlength in units of length, (e.g., m)

C = concentration in Molarity or g/mol

To increase the absorption of the analyte, and hence to increase the sensitivity of the detection long path cells are used. The most common long path cell is of the type designed by White. The long pathlength is obtained by multiple reflections of the infrared beam among three mirrors (see Figure 2.5). Such cells can be built so that by varying the number of reflections the pathlength can be changed. Because there are reflection losses at the mirror surfaces the number of reflections cannot be increased indefinitely. A point is reached where the decrease in SNR due to loss of light cancels the gain from a longer path.

The spectrum of water vapor in the mid-infrared region consists of three absorption bands centered at 1596, 3652, and 3756 cm^{-1}, due to three normal vibrational modes,[29] as shown in Figure 1.1. The vapor phase spectrum of hydrogen chloride and hydrogen bromide in the mid-infrared region consist of one rotational-vibrational band containing the P-R structure of diatomic molecules

centered at approximately 2900 cm^{-1} ,[30] and 2650 cm^{-1} ,[31] respectively. The fundamental absorption band of HCl is shown in Figure 1.2.

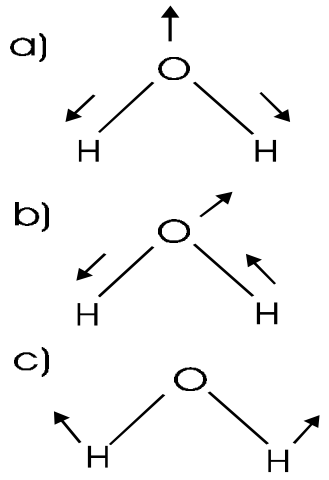

Figure 1.1 Vibrational modes in the H_2O molecule. a) Symmetrical stretching, $u_1 =$ 3652 cm^{-1}. b) Asymmetrical stretching, $u_2 =$ 3756 cm^{-1}. c) Bending, $u_3 =$ 1596 cm^{-1}.

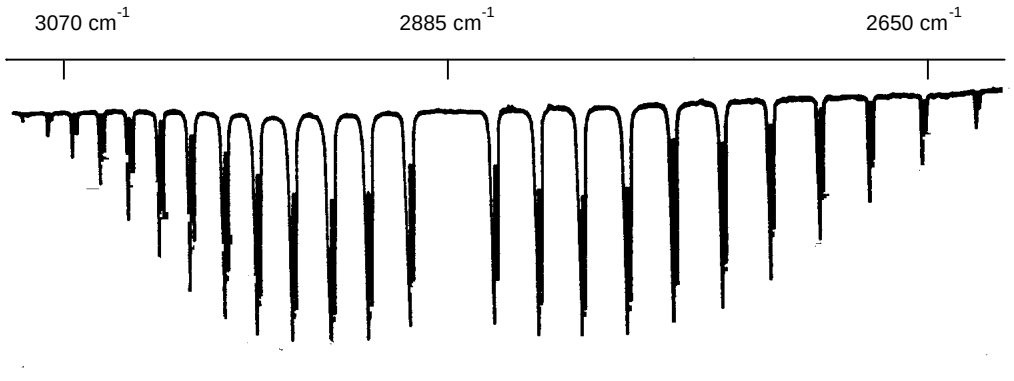

Figure 1.2 High resolution HCl fundamental absorption band. The lines are doubled due to the presence of two isotopes Cl^{35} and Cl^{37}.

The SNR for a FTIR spectrometer increases as the square root of the measurement time at a given resolution. The measurement time is varied by changing the number of scans that are signal-averaged to produce an interferogram. Resolution is changed by varying the length of travel of the moving mirror. High resolution spectra are noisier than low resolution spectra due to angular divergence, and the need to use apertures[28]. Also high resolution spectra

take more time to accumulate than do low resolution spectra because the mirror has to move a longer distance. If a high resolution spectrum is required, it takes longer, it is noisier, but the information content of the spectrum is increased compared to a low resolution spectrum. Lower resolution can be obtained with better SNR and shorter measurement time, but can hide some interferences. These are the trading rules for an FTIR instrument and often the optimum conditions for a specific experiment have to be determined empirically. The optimum resolution for accurate quantitative trace water vapor measurements will be discussed in section 5.6.

The most common infrared source used to provide energy in the mid-infrared region is the glowbar. It consists of a rod of silicon carbide that is heated to temperatures above 1400 K. It is also more rugged and has better emisivity at short wavelengths ($\lambda < 6\ \mu m$) than does another commonly used IR source, the Nernst glower, but water cooling is needed to cool the metallic electrodes attached to the silicon carbide rod.

Fourier transform infrared spectrometers commonly use deuterated triglycine sulfate, DTGS, detectors. They cover the mid-infrared range from 4000-400 cm^{-1}. The main drawbacks of pyroelectric detectors are that they are less sensitive than other detectors available, and they have relative slow response. Mercury cadmium telluride, HgCdTe or MCT, detectors are also commonly employed. It is a semiconductor photon detector for which cutoff and sensitivity vary on the composition of the semiconductor. MCT detectors cover the 5000-600 cm^{-1} range, and generally operate in the photoconductive mode. The major advantage of MCT detectors is their sensitivity. They are about 10 times more sensitive than DTGS detectors. They are also faster, but they must be cooled with liquid nitrogen, because the heat given off by the detector element itself is detected, giving rise to a large noise signal. Indium Antimonide, InSb, is another infrared detector used in the mid-infrared region. It is also a photon detector operating in the photovoltaic mode over the 8000-1800 cm^{-1} spectral region. It has the highest detectivity of the commonly used detectors. They are about 10 times more sensitive than MCT detectors. They must also be cooled with liquid nitrogen.

Chapter 5 will present a more detailed explanation of optimization of instrumental parameters to determine the best instrument setup for low level water vapor determination in corrosive gases.

1.2.2 Chemometrics Data Analysis

The use of chemometrics has become very popular for quantitative analysis based on molecular spectroscopic data. Specifically, multivariate calibration, a technique of chemometrics, has been successfully applied to the analysis of complex spectral data.[32] There exist a variety of multivariate techniques including classical least squares,[33-35] inverse least squares,[35-36] principal component regression,[37,38] and partial least squares.[37,38] The main advantage of these methods over conventional univariate analysis, is that the use of multiple frequencies, instead of one isolated frequency, improves the precision, accuracy, and reliability of determinations based on infrared spectral data. Furthermore, one

can also extract information about outlier samples in a calibration set or among unknown samples. The details and algorithms of these methods have been described thoroughly by Haaland and Thomas.[37]

The CLS multivariate calibration model is the simplest multivariate calibration method based on the Beer's law. During the calibration step the absorbance data at "n" frequencies of a set of "m" calibration samples, in which "l" component concentrations have been determined by a reference method, are considered as standards. Thus, the model can be written using matrix notation as:

$$A = KC + E_A \qquad .....(1.2)$$

where *A* is the n x m matrix consisting of the absorbance of each of the m samples at n frequencies (the spectra for the m samples), *C* is the l x m matrix of the l component concentrations in the m samples, and *K* represents the n x l matrix of pure component spectra. E_A is the n x m matrix of spectral noise (or model error) present in the spectra. Thus, in the calibration step the absorbances and concentrations of the standards are used to estimate the pure component spectra for each component at each frequency. Note that CLS can be considered as a factor analysis method based on Beer's law. Since it minimizes the error in the measured absorbances, the least squares solution for the pure component spectra is determined as:

$$\hat{K} = AC'/(CC') \qquad .....(1.3)$$

where *C'* is the transpose matrix of *C*, and $\hat{K}$ is used to represent the least squares estimate of the pure component spectra *K*. This least squares solution minimizes the sum of squares of the differences in the measured and estimated spectral intensities (called also the spectral residuals) at each frequency separately.

Qualitative information, like molecular interactions and matrix effects, can be extracted from the CLS calibration step by comparing the measured pure component spectra with the estimated pure component spectra.[34]

During the prediction step, an unknown spectrum is modeled using Beer's law as a column vector a of absorbances at n frequencies:

$$\mathrm{a} = Kc + e_a \qquad .....(1.4)$$

where *K* is the n x l matrix representing the pure component spectra and *c* is the vector of component concentrations in the sample. The least squares solution for the concentration of the unknown is obtained using $\hat{K}$ from equation (1.3):

$$\hat{c} = \hat{K}'\mathrm{a}/(\hat{K}'\hat{K}) \qquad .....(1.5)$$

where $\hat{c}$ is the estimated concentration in the unknown. This solution is a least squares curve-fitting procedure of a linear combination of the estimated pure component spectra, that minimizes the sum of squared differences between the sample spectrum and this linear combination of the estimated pure component spectra at all frequencies simultaneously. Also, the presence of unexpected components in the unknown sample, but not in the calibration samples, can be determined by examining the spectral residuals.[39]

Another advantage of CLS multivariate calibration method is its capability to fit spectral baseline variations even though nonlinear baseline variations are present.[40] Band-by-band analysis with linear baseline modeling can perform a

separate CLS analysis for each spectral region, band, selected and it will be discussed later. The main disadvantage of CLS over PLS and PCR is that all components that have spectral features in the spectral region being analyzed have to be included in the calibration set. Also, CLS is not useful for estimating chemical and physical properties of samples from their spectra, as the CLS model is based on Beer's law. Nevertheless, CLS is a multivariate calibration technique that is highly suited to trace gas analysis. The improvement in detection limits compared with the univariate classical method will be presented in section 5.5.

1.3 REFERENCES

1. P. Van Zant, “Microchip Fabrication, a Practical Guide to Semiconductor Processing,” 2nd edition, Mc Graw-Hill Inc., 1990, p. 81.
2. D. J. Elliot, " Integrated Circuit Fabrication Technology," 2nd edition, McGraw-Hill Publishing Company, 1989, pp. 345, 378.
3. S. Wolf and R. N. Tauber, Silicon Processing for the VLSI Era, Volume 1, Lattice Press, California, 1986, p. 215-216.
4. E. Flaherty, C. Herold, J. Wojiciak, D. Murray, A. Amato, and S. Thompson, “Reducing the Effects of Moisture in Semiconductor Gas Systems,” Solid State Technology, July 1987, p. 69.
5. P. Singer, " How to ensure Chemical Purity," Semiconductor International, May 1995, p.61.
6. J. J. McAndrew and D. Boucheron, Solid State Technology, 35 (2), pp. 55-60 (1992).
7. E. F. Ezell, K. Siefering, T. Kijima and A. Makihara, " Detection Capabilities of State-of-the-Art Trace Moisture Analysis Methods," Microcontamination Conference Proceedings, Oct. 1992, Santa Clara, CA.
8. K. Siefering and H. Berger, J. Electrochem. Soc., 139, 1442 (1992).
9. T. Ohmi, N. Nakamura, A. Ohki, K. Kawada and K. Hirao, J. Electrochem. Soc., 139, 2654 (1992).
10. "Standards Method of Measuring Humidity with Cooled-Surface Condensation (Dew Point) Hygrometer," ASTM Method D4230-83, American Society for Testing and Materials Annual Book of ASTM Standards, 11.03, 407-421 (1985).
11. W. I. Bailey, T. M. Booth, D. L. Grieble and P. B. Henderson, "Analytical Techniques for Speciality Gases," Air Products and Chemicals, Inc., private communication.
12. K. D. Cleaver, J. W. Epton, A. Tinkler, P. Clarke and R. Hogle, " The Application of FTIR Spectroscopy to the Determination of Impurities in Semiconductor Grade Special Gas Products," BOC Limited-Airco Electronic Gases, private communication.
13. D. E. Pivonka, Appl. Spectrosc., 45, 597 (1991).
14. K. Miyasaki, Y. Ogawara, and T. Kimura, Bull. Chem. Soc. Jpn., 66, 969-971 (1993).
15. D. M. Haaland, Anal. Chem., 60, 1208 (1988).
16. R. S. Inman and J. J. McAndrew, Anal. Chem., 66, 2471 (1994).
17. G. C. Bjorkland, Optics Letters, 5, 15 (1980).
18. J. A. Silver, Appl. Opt., 31, 707 (1992).
19. D. S. Bromse, J. A. Silver, and A. C. Stanton, Appl. Opt., 31, 718 (1992).
20. D. Herriot, H. Kogelnik, and R. Kompfner, Appl. Opt., 3, 523 (1964).
21. D. S. Bomse, and A.C. Stanton, Southwest Sciences Inc., Santa Fe, New Mexico, private communication.
22. S. J. Harris, Appl. Opt., 23, 1311 (1984).
23. D. A. Gilmore, P. Vujkovic Cvijin, and G. H. Atkinson, Opt. Comm., 103, 370 (1993).

24. J. J. Scherer, J. B. Paul, C. P. Coullier, A. O'Keefe, D. J. Rakestraw, and R. J. Saykally, Spectroscopy, 11, 46 (1996).
25. A. O'Keefe, and D. A. G. Bacon, Rev. Sci. Instrum., 59, 2544 (1988).
26. R. T. Jongma, M. G. H. Boogaarts, I. Holleman, and G. Meijer, Rev. Sci. Instrum., 66, 2821 (1995).
27. P. R. Griffiths and J. A. de Haseth, Fourier Transform Infrared Spectroscopy, John Wiley & Sons, New York, 1986.
28. B. C. Smith, Fourier Transform Infrared Spectroscopy, CRC Press, Boca Raton, 1996.
29. J. D. Ingle Jr. and S. R. Crouch, Spectrochemical Analysis, Prentice Hall, New York, 1988.
30 H. A. Szymanski, Theory and Practice of IR Spectroscopy, Plenum Press, New York, 1964, p. 94.
31. K. Nakamoto, Infrared and Raman Spectra of Inorganic and Coordination Compounds, John Wiley & Sons, New York, 1986, p. 105.
32. B. Wangmaneerat, J. A. McGuire, T. M. Niemczyk, D. M. Haaland, and J. H. Linn, Appl. Spectrosc., 46(2), 340 (1992).
33. D. M. Haaland and R. G. Easterling, Appl. Spectrosc., 34, 539 (1980).
34. D. M. Haaland and R. G. Easterling, Appl. Spectrosc., 36, 665 (1982).
35. D. M. Haaland and R. G. Easterling, Appl. Spectrosc., 39, 73 (1985)..
36. C. W. Brown, P. F. Lynch, R. J. Obremski, and D. S. Lavery, Anal. Chem., 54, 1472 (1982).
37. D. M. Haaland, and E. V. Thomas, Anal. Chem., 60, 1193 (1988).
38. D. M. Haaland, and E. V. Thomas, Anal. Chem., 60, 1202 (1988).
39 D. M. Haaland, and R. L. Barbour, Am. Lab., 17 (7), 14 (1985).
40. D. M. Haaland, Appl. Spectrosc., 40, 1152 (1986).

CHAPTER 2

EXPERIMENTAL INSTRUMENTATION

2.1 THE GAS HANDLING SYSTEM

Many industrial processes require extremely high purity input gases. In the microelectronics industry, for example, the specifications for moisture content is as low as 1 ppb for bulk gases (N_2, O_2, Ar, H_2, and He), and in the range of 0.1-1 ppm for electronic specialty gases (SiH_4, WF_6, HCl, HBr, CF_4, NF_3, etc.). This is because specialty gases are more reactive than bulk gases, which are generally supplied to the point-of-use via a distribution system, while specialty gases are commonly stored in cylinders, where they can pick moisture from the cylinder surface. In the semiconductor industry a typical gas distribution system consists of one or several gas manifolds with several Mass Flow Controllers (MFCs), valves, filters, dryers, pressure sensors and long piping and tubing configured to deliver the gases to the process equipment. It must be noted, however, that this system must meet ultraclean specifications to meet the desired gas purity levels. Conventional gas distribution systems are a source of impurities and often contaminate the high purity gas that it delivers to the process tool. For example, moisture can be desorbed by reactive gases from the surfaces in a conventional gas delivery system. The contamination can be attributed to: a) actuated components (seals and seats) in MFCs and valves , and b) interconnect tubing.

Conventional gas delivery systems use MFCs and valves with elastomer components that can shed particles when actuated. Elastomer components can absorb small amounts of moisture from the environment when manufactured, or when a gas delivery system is exposed to the ambient. The elastomer components in the MFC act as a moisture trap and can outgas the adsorbed moisture into the high purity gas being delivered over long periods of time. The other significant source of contamination is the internal surface of the delivery system tubing. A large internal surface area will provide areas for adsorption of moisture from the ambient. Conventional gas manifolds consist of single melt electropolished stainless steel surfaces with marginal surface roughness ≥ 20 Ra μin.[1] In single melt stainless steel tubing, oxide inclusions of Si, Ca, Al, and Ti are possible. Inclusions are a source of contamination, since they increase the tubing surface roughness and the internal surface area and are sites for moisture entrapment. Furthermore, they can leach into the gas stream or react with the gas producing undesirable contaminants.

The preferred method of producing a high purity gas delivery system is to use very smooth electropolished stainless steel tubing. Electropolished stainless-steel tubing with a Cr/Fe ratio of about 1.5 and a Cr_2O_3/Fe_2O_3 ratio of about 2.5 has surface characteristics suitable for gas delivery systems. This type of surface has low moisture adsorption and rapid desorption compared to untreated stainless-steel surfaces.[2] When halogen gases are used, the welding techniques used to prepare

the system as well as the metallurgical quality of the 316L stainless steel tubing are important.[3] Ultraclean manifolds are produced using double vacuum melt electropolished stainless steel tubing with all metal components in the MFCs and valves. Electropolished double vacuum melt stainless steel surfaces with marginal surface roughness ($\leq$ 5 Ra μin) provide a surface with minimal moisture adsorption and rapid desorption characteristics.[4]

In summary, maintaining the purity of a gas in a distribution system requires careful selection of designs, materials and procedures. The surface area of components gas lines must be reduced (i.e., internal volume), the dead space within components and piping must be minimized, metal seals instead of elastomers MFCs must be employed, the tubing has to be high quality electropolished stainless steel with all "wetted" surfaces (those that come into contact with the gas), improved gas filtration and purification technologies must be used, and strict procedures for installing and maintaining the gas distribution system, and for cylinder changeouts must be adhered to.[5]

The gas handling system used in this research is shown schematelly in Figure 2.1. It was designed and built in collaboration with Control Systems Incorporated of Rio Rancho, New Mexico. The 1/4" diameter tubing is 316L grade stainless steel, seamless, electropolished, and was thoroughly cleaned in a Class 100 clean room with hot deionized water. The stainless steel piping components were supplied by Valex Corporation according to their 401 specification for use in ultra-high purity process applications in semiconductor manufacturing systems.[6] Joints and bends are made with Cajon high purity Micro-Fit fittings that are specially cleaned, electropolished, and vacuum sealed in a Class 100 environment. At points where periodic disassembly is required, Cajon VCR metal gasket face seal fittings designed for ultra clean systems are used. Nupro diaphragm valves, model SS-DLBW4, are used throughout the gas system. The valves were also assembled in a Class 100 clean room following accepted procedures for ultra-high purity systems. MKS MFC 1100 Series was used to control the flow of nitrogen. The MFC 1100 Series wetted materials are 316L stainless steel and nickel with Viton seals. With corrosive gases, a Tylan 2900 series or a MKS Type 1359C were used as the flow controller. In these controllers, the wetted materials are 316 stainless steel and nickel with Kalrez seals. All components in the gas handling system were helium leak-tested.

The gas cabinet is a model GG100, two-cylinder cabinet from Air Products. The N_2 source is boil off from a large liquid N_2 tank located near the laboratory, in which the H_2O content is typically 200-250 ppb. The N_2 dryer is a Waferpure gas purification system, model WGPS 030-31, from Millipore. The HCl used for all experiments was Matheson semiconductor grade. The H_2O content of the HCl is specified to be less than 10 ppm. The HCl dryer is a Waferpure gas purification system for chloride gases, Millipore model WGPS 030-2C. The HBr is Airco ULSI grade. The H_2O content of the HBr is specified to be less than 3 ppm. The HBr dryer is a Waferpure mini XL integrated filter/purifier, Millipore model WPMV 200 SB. The Waferpure systems include

particle filtering to 0.05 μm and are specified to reduce moisture to < 1 ppb for N_2, < 10 ppb for HCl, and < 100 ppb for HBr.

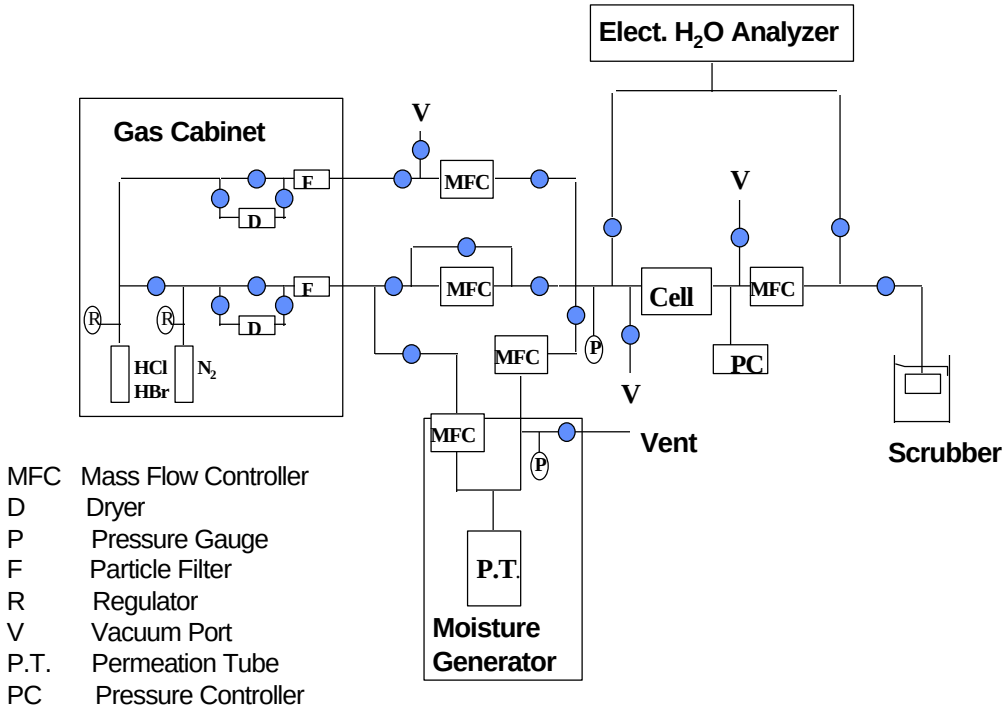

Figure 2.1 Schematic of the gas handling system.

As shown in Figure 2.1 three vacuum ports are attached to evacuate the gas handling system when corrosive gases are used. The vacuum system consists of a diaphragm pump, a liquid nitrogen cooled adsorption pump, and an ion pump. Before switching the system from a corrosive gas (HCl or HBr) to N_2, the diaphragm pump is used to cycle the system several times between rough vacuum and purge. The three vacuum pumps could also be used when high vacuum was needed to evacuate the gas cell to 10^{-6} torr. Also, the diaphragm pump is used to evacuate the gas bottle (through the regulator) when changing the bottle. An aqueous basic solution in a scrubber was used to neutralize both corrosive gases. The gas exhaust is monitored with a HCl/HBr sensor that insures no significant amount of corrosive gas is introduced into the environment.

A moisture generator and moisture electroanalyzer, shown in Figure 2.1, were used when experiments are carried out in N_2 . When flowing corrosive gases, these instruments were bypassed due to incompatibility with those gases.

2.2 THE L'EAU PRO MOISTURE GENERATOR

The preparation of very low and constant levels of water vapor is a difficult process. Standards for other atmospheric contaminants can accurately be prepared and stored in cylinders. That is not the case for ppm and sub-ppm moisture

standards due to the fact that adsorption-desorption processes can occur in the cylinder itself as discussed in section 2.1. Two complementary methods have been developed and validated for the generation of ppm and sub-ppm water vapor samples.[7]

The commercially available L'Eau Pro moisture generator, manufactured by Meeco Incorporated, uses a permeation-dilution principle to generate precisely controlled concentrations of water vapor at parts-per-billion levels. The generator consists of a permeation tube, manufactured by GC industries, enclosed in a temperature controlled chamber. Water vapor is released from the permeation device into a controlled flow of pre-dried diluent gas, as shown in Figure 2.2.

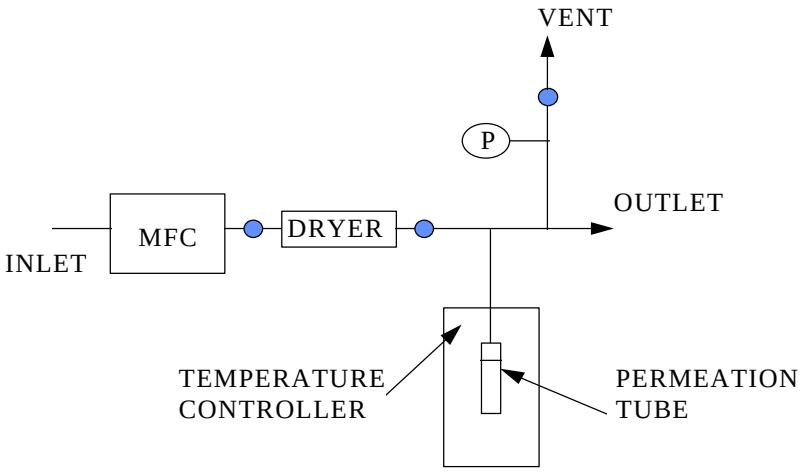

Figure 2.2 Schematic diagram of the moisture generator.

The permeation tube has a silicone permeation membrane between a sample of liquid water and a vapor phase moisture chamber, with a second membrane between the vapor phase chamber and the diluent gas. The use of two membranes reduces the effects of temperature compared to a single membrane, and also improves accuracy at the low permeation rates required to generate low ppb water vapor concentrations.[8] The concentration of water vapor is directly proportional to the permeation rate, P, and inversely proportional to the flow rate of the diluent gas that flows past the permeation tube, F, as shown in the following equation:

$$C = \frac{KP}{F} \qquad .....(2.1)$$

Where C = Generated water vapor concentration in ppm.

P = Permeation rate in nanograms per minute.

F = Flow rate in standards cubic centimeters per minute.

K = Proportionality constant

Using only one permeation tube, a ten-fold range of water vapor concentration is possible by varying the dilution flow (1 to 10 liters/minute). In order

to cover a broad water vapor concentration range four different permeation tubes were used that vary from 98-16200 ng/minute, calibrated at 50 or 60^{o}C and 20 Psig. The stated accuracy of the water vapor concentration is $\pm$ 12% or $\pm$ 2 ppb (whichever is greater).

2.3 THE AQUAMATIC PLUS MOISTURE ELECTROANALYZER

The Aquamatic Plus moisture electroanalyzer, manufactured by Meeco Inc., uses the electrolytic method to determine trace water vapor in nitrogen. It consists of a hollow tube cell containing two wrapped platinum wire electrodes coated with a hygroscopic phosphorus pentoxide (P_2O_5) film. The gas sample flows through the tube at a known flow rate and any water molecules in the gas sample are adsorbed on the film. The adsorbed water molecules are electrolyzed to produce H_2 and O_2. The electrode reactions are:

Cathode reaction:

$$2\ H_2O\ +\ 2\ e^-\ \rightarrow\ 2\ OH^-\ +\ H_2$$

Anode reaction:

$$2\ OH^-\ \rightarrow\ H_2O\ +\ 1/2\ O_2\ +\ 2\ e^-$$

The moisture concentration in the gas can be calculated from Faraday's law without the need for calibration with moisture standards. The amount of gas reaching the hygroscopic film is the critical part of this reference moisture determination and therefore the gas flow must be precisely measured by an accurate mass flow controller. The main drawback of the Aquamatic Plus is its slow response speed and loss of sensitivity after prolonged use under very dry conditions.[9] According to the manufacture its accuracy is $\pm$ 20 ppb or $\pm$ 2 % of the indicated reading, whichever is greater.[10] An enhancement of the Aquamatic Plus, the Turbo hygrometer, incorporates an improved cell design, that together with a microprocessor-controlled moisture addition feature (which keeps the cell wet under dry conditions) and signal integration, extends the measurement to 1 ppb moisture levels.[11]

2.4 THE FTIR SPECTROMETER

A Nicolet 800 Fourier transform infrared spectrometer with a glowbar source, a KBr beamsplitter, and deuterated triglycine sulfate (DTGS), HgCdTe (MCT) and InSb detectors was used to determine the trace water content in N_2, HCl, and HBr. Figure 2.3 is a layout of the optical components showing the infrared beam paths through the analysis system. The internal DTGS detector was used to monitor and correct for the background moisture present in the optical path of the spectrometer. A movable mirror inside the spectrometer allows us to direct the infrared beam to the external compartment of the spectrometer, where it can be directed to either of the two gas cells by the transfer optics. Two planar gold coated mirrors (not shown in the diagram) serve to align the beam accurately to the gas cells. The movable

mirror in the transfer optics is an off-axis parabola that approximately matches the numerical aperture of the White cell.

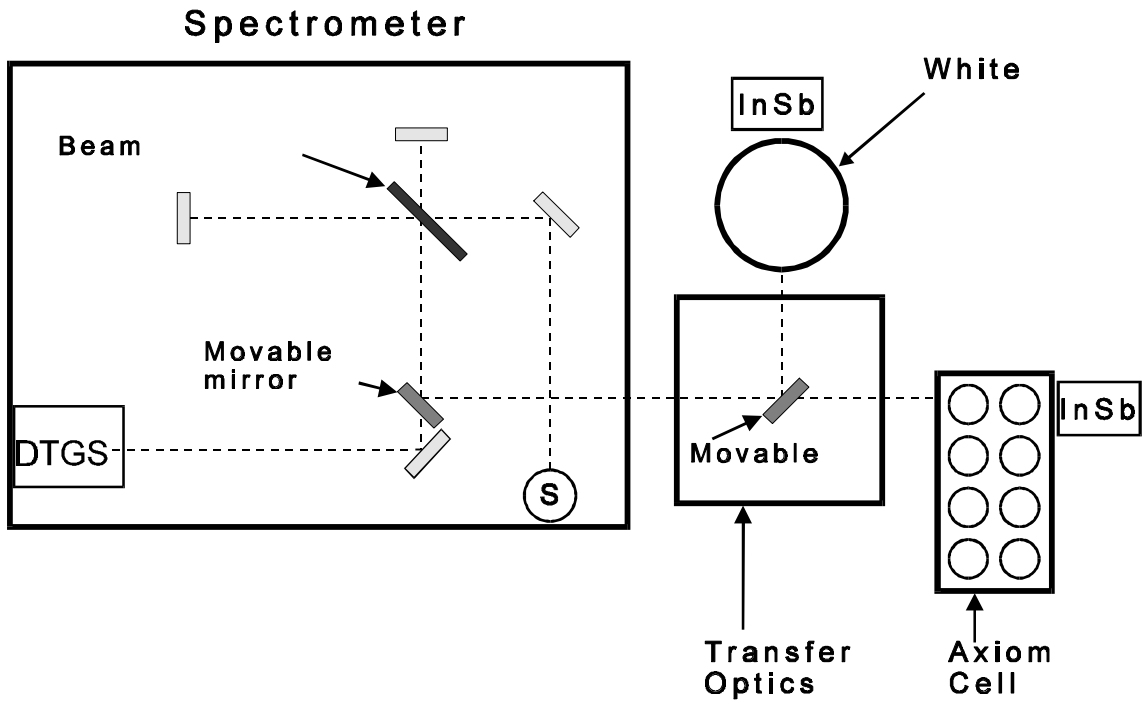

Figure 2.3 Optical layout showing the infrared beam paths through the analysis system. S is the glowbar source, and DTGS and InSb indicate the detector positions.

The external detectors are either MCT or InSb to measure the water vapor in the gas cells around 1600 cm^{-1} and 3800 cm^{-1} respectively. The 2 mm MCT or InSb detectors, purchased from Infrared Associates, are mounted in liquid nitrogen dewars. A standard Nicolet dual-use preamplifier circuit board (i.e., photovoltaic and photoconductive) is mounted on the base of the detector assembly so that the detector is readily coupled to the instrument's signal and control bus.

It was impossible to achieve a good purge in the spectrometer as delivered. The background moisture present in the environment has a typical water concentration of 10000 ppm. A normal purge in the spectrometer reduces the moisture to about 100 ppm. In order to improve the purge, perforated tubes were attached to the factory purge inlets and distributed around the spectrometer enclosure. While these improved purged inlets were an improvement, a good purge was not achieve until the entire spectrometer was placed in a polycarbonate box. After installation of the isolation box the water concentration in the optical path of the spectrometer, or background H_2O, could be reduced to low ppm values after several days of purging . The box was permanently attached to the underside of the spectrometer and extends about one inch beyond the top and four sides of the factory enclosure. Imperfections in the spectrometer box, transfer optics, sample

cells, and detector box, were plugged with Apiezon Q sealant. The spectrometer, transfer optic and detector boxes were purged with dried N_2 from a large liquid nitrogen tank located nearby. The typical moisture concentration of the purged nitrogen was about 150 ppb when entering the spectrometer.

The DTGS detector was used to monitor the background H_2O inside the spectrometer . It was chosen since it operates at room temperature, which eliminates the problem of breaking the instrument purge when adding liquid nitrogen which is required when using MCT or InSb detectors.

Figure 2.4 shows a typical drydown time of the enclosed spectrometer. The y scale for H_2O concentration is in arbitrary classical least square units that will be equated to ppb content of H_2O in section 4.2. Figure 2.4 shows that about 2 weeks of purging are necessary to reduce the background H_2O level in the spectrometer to a steady relative stable value of 2.1 arbitrary CLS units corresponding to about 1 ppm of H_2O. This introduces a time limitation in the determination of trace water contents that needs to be overcome using a spectrometer that purges more quickly or one that can be evacuated.

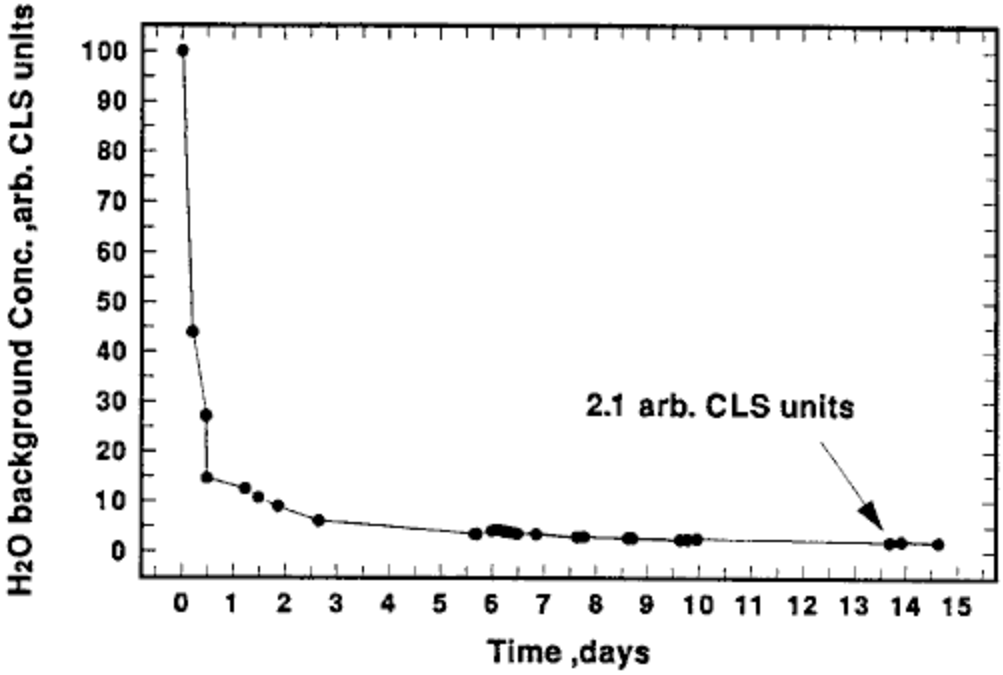

Figure 2.4 H_2O background drydown curve of the modified Nicolet 800 FTIR spectrometer as measured by the DTGS detector.

Another major difficulty is determining how to measure the background H_2O and differentiate it from the sample gas H_2O. The initial approach employed was to collect two measurements, the first using the internal detector (DTGS) and the second using the external detector (MCT or InSb). After a pathlength correction, the H_2O concentration in the sample gas cell is determined by subtracting the results from the two detectors as will be shown in section 4.1. The enhancements achieved using an optimized spectrometer design will be presented in chapter 5. The problems associated with calculating an absorbance spectrum, especially in the

situation where the background H_2O concentration is changing, will be discussed in chapter 3.

2.5 THE GAS CELLS

Two different optical cells, shown in Figures 2.5 and 2.6, were used in these experiments. The most common gas cell used in environmental studies is the White cell (Figure 2.5).[12] The White cell (Infrared Associates) used here consists of a permanently aligned path enclosed in a 6" diameter pyrex with anodized aluminium end caps. It is a multiple-pass design based on reflection by the three 4" gold mirrors. The cell has a base pathlength of 55 cm. The light make 40 passes through the cell resulting in a total path of 22 m, the cell volume is approximately 4.7 liters, and the cell has a numerical aperture of 0.125. The measured throughput of the White cell is about 40% that represents an energy loss of about 2% at each reflection.

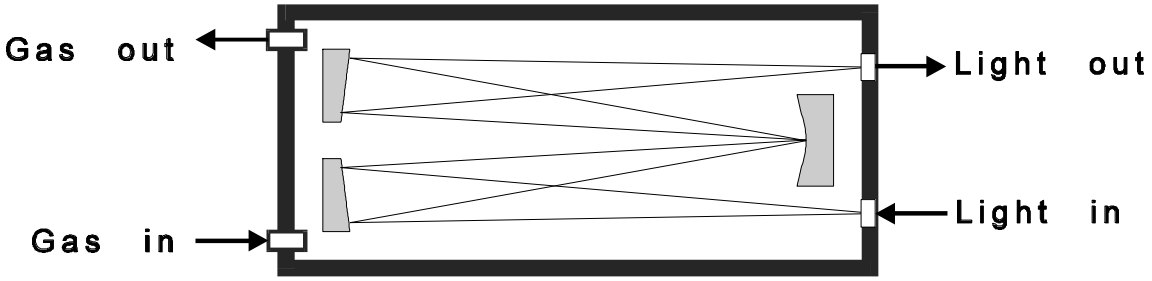

Figure 2.5 A multiple-pass White gas cell. Only four passes are shown for simplicity.

The second gas cell, shown in Figure 2.6, was purchased from Axiom Analytical Incorporated.[13] Unlike the White cell, it is a single pass design based on a folded optical path through eight nickel-coated brass tubes of 2m length and 1.25" diameter with 45^o gold mirrors at the end of each tube. The mirror assemblies can be repositioned on the tubes to give configurations of 4, 8, or 16 m pathlength. Since the output beam of an FTIR spectrometer is collimated, the infrared beam can be directed into the Axiom cell using simple plane mirrors and optical transfer tubes, to maintain a purged optical path. The interior of the transfer tubes and the cell tubes are highly polished. The transmission of the Axiom gas cell per 2 m tube is about 0.70, therefore the throughput is about 6 % when using a 16 m pathlength. The volume per 2 m tube is about 1.6 liters. Heating tape was permanently affixed to the cell tubes to heat the cell to about 150^o C.

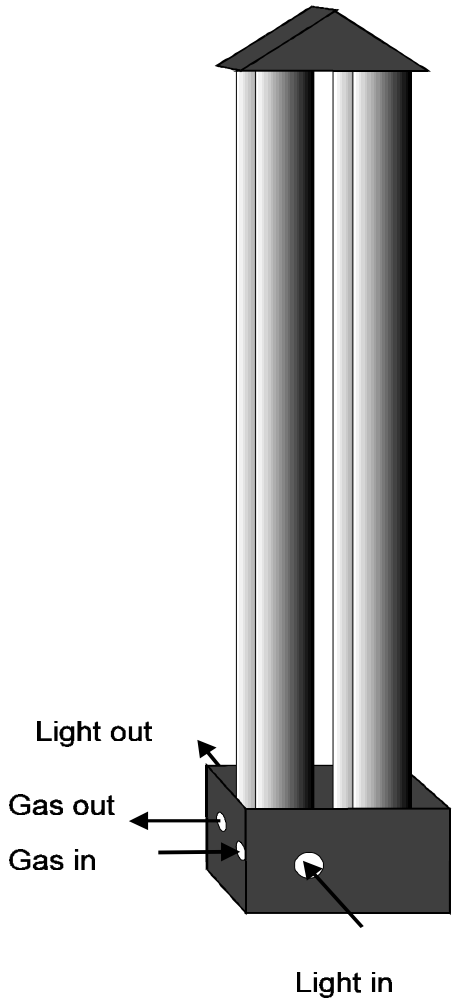

Figure 2.6 A single-pass, folded Axiom gas cell. The linear flow gas cell is made of 2m tubes (only 4 tubes are shown) connected by gas- and light-tight endcaps that guide both the gas and light through the system.

2.6 REFERENCES

1. S. Krishnan, A. Tudhope, O. Laparra, and J. Grob," Case Study: Ultraclean Gas Delivery," Semiconductor International, April 1995, p. 89.
2. S. Krishnan, S. Grube, A. Tudhope, O. Laparra, "Particle Generation in Corrosive Gas Delivery Systems," Conference Proceedings, 18th Annual Adhesion Society Meeting, SC, Feb. 1995.
3. . S. Krishnan, S. Grube, A. Tudhope, O. Laparra," Site-specific Corrosion in Gas Delivery Tubing Exposed to Semiconductor Grade HCl, "Semiconductor International, October 1995, p. 11.
4. K. Sugiyuma, T. Ohmi, T. Okumura, F. Nakahara, "Electropolished, Moisture-free Piping Surface Essential for Ultrapure Gas Systems," Microcontamination, Vol. 7, No. 1, Jan. 1989.
5. P. Singer, " Effective Gas Handling: A Balance of Cost and Purity," Semiconductor International, September 1994, p. 64.
6. Valex Corporation, 401 Specification for Ultra-high purity, Electropolished, ASTM Grade TP316L (UNS S31603) Stainless Steel Piping Components, Valex Corp., 6080 Leland St. Ventura, CA 93003.
7. F. Mermoud, M. D. Brandt, and J. McAndrew, Anal. Chem., 63, 198 (1991).
8. Meeco Incorporated, L'Eau Pro Moisture Generator Catalog, Meeco Inc., 250 Titus Av., Warrington, PA 18976.
9. E. Flaherty, C. Herold, J. Wojiciak, D. Murray, A. Amato, and S. Thompson, “Reducing the Effects of Moisture in Semiconductor Gas Systems,” Solid State Technology, July 1987, p. 69.
10. Meeco Incorporated, Aquamatic Plus Moisture Analyzer Catalog, 250 Titus Av., Warrington, PA 18976.
11. C. Ma, F. Shadman, J. Mettes, and L. Silverman," Evaluating the trace moisture measurement capability of coulometric hygrometry", in Microcontamination, April 1995.
12. Infrared Analysis Incorporated, Catalog 91, 1424 North Central Park Ave., Anaheim, CA 92802.
13. Axiom Analytical Incorporated, LFG Long Path Infrared Gas Cell Catalog, 18103-C Sky Park South, Irvine, CA 92714.

CHAPTER 3

SYNTHETIC GENERATION OF WATER BACKGROUND

3.1 INTRODUCTION

There are countless applications of spectroscopy where absorbance of an analyte is related to its concentration by application of Beer's law. The calculation of an absorbance spectrum depends on the measurement of a background spectrum. In most cases, the measurement of a background spectrum is straightforward. There are, however, some spectroscopic applications where the measurement of a background spectrum is difficult. Such applications include the determination of atmospheric components using infrared spectroscopy,[1] or determination of the concentration of H_2O in a gaseous sample using infrared spectroscopy. Ideally, a background spectrum is obtained by measurement of a blank (i.e., a sample that contains everything except the analyte). In the atmospheric studies it is nearly impossible to eliminate the analytes from the optical path of the measurement, and in the case of water vapor measurement it is very difficult to remove completely all water from the optical path of the spectrometer.

A number of approaches have been developed to deal with the problem of generating a background spectrum in these situations. In the case of water vapor determination in an enclosed cell, the water vapor in the spectrometer can be eliminated by using an evacuable spectrometer. More commonly, however, approaches that involve fitting a baseline to a single beam spectrum are used.[2] Baselines employing multiple straight lines as well as high order polynomials have been used.[3] Note that the result of this baseline fit is the removal of the high frequency information, the narrow gas phase absorption peaks, from an otherwise broad, slowly changing spectrum.

In 1979, Hirschfeld suggested that a background spectrum could be generated by removing the narrow absorption bands due to gaseous molecules in the optical path of the spectrometer, or in the sample cell, by filtering the high frequency information from the single beam spectrum.[4] The filtering operation is most conveniently carried out by truncating the interferogram prior to performing the Fourier transform. We have investigated this approach to the development of a "synthetic background" spectrum for the specific case of determination of trace water in a gaseous sample. We present a procedure for performing the filtering operation and discuss the conditions in which the process can be used to produce accurate and precise determinations.

3.2 EXPERIMENTAL

All spectral data were collected using a Nicolet Model 800 FTIR spectrometer equipped with an InSb detector and KBr beamsplitter. The gas cell used in these experiments was an eight-meter Axiom cell consisting of four two-meter, 1.25 inch

diameter nickel-coated brass tubes in a folded configuration. The gas handling system consists of a specially designed and constructed apparatus with moisture generation and reference measurement components as it was described in chapter 2.

All data were collected at a nominal resolution of 1 cm^{-1}, which corresponds to 24576 point interferograms using a fixed ten minute signal averaging period.

The program to generate the synthetic background spectra was written in array BASIC to operate within the Lab Calc or GRAMS (Galactic Industries) environment. The program initially finds the zero-path-difference (ZPD) point in the interferogram, then multiplies the interferogram by the filter function centered on the ZPD point. This process is similar to apodization. The Gaussian filters are characterized by their width in interferogram points (1 cm^{-1} resolution). The width is the full width at 1/e height. The single beam background spectra were then generated by Fourier transforming the filtered interferogram. The single beam sample spectra were generated by apodizing (Happ Genzel) the sample interferogram followed by Fourier transformation. The modeling studies were carried out using programs written in MATLAB. The classical least squares (CLS) calibrations were carried out using software written in array BASIC to operate in the Lab Calc or GRAMS environment.[5]

3.3 RESULTS AND DISCUSSION

A number of considerations must be taken into account when generating the synthetic background spectrum. Most important are the form and width of the filter function. The most straightforward approach to filtering the interferogram is to use a boxcar function. The single beam synthetic background spectrum that results from the multiplication of the interferogram by a 200 point boxcar function is shown in Figure 3.1. Note the “ringing” in the spectrum. The ringing causes errors in determinations based on the absorbance spectra calculated from these synthetic background spectra. The ringing can be avoided by using a wider boxcar filter, but by the time the ringing becomes insignificant, the boxcar filter is wide enough to let enough high frequency information through so that the water peaks, though somewhat muted, become visible in the synthetic backgrounds. No suitable compromise between the ringing and incomplete filtering of the water peaks could be found.

The ringing problem noted above is similar to that seen in high resolution spectra when a boxcar apodization is used. The problem is avoided by using different functional forms for the apodization; one potentially useful filter function is a Gaussian. An interferogram, the result of signal averaging 620 scans of the interferometer for a 500 ppb sample of water, was multiplied by a Gaussian function centered at the ZPD point. The single beam background spectrum resulting from a filtering using a 78 point wide Gaussian function is shown in Figure 3.2. The entire single beam sample spectrum, and a blowup of the water region (3600-3900 cm^{-1}) is shown in Figure 3.3. The absorbance spectra obtained by rationing the sample spectrum to the synthetic background spectra created using the two different widths

Gaussian filters is shown in Figure 3.4. Note that the water vapor peaks in Figure 3.4.a and 3.4.b look similar, but there is a significant difference in the baselines. A peak-by-peak CLS analysis of data processed by either width of the Gaussian filter produces a good calibration, but that might not always be the case. The accuracy of the CLS calibration is affected by the analyte peak height and width, and the relationship of those variables to the width of the filter function.

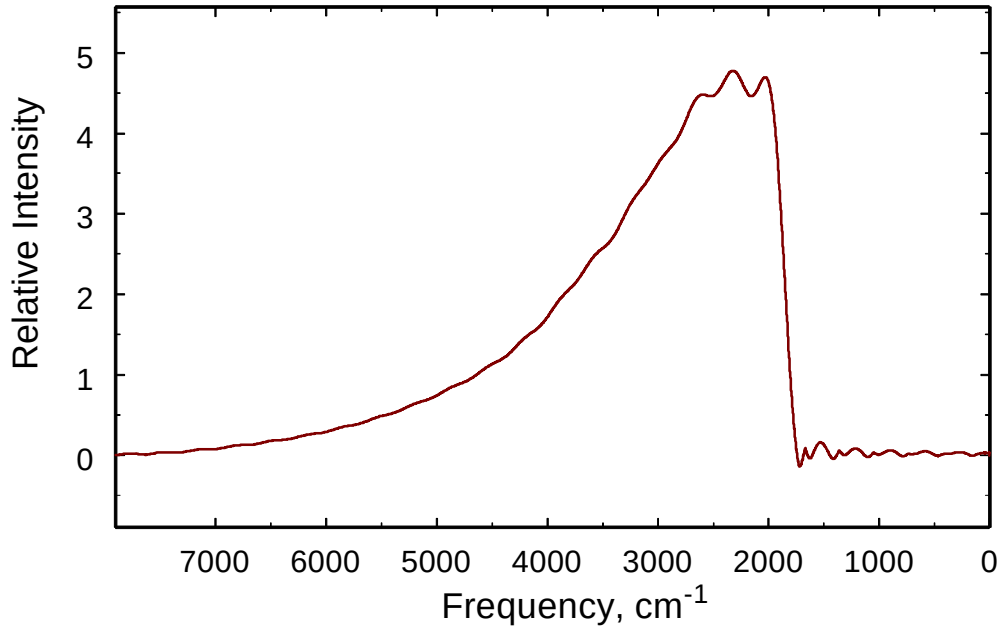

Figure 3.1 Single beam spectrum obtained after Fourier transform the multiplication of an interferogram with a 200 point boxcar function.

The effects of these variables can most easily be examined in a modeling study where the effects of analyte peak width, peak height, and filter function can be readily determined. The basic approach taken in the modeling study was to add peaks of known height and width to a water-feature free single beam background spectrum, create an interferogram from the resulting spectrum, perform the filtering operation, then use the filtered interferogram to produce a single beam synthetic background spectrum and take note of the effects of the filtering operation on the recovery of the known peak.

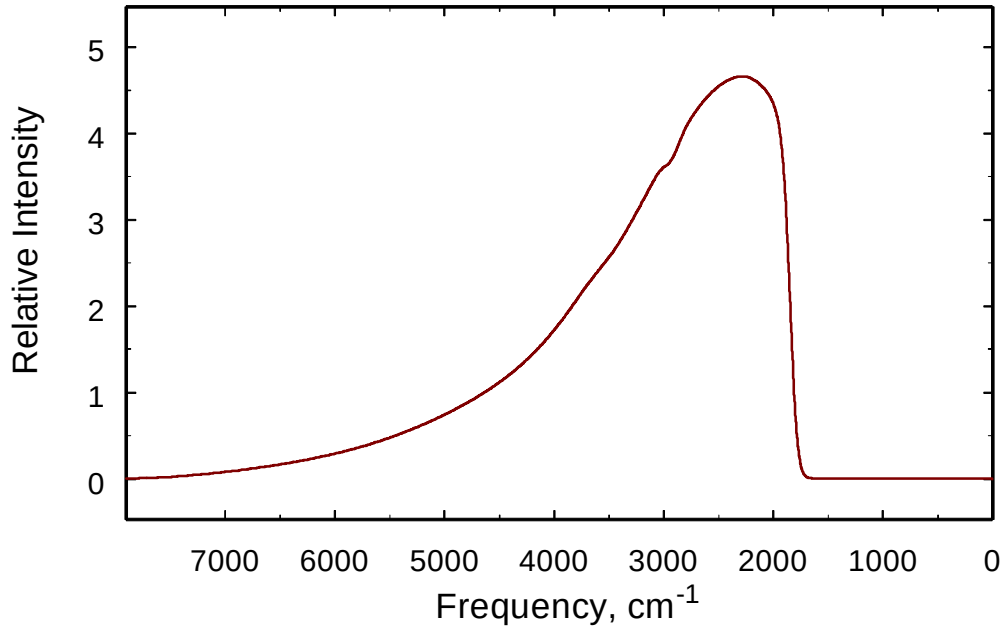

Figure 3.2 Single beam spectrum obtained after Fourier transform the multiplication of an interferogram with a 78 point Gaussian function.

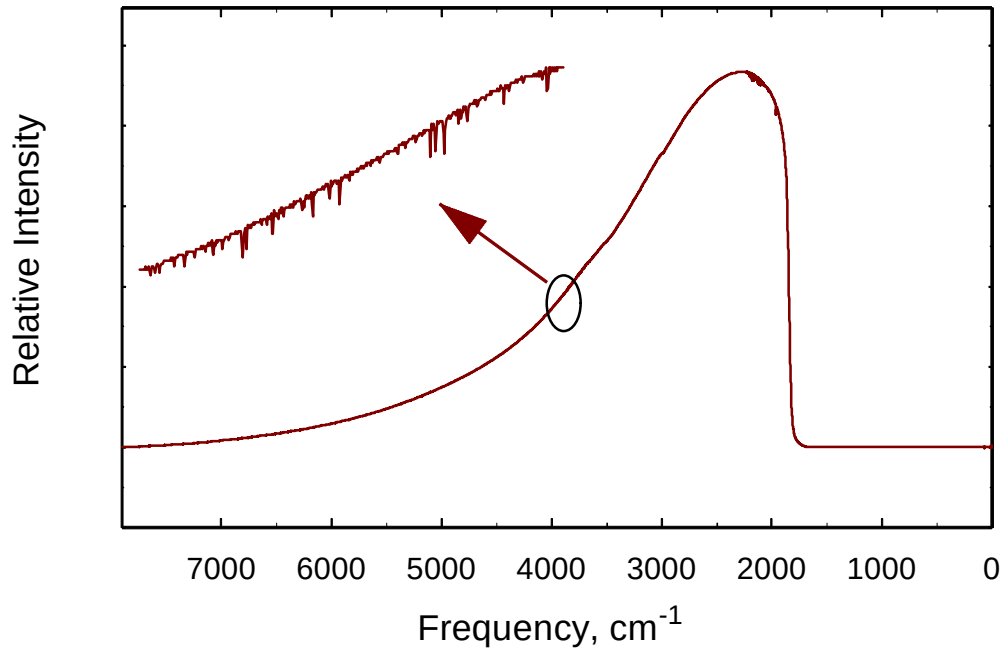

Figure 3.3 Sample single beam spectrum of 500 ppb H_2O.

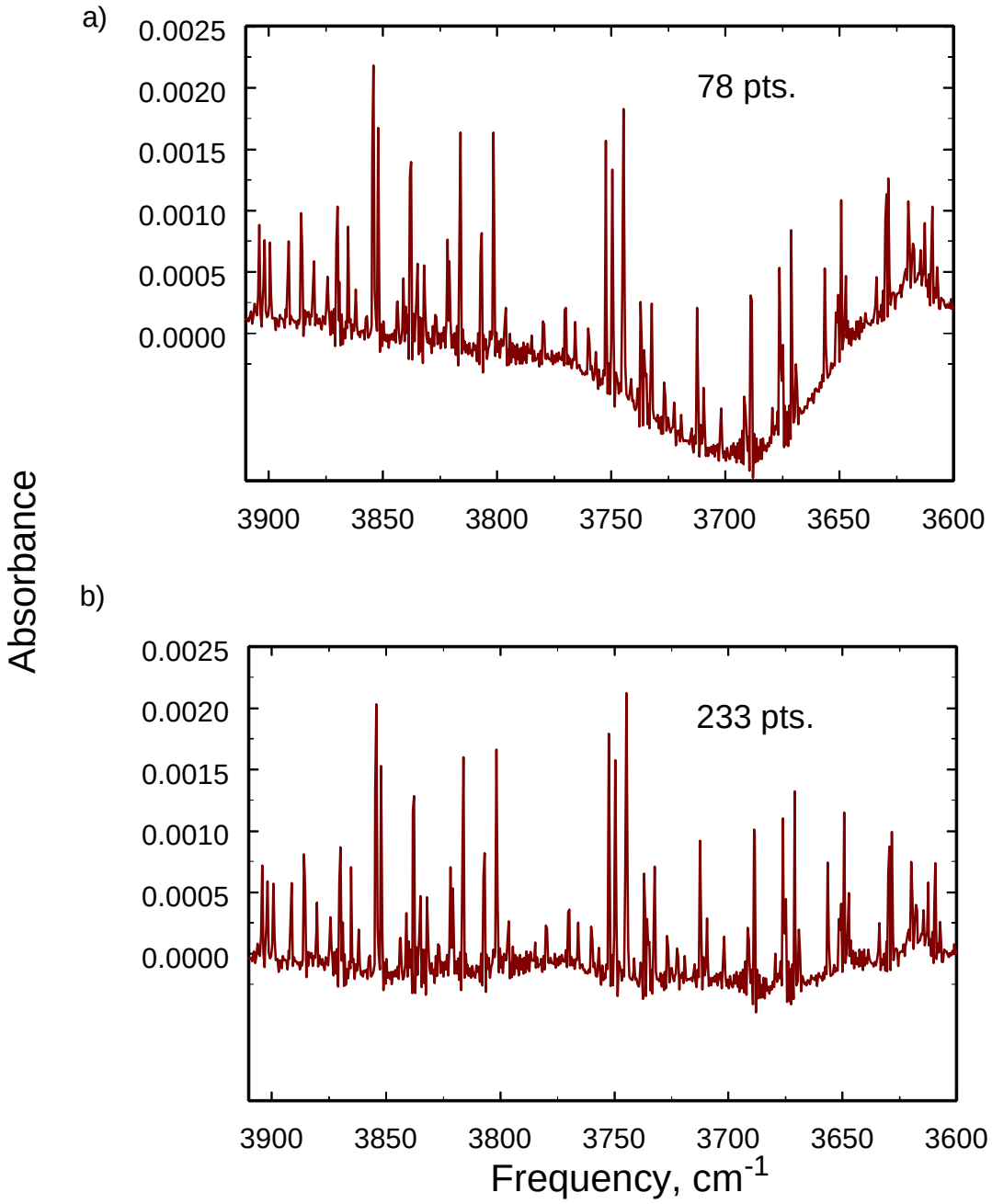

Figure 3.4 Absorbance spectra obtained using a 78 and 233 point width in the Gaussian filter, respectively.

The water-feature free single beam background spectrum was generated by recording a single beam spectrum after the spectrometer and sample cell had been thoroughly dried. The residual water features, corresponding to about 1 ppm of water in the optical path, in this single beam spectrum were removed by

application of a 310 point wide Gaussian filter to the interferogram prior to Fourier transforming to produce the spectrum. A model spectrum was then created by adding a Gaussian peak of specific height and width to this single beam background. Such a model single beam sample spectrum is shown in Figure 3.5. The overall shape of the spectrum in Figure 3.5 is the result of the use of a Barr Associates bandpass filter (3448-4081 cm^{-1}) which limits the bandpass of the spectrometer to the region of the water absorption.

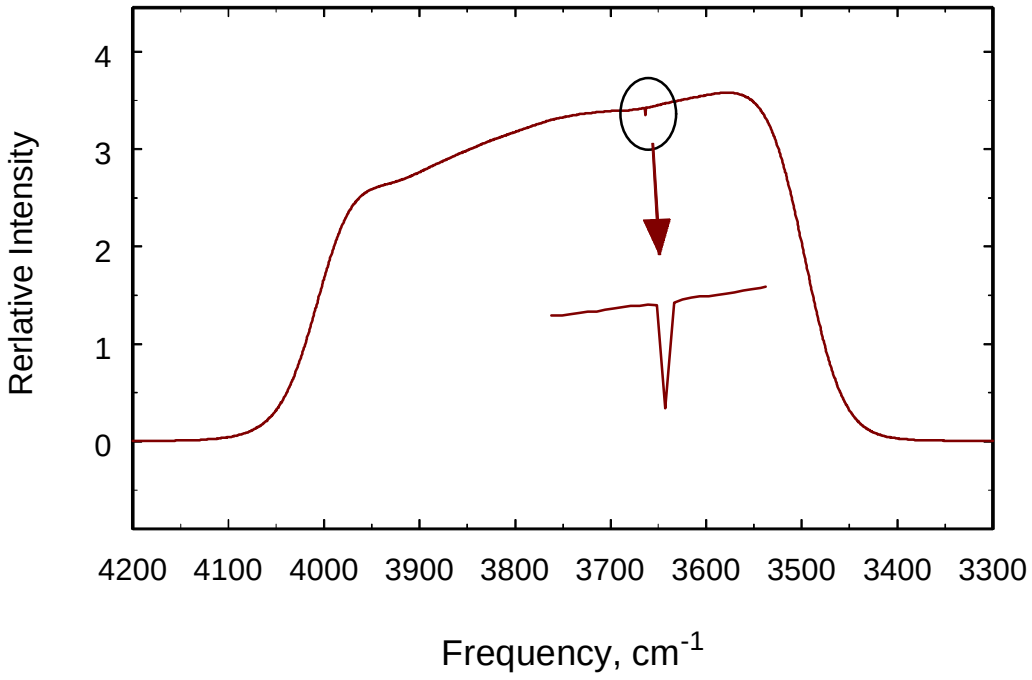

Figure 3.5 Model single beam spectrum showing an added Gaussian peak of known peak height absorbance and peak width.

The values of the absorbance peaks selected for the modeling are in the range of those actually measured in an experiment monitoring trace water contamination in semiconductor grade gases (0.1-0.001). We have found that optimal quantitative results are achieved when making determinations from these gas phase IR data via the use of a CLS calibration (see section 5.5). Thus, the errors in quantification due to the generation of the synthetic background were also determined using a CLS calibration. In practice, the CLS model is applied across a number of the analyte bands in the spectral data. Much of the precision improvement achieved through the use of CLS calibration , when compared to univariate determinations, is the result of signal averaging across the several bands. The modeling studies are limited to a single band, with the assumption that a suite of bands, of like strength and width, would be affected in a similar manner by the background generation process.

The CLS model used in the model studies was based on an absorption spectrum calculated for the largest of the peaks studied, peak height of 0.1 absorbance units, for a given peak width. This reference absorbance spectrum was calculated by taking the log of the ratio of the water-free single beam background to the model single beam spectrum. This model absorbance spectrum should be perfect, as it is created by ratioing a background plus a perfect Gaussian to the identical background.

The modeling studies were carried out by performing the following steps: (1) adding the Gaussian peak of known height and width to the water-free single beam background spectrum; (producing the single-beam model spectrum) (2) inverse Fourier transforming to produce an interferogram; (3) performing the filtering step to produce a synthetic background interferogram; (4) Fourier transforming to produce the synthetic background; (5) ratioing the model spectrum to the synthetic background to produce a model absorbance spectrum; and (6) applying the CLS calibration to the model absorbance spectrum to return a concentration. CLS modeling assumes a linear relationship between concentration and absorbance, an assumption that has been shown to be valid for the range of absorbances, 10^{-3} to 10^{-1} absorbances unit peaks modeled. The relative error in the concentration is equivalent, based on the linear relationship between absorbance and concentration, to the relative error in absorbance.

The errors measured that result from the generation of the synthetic background are a function of the width of the filter function used on the interferogram, the strength of the absorbance peak, and the absorbance peak width. Figures 3.6 show the relative error measured as a function of the absorbance peak height and peak width for two different filter functions. The filter function used in Figure 3.6.a was a 156 point wide Gaussian, which corresponds to about 210 cm^{-1} resolution, and the filter function used in Figure 3.6.b was 1244 points wide, which corresponds to approximately 26 cm^{-1} resolution. When using the 156 point wide Gaussian filter function, errors greater than 1% are only seen for the 8 and 16 cm^{-1} wide peaks – and then only for the weakest, smallest absorption, of these peaks. The errors noted for the 1244 point wide Gaussian filter function, shown in Figure 3.6.b, are much more significant. Again, however, the errors are much more significant for the broader absorption peaks, reaching 50%. Relatively little error is seen for the peaks of 1 and 2 cm^{-1} in width. Plots for filter functions intermediate to these look similar; i.e., there are insignificant errors for narrow absorption peaks regardless of the absorption strength, but significant errors for wider peaks. Similar plots using filter functions wider than 1244 points show significant errors regardless of the absorption peak height or peak width.

Figure 3.7 is a plot of relative error versus filter width for an absorption peak that is 0.002 absorbance units high and different peak widths. The general trend shown in Figure 3.7 is that seen in Figures 3.6.a and 3.6.b, i.e., errors are much more significant for broader peaks. Note, however, that there are minima in the curves for the peaks of 4 and 8 cm^{-1} widths. The reason for the minimum is that when too narrow a filter function is used, the baseline of the background spectrum generated is not very smooth. The undulating background affects broader peaks

much more significantly than it does very narrow peaks. This is especially the case when using a band-by-band CLS calibration, such as that used to process these data.

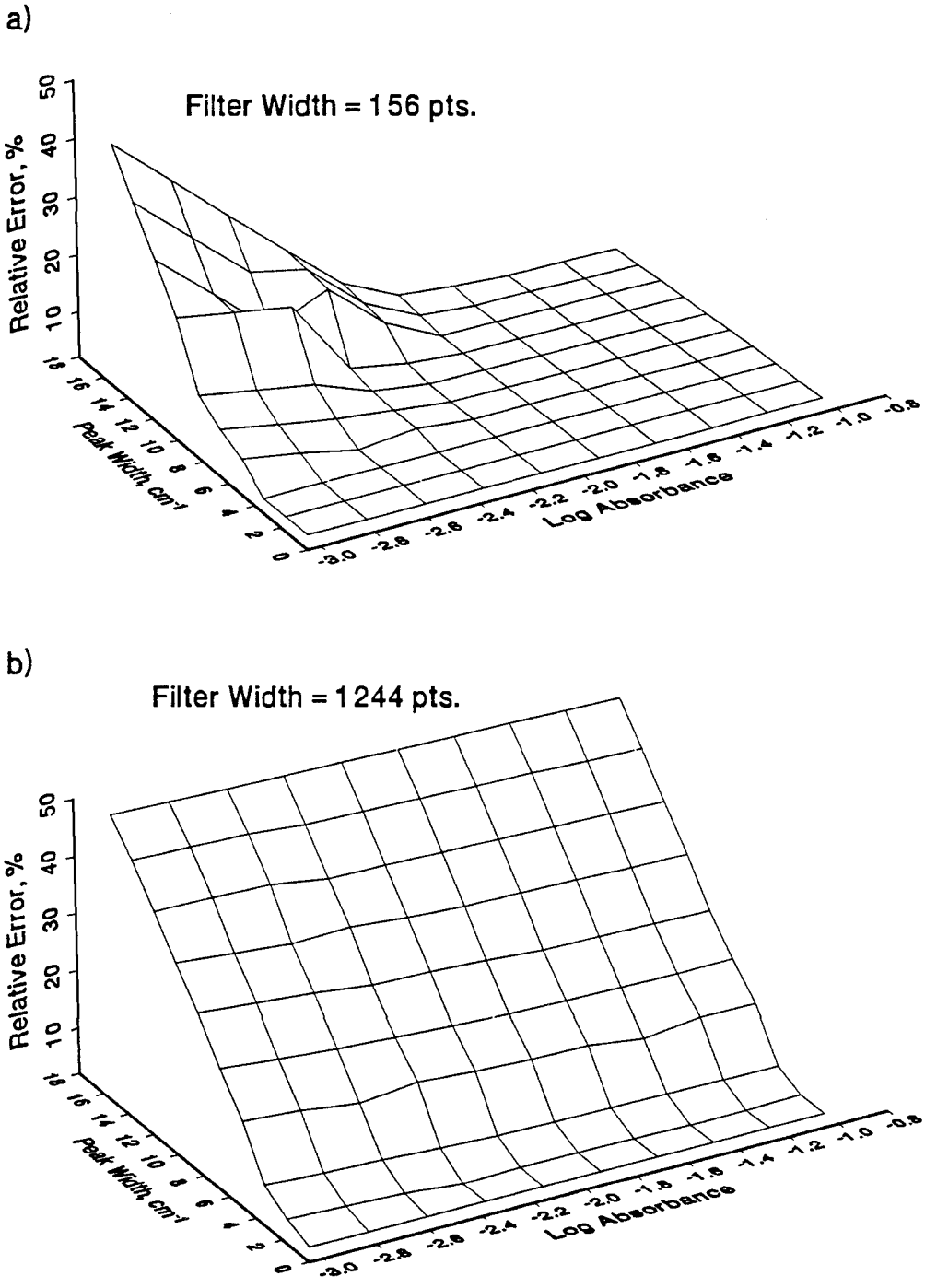

Figure 3.6 Plots showing the relative errors as function of the absorbance peak height and peak width for 156 and 1244 point filter width, respectively.

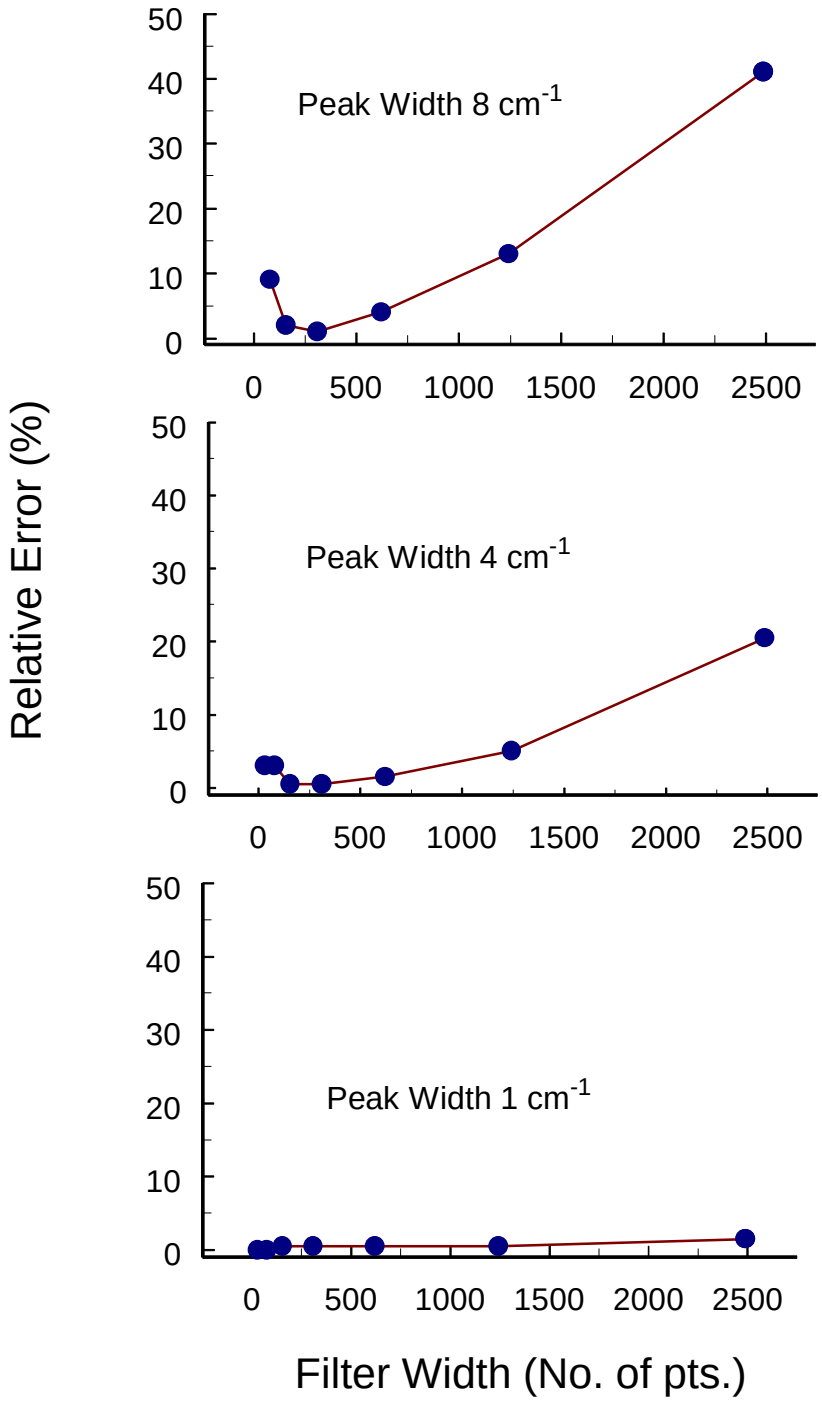

Figure 3.7 Plot showing the relative error vs. filter width for an 0.002 absorption peak height and different peak widths.

The practice of generating a synthetic background by filtering the interferogram cannot be tested for absolute accuracy against experimental data because all of the calibrations are based upon a linear relationship between a value

returned from the CLS analysis and a water concentration based on a reference determination. We can, however, explore the how the background generation process changes the CLS value returned for a particular sample.

A CLS model was generated based upon a 500 ppb sample of water vapor in nitrogen. The spectral data for this model were collected at 1 cm^{-1} resolution and a ten minute signal integration. The CLS model was created using the two water absorption peaks at 3852.2 and 3854.1 cm^{-1}. The interferogram was filtered using different width Gaussian filters. The results of three of these filtering operations are shown in Figure 3.8. As had been seen before, very narrow filters result in curved baselines. The 156-point filter, according to the modeling studies above, ought be a width filter that produces good quantitative results. Although no apparent differences exist between the absorbance spectra produced with the 156 and 1244 point filters, the wider filter does not entirely remove the water features in the background. Although the spectrum produced by the wider filters looks similar to that produced using intermediate filters, the areas under the peaks and the peak heights are decreased. This cause a significant error when the data are subject to CLS analysis.

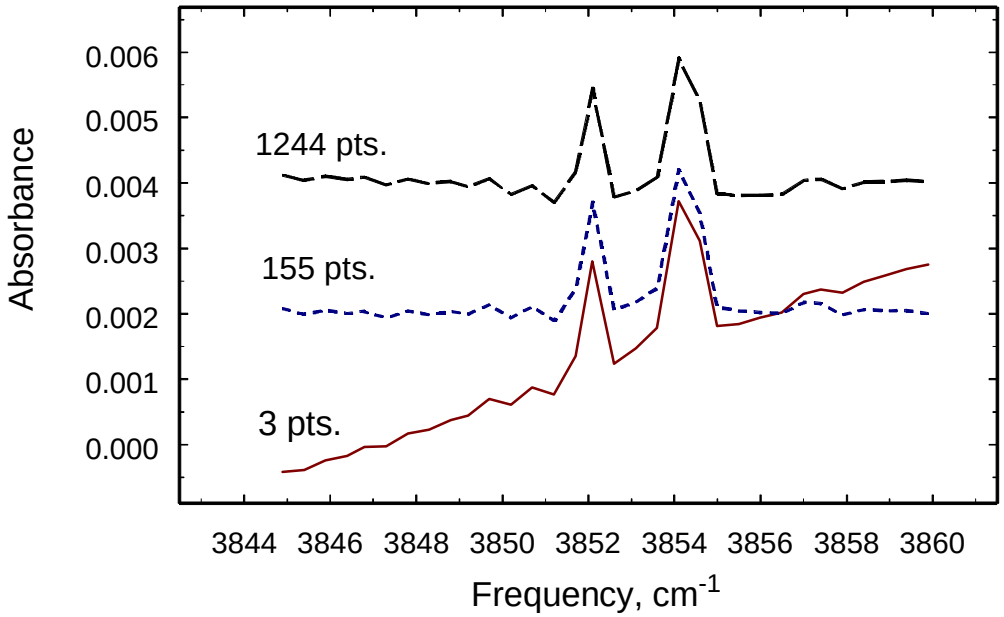

Figure 3.8 Water vapor spectra showing two absorption peaks generated by using different number of points in the Gaussian filter.

The change in the concentration as predicted by the CLS model, in CLS units, is plotted against the number of points in the Gaussian filter in Figure 3.9. As can be seen, there is a small error for extremely narrow filters, then a region with almost no error at all, followed by a region of increasing error in the CLS value return. Based on the modeling studies, the changes in the CLS value returned from

the intermediate region will directly correspond to concentration errors in the determination.

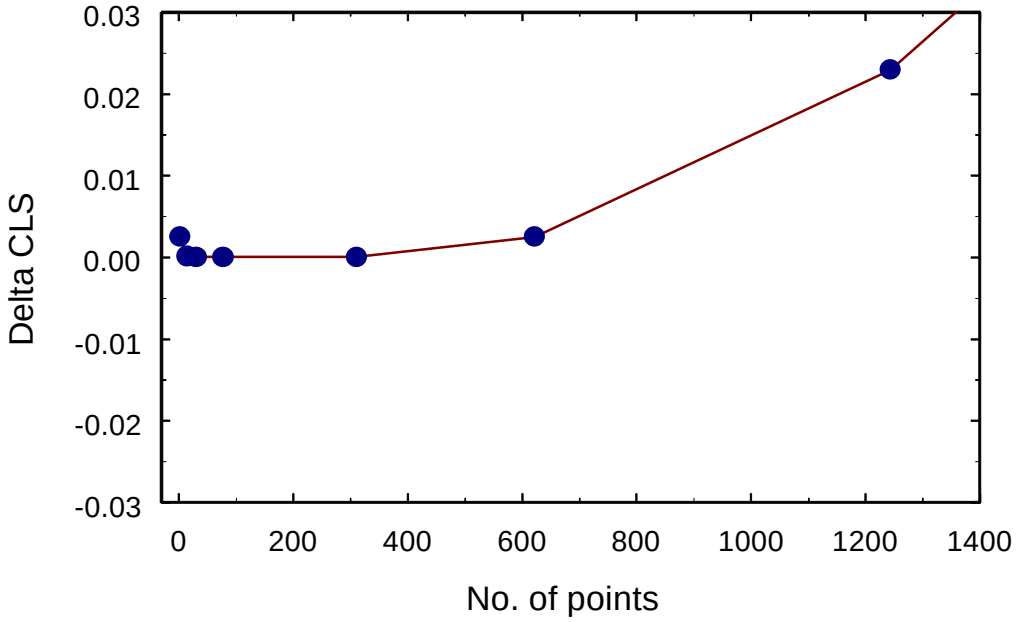

Figure 3.9 Plot showing the change in concentration as predicted by the CLS model against the number of points in the Gaussian filter.

3.4 CONCLUSION

It is difficult, if not impossible, to develop an appropriate background spectrum to use in the generation of an absorbance spectrum for some gas phase samples. The method of filtering the high frequency information, the sharp absorption bands due to gas phase species, from the interferogram and then using the filtered interferogram to generate a synthetic background spectrum produces good quantitative results as long as some guidelines are followed. First, the filtering process can only be successfully applied when the absorption bands are very narrow. Our results, both experimental as well as modeling studies, indicate that there is no problem working with data where the absorption bands are 2 cm^{-1} or less in width. Further, our results indicate that filters that are too narrow cause curving baselines, hence potential for error in the data analysis step. Filters that are too wide do not effectively filter out all the high frequency information, thus resulting in changes in the peak heights when an absorption spectrum is generated. The range of filters that we have found to work successfully are filters of 78 points in width (corresponds to about 420 cm^{-1} resolution) to 310 points in width (approximately 106 cm^{-1} in resolution).

3.5 REFERENCES

1. P. L. Hanst, A. S. Lefohn, and B. W. Gay, Appl. Spectrosc., 27, 188-190 (1973).
2. G. M. Russwurm and J. W. Childers, Laser Focus World, 31 (4), 79 (1995).
3. P. L. Hanst, Spectroscopy, 8 (9), 44 (1993).
4. T. Hirschfeld, Appl. Spectrosc., 33 (5), 525 (1979).
5. Grams/ 386™, Array Basic™ User's Guide, Galactic Industries Corporation, 395 Main Street, Salem, New Hampshire, 03079.

CHAPTER 4

EXPERIMENTAL RESULTS (NICOLET 800)

4.1 EXPERIMENTAL PROCEDURES

The initial experiments that were carried out were targeted at the determination of the optimal conditions needed to measure trace H_2O in corrosive gases using a Nicolet model 800 FTIR spectrometer. Two different gas cells, an 8 m single folded pass Axiom cell, and a 22 m multiple pass White cell, were used to perform H_2O calibrations in N_2 and to determine detection limits in N_2, HCl, and HBr. When experiments were carried out in N_2, the electrolytic cell analyzer was used as a reference method. Alternatively, the moisture generator can be used as a reference by calculating the concentrations of H_2O using equation 2.1 shown in section 2.2. The assumption that the calibrations for low levels of H_2O in the various gases are identical is made. The difference in H_2O calibration in N_2 versus the one in HCl or HBr has been discussed in the literature,[1-3] and is a topic of further investigation (see section 7.2.1).

The two major challenges when performing a H_2O calibration in N_2 or estimate detection limits are dealing with the H_2O background in the spectrometer and conditioning the gas cell for H_2O equilibration. Experimental as well as data analysis procedures are described below that were developed to meet these challenges.

4.1.1 Spectrometer H_2O background procedure

The first issue addressed in the determination of trace H_2O by FTIR spectroscopy was the reduction and monitoring the background H_2O in the spectrometer. Therefore, after enclosing the spectrometer in a polycarbonate box, a standard spectrum was collected using the internal DTGS detector to monitor the background H_2O. It was assigned an arbitrary value of 100.000 CLS units. This number serves only as a reference point. At low levels of moisture Beer's law should be followed. Thus, the change in the water background concentration in the spectrometer will be monitored using the DTGS detector. After two weeks of purging, the background level of H_2O in the instrument, was reduced to a signal level of about 2.1 CLS units (see figure 2.4). By comparing the water absorption bands in the background spectrum to calibration spectra obtained using the 8 m Axiom cell, it can be estimated that the equivalent background water concentration was about 250 ppb. Most of the following experiments were done with a moisture background in this range. The true concentration of H_2O in the instrument is about 1 ppm since the pathlength inside the spectrometer is about 1/4 of the Axiom cell. Achieving a low and stable H_2O background is critical to the analysis. It is a challenge to accurately determine low trace levels of H_2O in the gas cell with

background levels in the optical path of the spectrometer that are 10 to 100 times those in the gas cell.

4.1.2 Cell conditioning procedure

Conditioning the gas cells is another procedure that is necessary to achieve reproducible calibrations of H_2O in N_2 over the range 40 to 400 ppb. The first step in the conditioning process was to heat the gas cell for three days. The gas cell and the gas handling system were then purged at 1-4 liters/minute with dried N_2 to reach a moisture level of 20-30 ppb (determined using the moisture analyzer). This level of H_2O was achieved using the 8m Axiom cell, but the White cell could not be heated, hence could not be dried lower than 150 ppb of H_2O. Because of this the Axiom cell was selected to do a calibration in the lower range. Prior to any measurement, the pressure and the water level were adjusted and about two hours were allowed for the cell to come to equilibrium. Then two interferograms, one using the internal DTGS detector and the second using the external InSb detector, with as short a time interval between them as possible, were collected. The total acquisition time for each interferogram was ten minutes. The background H_2O, that represents the absorption of water in the optical path of the spectrometer, was determined using the internal DTGS detector. The sample plus background concentration of H_2O was determined using the external InSb detector. Subsequent points at different levels of H_2O were preceded by heating the cell and purging the system with dried N_2 for about five hours. The desired H_2O concentrations were produced by varying the flow of nitrogen past the permeation device.

4.1.3 Data analysis procedures

Calculating the concentration of H_2O based on the spectroscopic data collected involves several steps. The two interferograms collected at each calibration point were transferred from the Nicolet SX computer to a 486/50 personal computer, where they were converted to the ".spc" format using the Nicolet PCIR software so that the data could be manipulated using the Lab Calc or GRAMS spectroscopic software (Galactic Industries). Absorption spectra were produced using the procedure discussed in Chapter 3.

Figure 4.1 shows the scheme that was used to estimate the H_2O concentration in the sample cell. The CLS estimate of the background H_2O was determined using the DTGS detector. The CLS estimate of the background H_2O plus the sample cell H_2O was determined using the external InSb detector. A correction factor (discussed below) is used to scale for the pathlength differences in the optical paths. Finally, a simple subtraction gives the CLS estimate of the water concentration in the sample.

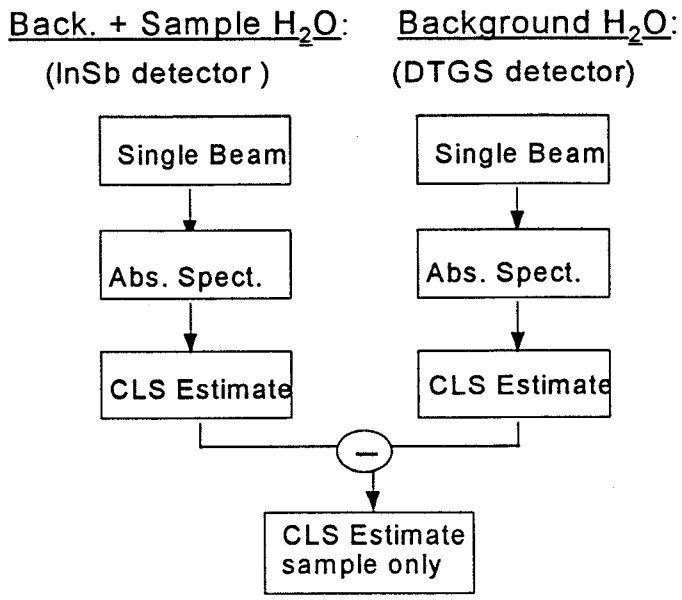

Figure 4.1 CLS data analysis scheme.

The DTGS reference spectrum, used in the calculation of the absorbance spectra, was acquired during the drydown of the spectrometer. To ensure a high SNR , 1250 scans (about 60 minutes) at 1 cm^{-1} resolution were collected. It was calculated a value of 20.148 CLS arbitrary units (relative to the 100.000 CLS unit scale) by comparing the peak areas around 3600-3910 cm^{-1} with the 100.000 CLS arbitrary units spectrum. A separate InSb reference spectrum was acquired, where 4000 scans (about 60 minutes) at 1 cm^{-1} resolution were collected. It was calculated a value of 23.193 by comparing peak areas with the 100.000 CLS arbitrary units spectrum. Figure 4.2 shows the reference DTGS H_2O spectrum at a resolution of 1 cm^{-1} after its interferogram has been converted to an absorbance spectrum. The concentration of H_2O is about 2 ppm. The ten indicated regions, encompassing the strongest water bands in this frequency range, were chosen for the CLS band-by-band calculation. In each region the CLS algorithm fits the unknown spectrum with the reference spectrum and a linear baseline. This gives a value for the intensity of the unknown spectrum, relative to the reference spectrum in each region. A weighted average yields the final concentration result, where the weighting factors are inversely proportional to the square of the spectral residuals. The CLS software written at Sandia National Laboratories, as part of the multivariate analysis program PLSSNL[4] for used in Lab Calc or GRAMS, was used in this determination.

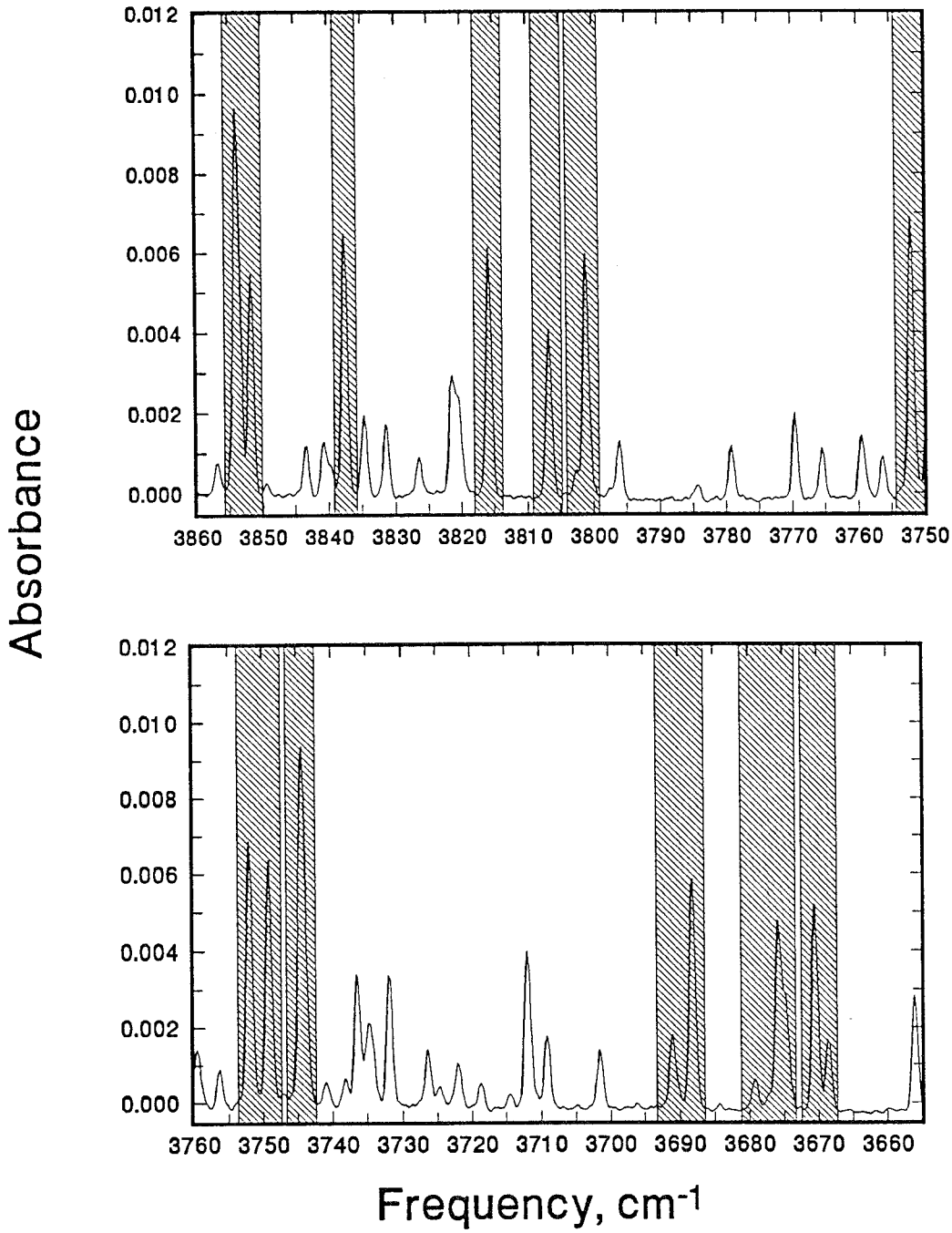

Figure 4.2 H_2O absorption spectrum with superimposed cross-hatching indicating the 10 regions used for most of the CLS calculations.

To determine the scaling factor required to correct the DTGS measurement of the background H_2O for the difference in pathlengths, the optical cell was removed from the InSb beam path and replaced with a short section of Axiom light pipe. This allowed for the entire InSb path to be purged to the identical background water level as the DTGS path. Repeated CLS measurements of the H_2O concentration in the DTGS and InSb paths were made over a period of seven days. The ratio of InSb to DTGS is plotted in Figure 4.3. The mean of 1.103 is the scaling

factor that accounts for the difference in pathlengths. The precision of this determination is obtained by calculating the standard error of estimate (SEE), which is the root-mean-square (RMS) error relative to the model, which, in this case, is a second order polynomial fit to the data (the solid line). The standard errors of the polynomial coefficients describing the curve in Figure 4.3 are not statistically different from zero, which implies that the fit is not distinguishable from a horizontal straight line.

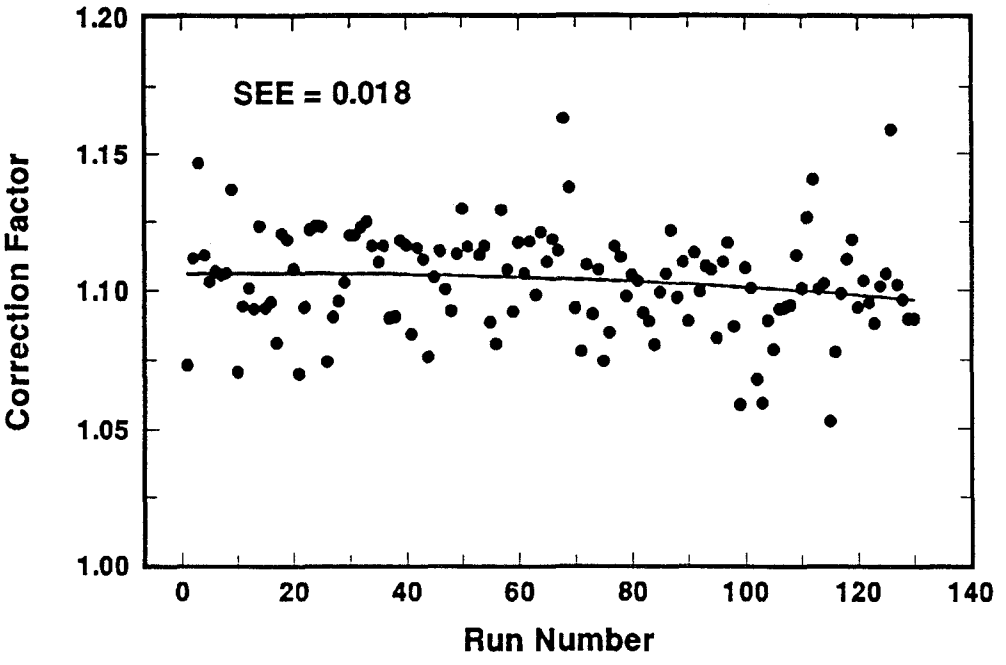

Figure 4.3 Plot to determine the scale factor to apply to the CLS estimate of the background H_2O concentration as derived from the DTGS spectra.

When the White cell was employed in the system the InSb optical path was necessarily altered from that used when the Axiom cell was installed. A similar procedure was employed to determined a pathlength scaling factor of 1.130 for the optical setup employing the White cell.

Another important procedure involves measuring the spectral noise to signal ratio (NSR) using a 100% line. A 100% line is obtained by ratioing two consecutive single beam background spectra collected using identical conditions. Figure 4.4 gives two examples of 100% lines. A 100% line contains noise, a slight slope, and often H_2O and CO_2 bands.[5] The estimation of spectrometer noise in the regions of the water bands can give us information about the quantification capabilities of FTIR spectroscopy under certain conditions. Noise is typically expressed as peak-to-peak noise or as root-mean-square (RMS) noise. The peak-to-peak noise is the difference in the % T values for the lowest and highest points in a given wavenumber region.. The RMS noise can be calculated by estimating the RMS deviation of the signal derived from n measurements.[6] To assure that the measurement reflects the noise and not improper cancellation of water bands, the

measurements were carried out after a very careful purge. The cancellation of the H_2O bands was confirmed by plots such as Figure 4.5, where twenty spectra of 50 scans each were collected at 1 cm^{-1} resolution. Spectrum #1 was ratioed to #2 to produce the first point. Spectra #1 + #3 were ratioed to #2 + #4 to produce the next point and so on. Array BASIC programs were written to perfom the spectral ratios and to calculate the RMS noise within a spectral region. The RMS noise of the 100% lines follows the expected dependence, (# scans)$^{-1/2}$.[7]

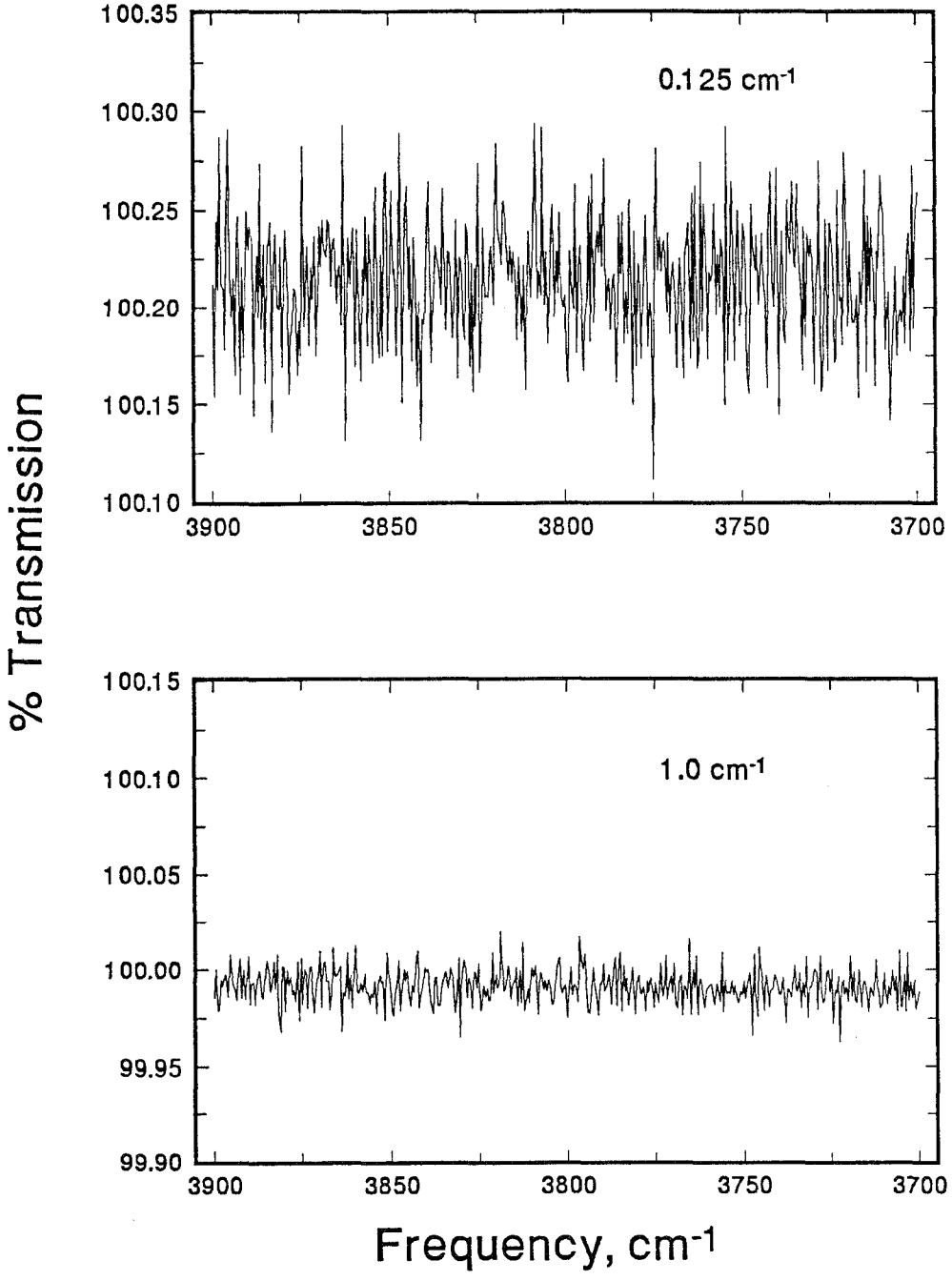

Figure 4.4 Examples of 100% lines for 1/8 cm^{-1} and 1 cm^{-1} spectral resolution.

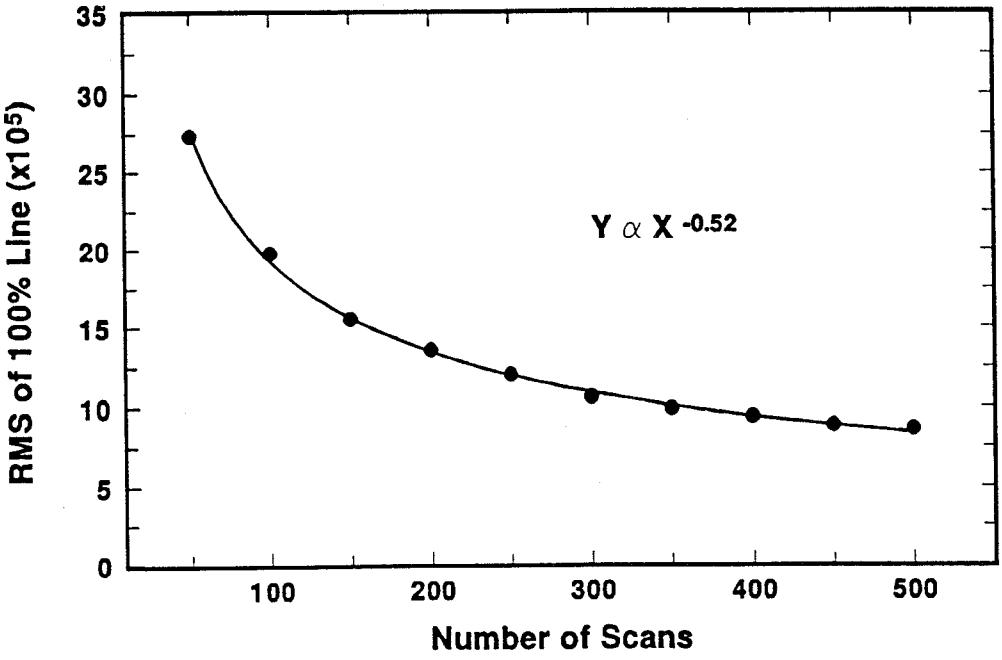

Figure 4.5 Spectral noise vs. the number of accumulated scans for 1 cm^{-1} resolution.

4.2 EXPERIMENTAL RESULTS

4.2.1 H_2O calibration in N_2

Table 4.1 shows one of the first calibration set of H_2O concentration in N_2 using the following experimental conditions:

a) Axiom Gas Cell: 8m (4 tubes).
b) Spectral resolution: 1.0 cm^{-1}.
c) Number of scans, DTGS: 180 (10 min.).
d) Number of scans, InSb: 620 (10 min.).
e) Source: Glowbar
f) Beamsplitter: KBr.
g) Optical cell windows: KBr.
h) Spectral region: 3600-3910 cm^{-1}.
i) CLS regions: See Figure 4.2, with band by band analysis.
j) Apodization: Happ-Genzel
k) Zero-filling: Two times, yielding one point per 0.25 cm^{-1}.
l) Optical filters: None
m) Temperature: 23° C, ± 2°.
n) Pressure: Atmospheric = 0.822 ± 0.013 atm, Cell pressure = 0.544 ± 0.014 atm, Total = 1.37 ± 0.03 atm.
o) Flow rate of sample: 2 to 7 liters/minute as dictated by the 420 ng/minute moisture generator.

Table 4.1 Results of H_2O calibration in N_2. The last three columns are the values determined spectroscopically by the CLS method.

Flow H_2O Generator (liter/min.)	Measured H_2O Conc. Analyzer (ppb)	Measured H_2O Conc., InSb det. (arb. CLS units), a	Measured H_2O Conc., DTGS det. (arb. CLS units), b	Sample Cell H_2O Conc. (a - 1.103 b) (arb. CLS units)
4	176	4.249	2.187	1.837
4	180	4.314	2.020	2.086
2	316	5.689	2.208	3.254
5.5	128	3.582	2.126	1.237
2	280	4.882	2.153	2.507
4	156	3.573	1.971	1.399
4	145	3.525	1.929	1.397
2	241	4.404	1.821	2.395
5.5	112	3.348	1.993	1.150
4	136	3.688	2.001	1.481
N./A.[a]	44	2.605	1.931	0.475
7	98	3.427	1.981	1.242

The first column of table 4.1 shows the flow settings of the MFC controller in the moisture generator used to produce different concentrations of H_2O. The second column is the readout from the moisture Meeco electroanalyzer during spectral collection. The third and fourth columns are the estimated H_2O concentration from the CLS standard as described in section 4.1.3. Finally the last column represents the spectroscopically estimated H_2O concentration in the sample only after the scaled subtraction of background moisture signal. The whole calibration set was obtained a point per day after carefully conditioning the cell and letting the H_2O concentration equilibrate for hours. It can be seen that repetitions of the same calibration point gave an indication of some irreproducibility in the experiment. For example, setting the moisture generator at 4 liters/minute should produce a H_2O concentration of 143 $\pm$17 ppb. The Meeco moisture analyzer has a specified precision of $\pm$20 ppb over the range of moisture values generated. Assuming the specified ranges to be standard deviations the generated moisture level should be in the range of 143 $\pm$26 ppb. Two of the measurements are outside this range, a fact that calls the reliability of the reference determinations into question. In Figure 4.6 the sample cell H_2O concentration in N_2 determined spectroscopically in arbitrary CLS units is plotted versus the H_2O concentration determined by the reference electroanalyzer method in ppb. The inverse of the slope of the best fit line gives a calibration for the arbitrary CLS units that is 106 ppb per CLS unit (standard error = 7 ppb). The 22 m White cell was used to obtain a second calibration curve over a higher range of H_2O concentration. The same experimental conditions were used , but different CLS standards and a different pathlength correction were used. Figure 4.7 shows the White cell calibration curve.

[a] Generator was off .

In this case the inverse of the slope gives a calibration factor of 44 ppb per CLS unit (standard error = 1 ppb). In comparing the two calibration results, a correction is necessary to account for the pathlength difference between the two cells. Correcting the calibration factor from the White cell to an 8m path, yields a calibration factor of 121 ppb per CLS unit (standard error = 3 ppb).

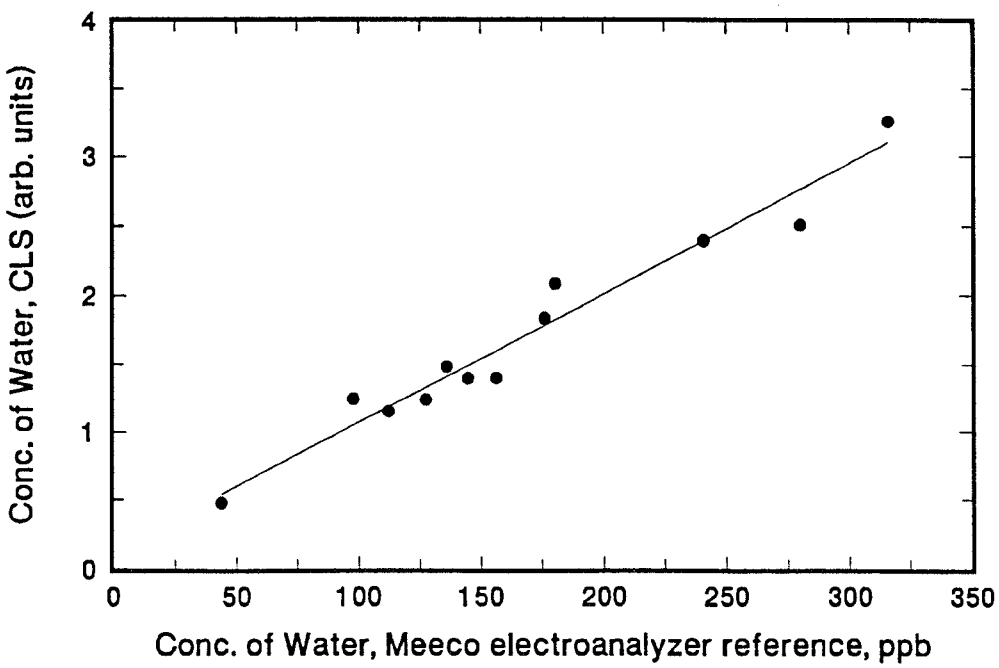

Figure 4.6 Measured H_2O concentration in N_2 vs. the reference values from the Meeco electroanalyzer (8 m Axiom cell). The solid line is a linear regression.

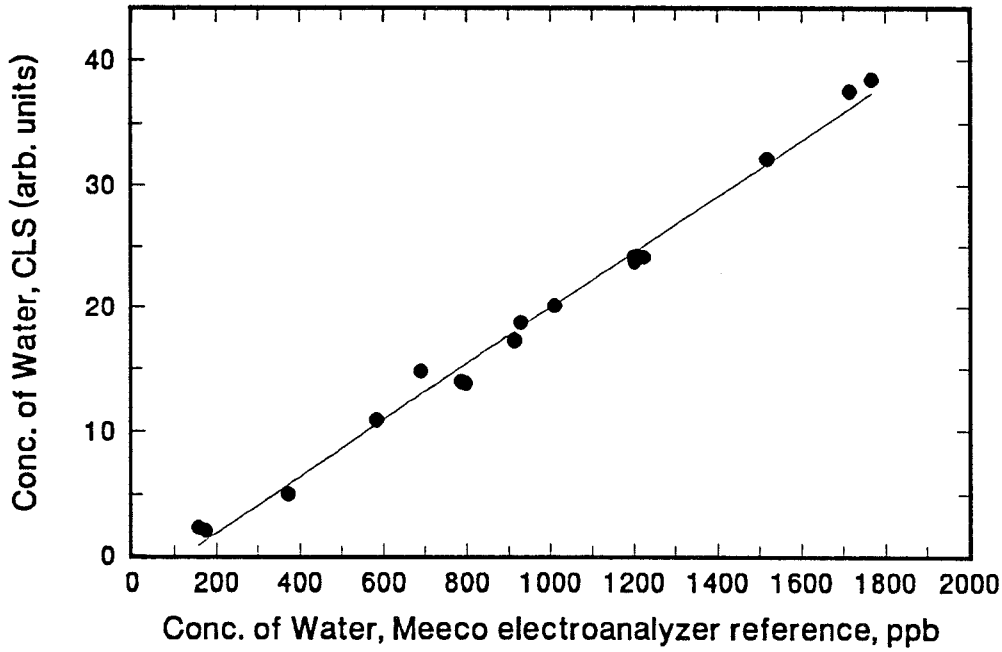

Figure 4.7 Measured H_2O concentration in N_2 vs. the reference values from the Meeco electroanalyzer (22 m White cell). The solid line is a linear regression.

Another H_2O calibration curve in N_2 was attempted six months later using the 8m Axiom cell with the same experimental conditions, except that BaF_2 windows and a total pressure of 2.19 ± 0.03 atm (atmospheric = 0.822 ± 0.013, cell pressure = 1.370 ± 0.014) were used. Two H_2O permeation devices of 2860 and 420 ng/minute were alternated to produce a range of 70-2000 ppb H_2O concentration. Both the Meeco Aquamatic Plus electroanalyzer and the permeation tube were used as reference methods. The H_2O concentration measured by the reference methods, as well as the spectroscopic CLS estimations are presented in Table 4.2. Figures 4.8 and 4.9 are plots of the H_2O concentration in N_2 determined spectroscopically (column 5 in Table 4.2) using the arbitrary CLS multivariate method versus the H_2O concentration determined using the permeation tube and electroanalyzer reference methods. It can be seen that the linear regression gave a better fit when the permeation tube is used as the reference method. The calibration factors calculated from the inverse of the slopes of the plots in Figure 4.8 and 4.9 are 115 ppb (standard error = 1 ppb) and 92 ppb (standard error = 2 ppb) per arbitrary CLS units. Considering all calibration curves presented so far, an average of the calibration factor is 109 ppb per CLS unit, with a relative standard deviation of 12%. This is an indication of the reliability of the calibration results.

Table 4.2 Results of H_2O calibration in N_2. The first two columns are the reference H_2O concentration measured by the permeation tube and Meeco electroanalyzer, respectively.

Generated H_2O Conc. (ppb)[a]	Measured H_2O Conc. Analyzer (ppb)	Measured H_2O Conc., InSb det. (arb CLS units),a	Measured H_2O Conc., DTGS det. (arb CLS units),b	Sample Cell H_2O Conc. (a - 1.103 b) (arb. CLS units)
806	793	10.261	2.506	7.497
409	419	6.949	2.651	4.025
575	563	7.594	2.032	5.352
1353	1182	14.544	2.097	12.231
1009	896	11.433	1.815	9.431
2022	1649	19.774	1.782	17.808
492	477	6.697	1.990	4.502
668	608	8.566	2.055	6.299
1612	1289	16.394	1.768	14.444
409	433	6.397	2.335	3.821
1014	895	11.987	2.531	9.195
668	607	8.631	2.085	6.331
149	163	3.840	1.978	1.658
299	257	5.317	1.872	3.252
73	87	2.990	1.781	1.025

[a] A 2860 ng/min were used to generate the water concentration except the last three point that were generated using a 420 ng/min permeation tube

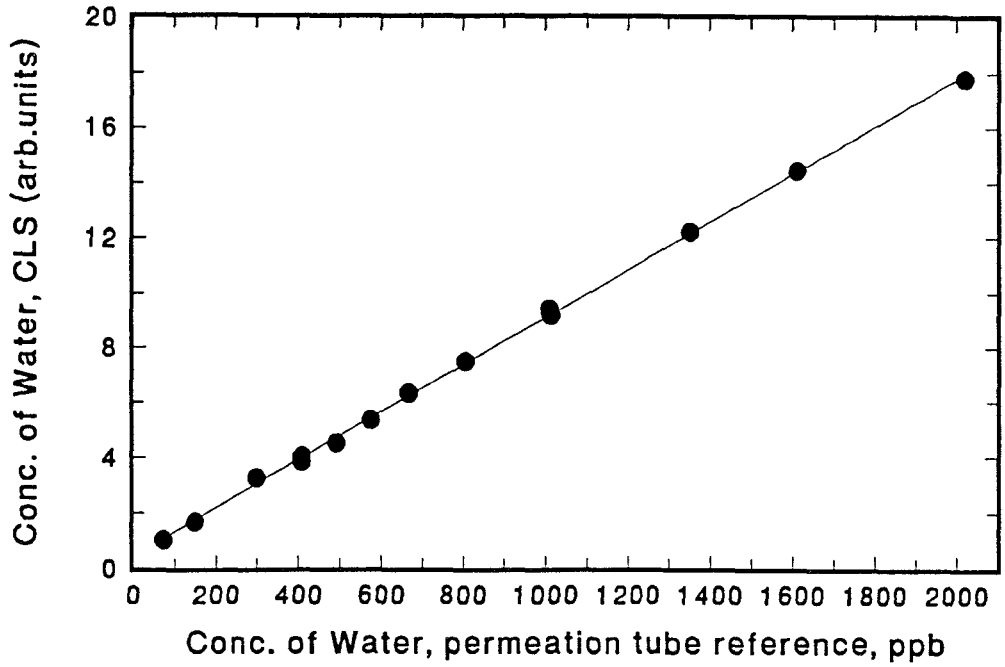

Figure 4.8 Measured H_2O concentration in N_2 vs. the reference values from the permeation tube (8 m Axiom cell). The solid line is a linear regression.

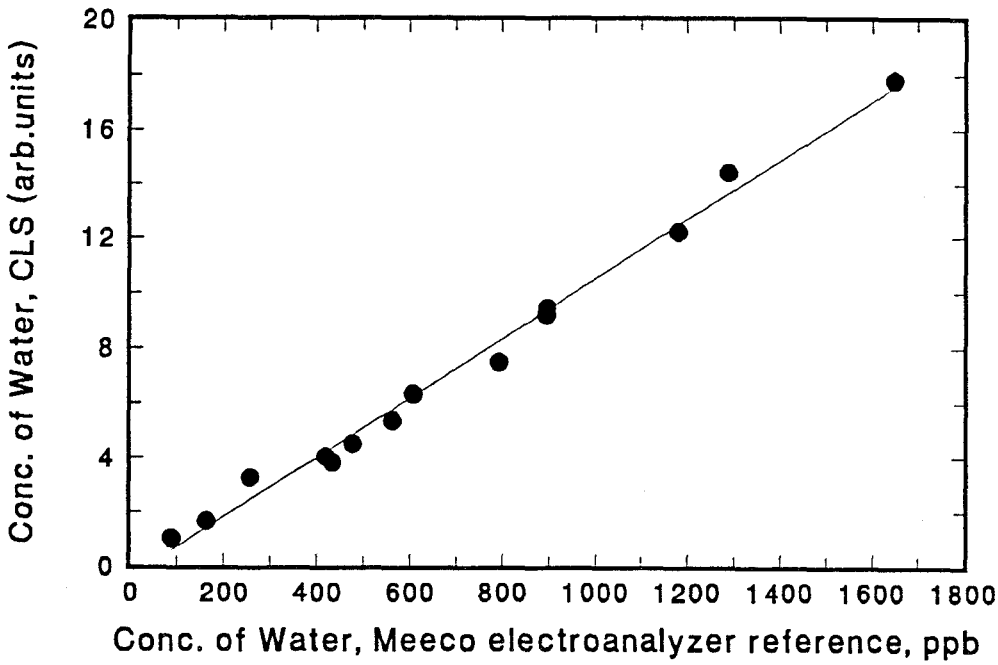

Figure 4.9 Measured H_2O concentration in N_2 vs. the reference values from the Meeco electroanalyzer (8 m Axiom cell). The solid line is a linear regression.

From the calibration curves discussed above, it is possible to calculate an absorptivity for each H_2O band in the spectrum. The absorptivities found for the

strongest 12 peaks in this work (using 109 ppb per CLS unit) are listed in Table 4.3. The absorptivities are, after adjustment for operating parameters, on average, 1.4 times those derived from the HITRAN data base.[8] The discrepancy in the absorptivities is considered acceptable since the precision of the cross-section values for the H_2O absorption bands in the HITRAN data base are listed as undetermined, indicating that the original experiments were not done with exact quantification in mind. Also, manipulating the HITRAN data to duplicate the spectrometer conditions can be a significant source of error, especially in gas phase analysis, where the intensity at an absorption peak is a very sensitive function of spectral resolution and apodization.

Table 4.3 H_2O absorptivity values calculated in our work compared to those calculated by the HITRAN data base.

Peak Position (cm^{-1})	IR Absorptivity Coefficient ($ppb^{-1}m^{-1}$) x 10^7	HITRAN Absorptivity Coeff.($ppb^{-1}m^{-1}$) x 10^7
3670.7	3.1	2.3
3675.9	2.9	2.1
3688.4	3.6	2.4
3744.5	5.5	4.2
3749.3	3.7	2.9
3752.1	3.9	3.1
3801.3	3.5	2.7
3806.9	2.5	1.6
3816.0	3.5	2.6
3837.8	3.9	2.6
3852.0	3.2	2.4
3854.1	5.5	4.0

4.2.2 Detection Limits

The Standard Error of Prediction (SEP) is used in multivariate calibrations to estimate the precision of a determined concentration.[9] It is calculated using cross-validation, where a calibration sample is removed from the calibration set. A calibration is performed using the remaining samples, and the resulting calibration is used to predict the properties of the removed sample. The removed sample is returned to the calibration set, a new sample is removed, a new calibration is performed and used to predict the properties of the new sample. This process is continued until all samples have been removed one at a time and their properties predicted. The SEP is calculated by:

$$SEP = [\sum_{i=1}^{n} (y_i - \hat{y}_i)^2 / n]^{1/2} \qquad .....(4.1)$$

where y_i and $\hat{y}_i$ are the reference value and the estimated value for the ith sample respectively, and n is the total number of calibration samples. Figure 4.10 presents the data of Figure 4.8 as a cross-validated calibration plot, where the SEP is calculated and found to be equal to 18 ppb. Similar plots of the above calibration plots gave SEP values of 18-49 ppb. Nevertheless, in all cases, the precision of the reference methods was the main source of error contributing to the SEP. In order to determine the precision inherent to the FTIR system, i.e., determine the FTIR detection limit, repeatability experiments were performed.

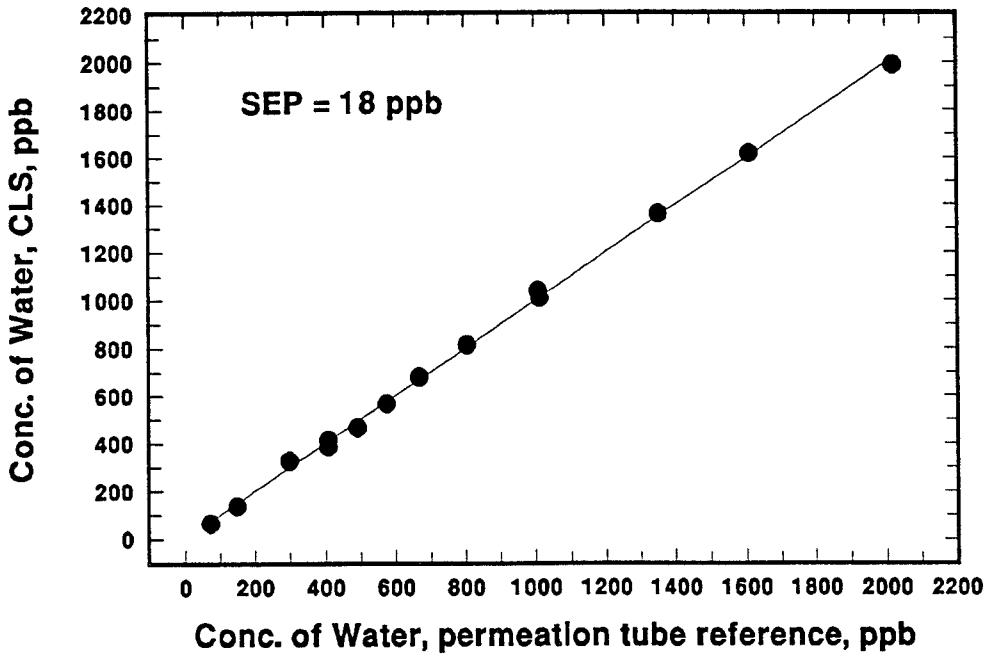

Figure 4.10 The cross-validated prediction plot for the data in Figure 4.8. The SEP is essentially the precision of the determination including errors in the reference method.

The simplest approach to determine detection limits in an analytical technique considers only the variance in the measurement[10] as determined from the detector noise. As discussed in section 4.1.3 the H_2O concentration in the gas cell is derived using two detectors, therefore the noise of these two detectors can be measured separately and combined to estimate the total noise for the measurement. The detection limit, or the two sigma precision of the measurement, was determined by 54 repeat measurements on a low and stable sample of H_2O in N_2 over a 9 hour period using the DTGS (background water) and InSb (background plus cell water) detectors, where each spectrum was measured for 10 minutes. The H_2O concentration in the background and the background plus cell was calculated using the CLS analysis described above. The water concentrations in the background and background plus cell over the nine hour period are shown in Figures 4.11 and 4.12 respectively. Because of the low H_2O concentration and the length of the experiments, a drift in the value of the H_2O was unavoidable. This drift was

accounted by fitting a second-order polynomial to each data set as shown by the solid line in the plots. The precision of both measurements was obtained by calculating the standard deviation (or standard error of estimate, SEE) of the data relative to the polynomial fit. The SEEs of the DTGS and InSb detector measurements were 9.1 ppb and 3.3 ppb, respectively. Thus, the total measurement error, or the two sigma detection limit is calculated using $2\sqrt{(DTGS)^2+(InSb)^2}$ and is equal to $2\sqrt{(9.1)^2+(3.3)^2}$ = 19 ppb for the H_2O determination in N_2 using both detectors, 1 cm^{-1} resolution, a 8m path length, and a total of 20 minutes scanning time.

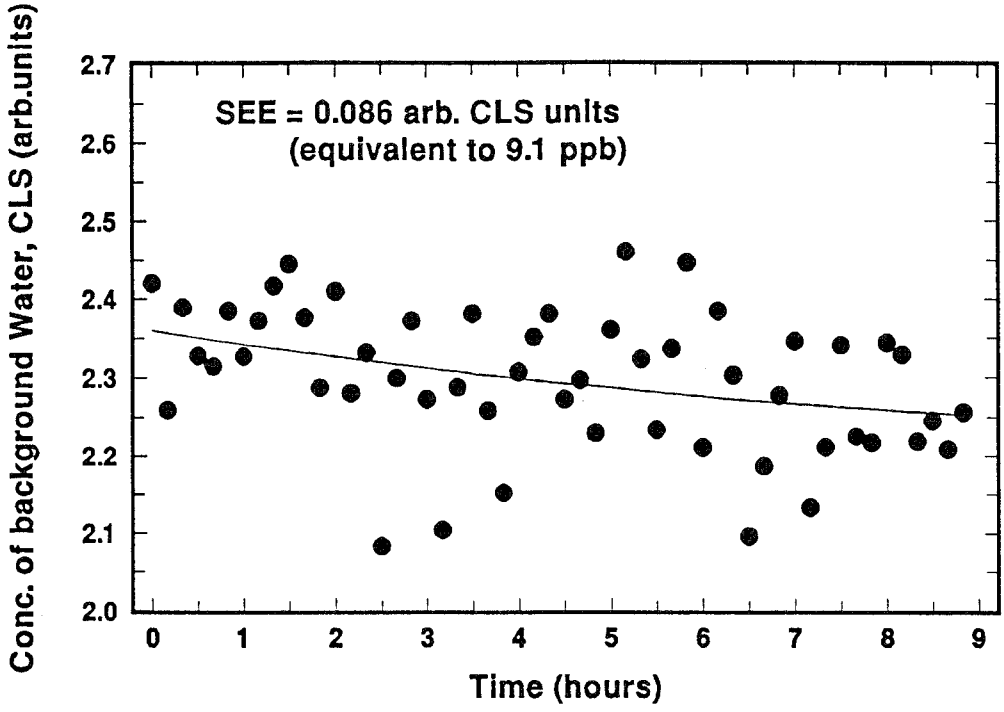

Figure 4.11 Experimental data showing the precision of the measurement of the background H_2O concentration in N_2 over a nine-hour period using the DTGS detector. The solid line is a second-order polynomial fit.

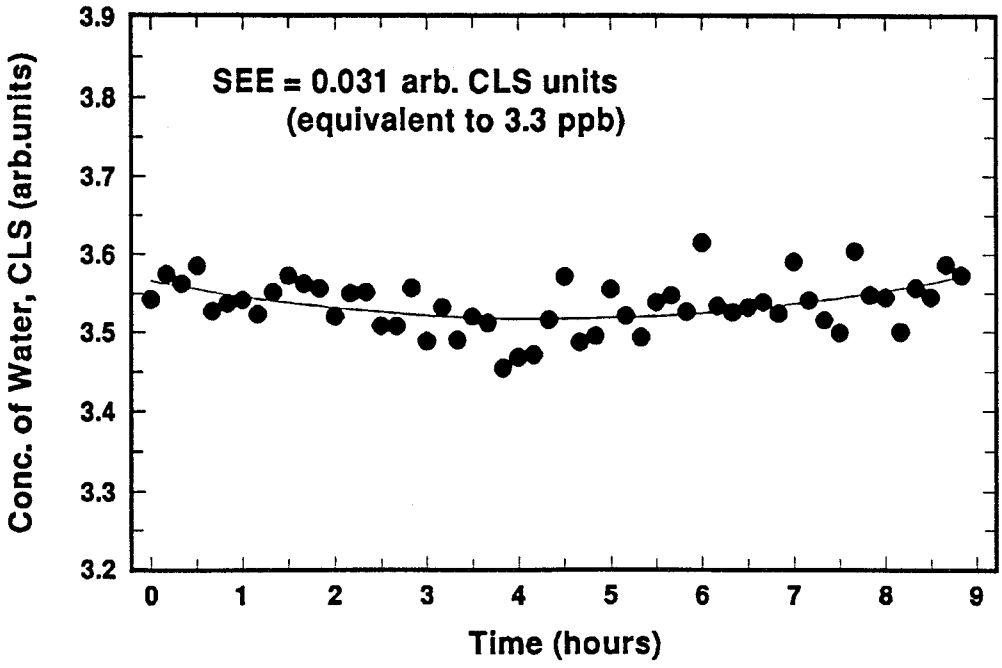

Figure 4.12 Experimental data showing the precision of the measurement of the background H_2O plus cell concentration in N_2 over a nine-hour period using the InSb detector and an 8 m Axiom cell. The solid line is a second-order polynomial fit.

Figure 4.13 is a spectrum of about 0.5 ppm of H_2O in semiconductor grade HCl. A spectral interference from CO_2 contamination in the HCl about 3615 cm^{-1} and 3715 cm^{-1} can be seen. The CO_2 bands overlap some the water bands in the 3600-3910 cm^{-1} region, hence the CLS calibration for water in HCl is limited to five interference free bands. Alternatively the whole spectral region in the determination could be used if other contaminants are also included in the CLS calibration. According to the specifications of semiconductor grade HCl, CO_2 and CH_4 are the major contaminants, other than H_2O, with concentrations of less than 10 ppm and 2 ppm, respectively. As explained above, conditioning the cell is a standard procedure to accurate measure the H_2O concentration in gaseous samples. When the gas being tested is HCl or HBr, it takes much more time for the cell to reach equilibrium than in N_2. There is considerable H_2O adsorbed onto the cell walls when equilibrium is reached when N_2 is flowing through the cell. After switching the gas stream to HCl or HBr the cell acts as a significant source of H_2O. Figure 4.14 shows the response of the cell when the supplied gas is switched from dry N_2 (about 50 ppb H_2O) to dry HBr (< 100 ppb H_2O). Experimentally we determined that HBr is more aggressive than HCl in stripping H_2O off the cell walls.

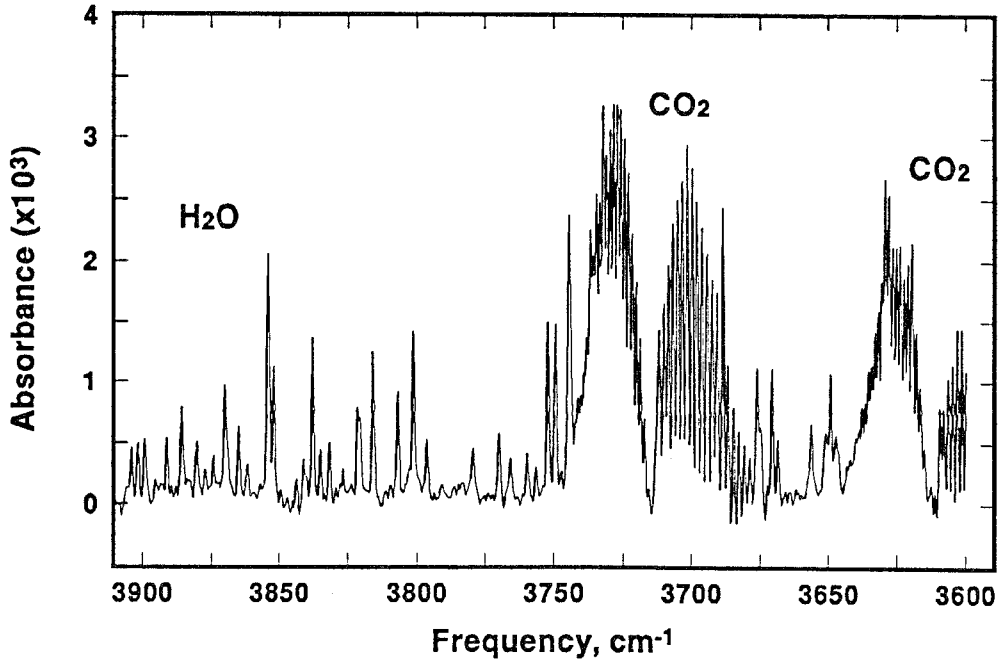

Figure 4.13 Spectrum of H_2O at about 0.5 ppm in semiconductor grade HCl. The spectral interference from CO_2 present at less than 10 ppm is evident.

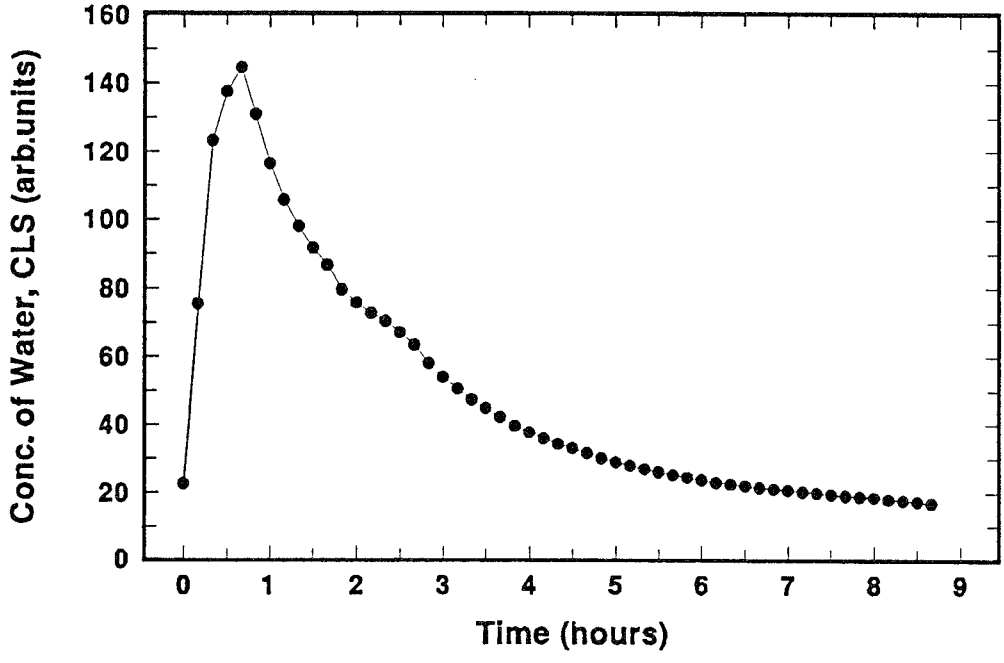

Figure 4.14 Experimental data showing the H_2O concentration when the supplied gas is switched from dry N_2 to dry HBr.

Figure 4.15 shows the H_2O concentration in HCl (CLS estimates) of 54 consecutive spectra, after conditioning the gas cell with N_2 and then letting the H_2O equilibrate for several hours with the sample of dry HCl (<10 ppb H_2O). Since the H_2O concentration is decreasing with time the SEE was calculated to be 8.4 ppb by fitting the points to a second order polynomial. The reduced sensitivity when comparing the precision in HCl to that in N_2 is due to the spectral interference found in HCl. For HBr the SEE of the InSb measurement was 5.1 ppb with no interference observed in the H_2O 3600-3910 cm^{-1} absorption region. The detection limits of the H_2O determination in HCl and HBr are 25 ppb and 21 ppb, respectively. Note that the noise level of a DTGS detector is much greater than that of the InSb detector. Hence, replacement of the DTGS detector with an InSb detector should result in a lowering of the detection limit of the determination. Taking both the InSb noise level and the light level reaching the detector in the background determination into account we expect to improve the precision of the determination from 9.1 ppb to 0.8 ppb (3.3×0.7^4 ppb). The two sigma detection limits would be 7 ppb (0.8 ppb, 3.3 ppb) for H_2O in N_2, 17 ppb (0.8 ppb, 8.4 ppb) for H_2O in HCl and 10 ppb (0.8 ppb, 5.1 ppb) for H_2O in HBr. Table 4.4 summarizes the detection limits for the FTIR Nicolet 800 instrument.

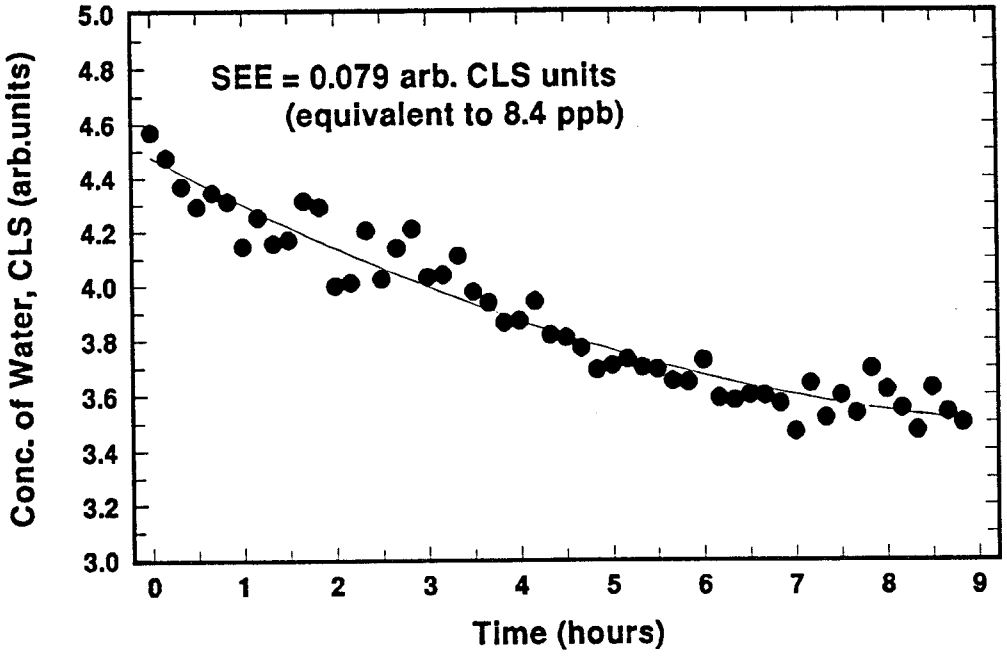

Figure 4.15 Experimental data showing the precision of the measurement of the H_2O concentration in HCl over a nine-hour period using the InSb detector and an 8 m Axiom cell. The solid line is a second-order polynomial fit.

Table 4.4 FTIR estimated detection limits (Nicolet 800)

	2 σ Detection Limits (ppb)	
	DTGS + InSb detectors	2 x InSb detector
H_2O in N_2	19	7
H_2O in HCl	25	17
H_2O in HBr	21	10

4.3 CONCLUSIONS

An initial estimate of the capabilities of FTIR spectroscopy applied to trace water vapor determination in corrosive gases has been accomplished. Multivariate classical least squares data analysis has been shown to lower the detection limit relative to univariate analysis. Problems, mostly associated with obtaining an adequate spectrometer purge, were identified and methods of dealing with them developed. The performance of the resulting system was characterized over a wide range of H_2O concentrations and operating conditions. Detection limits of about 10 ppb H_2O in N_2, HCl, and HBr are possible for FTIR spectroscopy. This performance is better than any commercial instrument capable of a quantitative determination of water vapor in corrosive gases. More important, however, is that these studies point out the design features necessary in an optimized trace water detection system. Instrument optimization will be discussed in Chapter 5.

4.4 REFERENCES

1. D. Pivonka, Appl. Spectrosc., 45, 597 (1991).
2. K. Miyasaki, Y. Ogawara, and T. Kimura, Bull. Chem. Soc. Jpn., 66, 969 (1993).
3. R. S. Inman and J. F. McAndrew, Anal. Chem., 66, 2471 (1994).
4. D. M. Haaland and D. Melgaard, PLSSNL software, Sandia National Laboratories, Albuquerque, NM 87185.
5. B. C. Smith, Fourier Transform Infrared Spectroscopy, CRC Press, Boca Raton, p. 52, (1996).
6. J. I. Ingle Jr. and S. R. Crouch, Spectrochemical Analysis, Prentice Hall, New York, p. 136, (1988).
7. P. R. Griffiths and J. A. de Haseth, Fourier Transform Infrared Spectroscopy, John Wiley & Sons, New York, p.254, (1986).
8. L. S. Rothman, R. R. Gamache, R. H. Tipping, C. P. Rinsland, M. A. H. Smith, D. C. Benner, V. M. Devi, J. M. Flaud, C. Camy-Peyret, A. Perrin, A. Goldman, S. T. Massie, L. R. Brown, and R. A. Toth, J. Quant. Spect. Radiat. Transfer, 48, 469 (1992).
9. J. Workman Jr. and H. Mark, Statistics in Spectroscopy, Spectroscopy, 7, p. 14, (1992).
10. G. L. Long and J. D. Winefordner, Anal. Chem., 55, p. 712A, (1983).

Intentionally Left Blank

CHAPTER 5

INSTRUMENT OPTIMIZATION

The work presented in the preceding chapters shows that it is possible to perform low ppb water determinations using standard laboratory infrared equipment. There are, however a number of design choices and optimizations improvements that can be made if an infrared spectrometer dedicated to trace water determination is being developed. The development of such an instrument is the subject of this chapter.

5.1 BEAM PATH DESIGN

There are three possible approaches when using an FTIR system for trace water determination to account for the amount of background H_2O present in the optical path of the spectrometer. The two beam-two detector approach, like the one used with the Nicolet 800 FTIR system, as it was described in chapter four, is too complex and cumbersome to achieve optimum performance. A system designed for trace water measurements from the start would take one of two approaches to the dealing with the background water. The first is to completely eliminate water from the background, i.e., evacuate the system. The second is to employ a dual-beam single detector design.

5.1.1 Evacuable FTIR system

One alternative is a single beam system with an evacuable FTIR, where the background H_2O can be reduced to a negligible level. Assuming an instrument pressure of 10^{-5} torr, and 10% of the vapor water, the background water will correspond to about $10^{-6} / 760 = 1.3$ ppb of H_2O at atmospheric pressure. The ability to measure the water concentration in a sample should improve when ratioing the sample spectrum to a "zero H_2O" spectrum. The cost and complexity of an evacuable spectrometer are high relative to a purged system. There are however commercially available vacuum spectrometers. An example is the system being marketed by the Midac Corporation. It is designed to be small and robust, hence an ideal spectrometer for our purpose.

5.1.2 Purged dual beam FTIR system

A second alternative is a purged system with a dual beam accessory as shown in Figure 5.1, where an alternate beam path bypasses the sample cell. The second path, called the reference channel, can be used to monitor the background H_2O. Note that it is possible to make the optical pathlengths of the two channels equal. By moving the mirrors to direct the beam through the reference channel the background H_2O is measured, and by moving the mirrors to direct the beam through

the cell channel, the background plus sample H_2O is measured. By collecting data in one channel, then rapidly switching to the other channel for a data collection, the effects of drift in the background water concentration can be minimized. The background H_2O drift was found to be about 10 ppb during a 10 minutes data acquisition. Ultimately the data acquisition time will be reduced to one minute which will make the drift negligible.

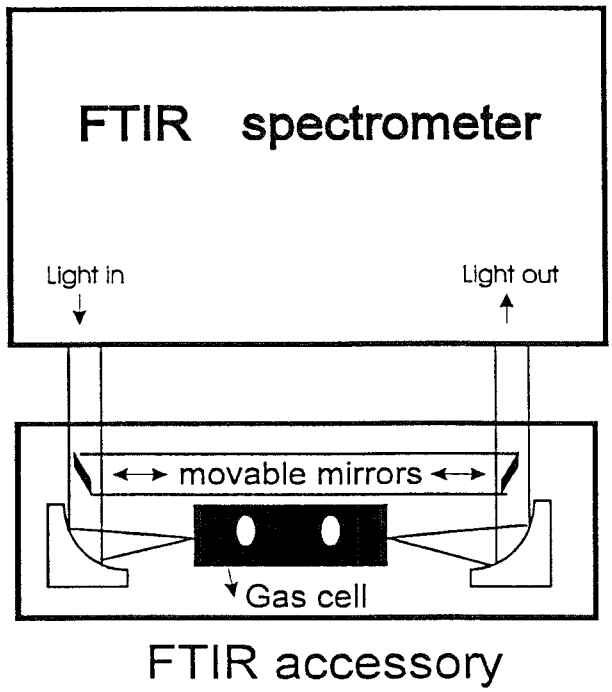

Figure 5.1 Schematic of a dual-beam accessory attached to an FTIR instrument for trace water determination.

The most significant concern when using a purged spectrometer to measure trace water concentration is to have an excellent purge to bring the H_2O background down to low and stable levels. In the Nicolet 800 FTIR spectrometer a 1 ppm H_2O background was achieved only after enclosing the spectrometer in a secondary box and by purging with dried N_2 for about two weeks. Smaller spectrometers with leak free enclosures should purge more efficiently and reach the 1 ppm H_2O background level in a much shorter time. Finally, we expect that coupling a rugged, sealed and compact FTIR spectrometer to this dual beam accessory will be as close as possible to the optimum system for the infrared determination of trace levels of water vapor in corrosive gases. Test results obtained from such a system will be discussed in chapter 6.

5.2 DETECTOR AND SPECTRAL REGION

Figure 5.2 shows the water absorption bands in the mid-infrared region, at approximately 1600 cm^{-1} and 3800 cm^{-1}. The magnitude of these absorption bands are roughly equivalent, making the decision of which region to use based largely on the characteristics of available detectors.

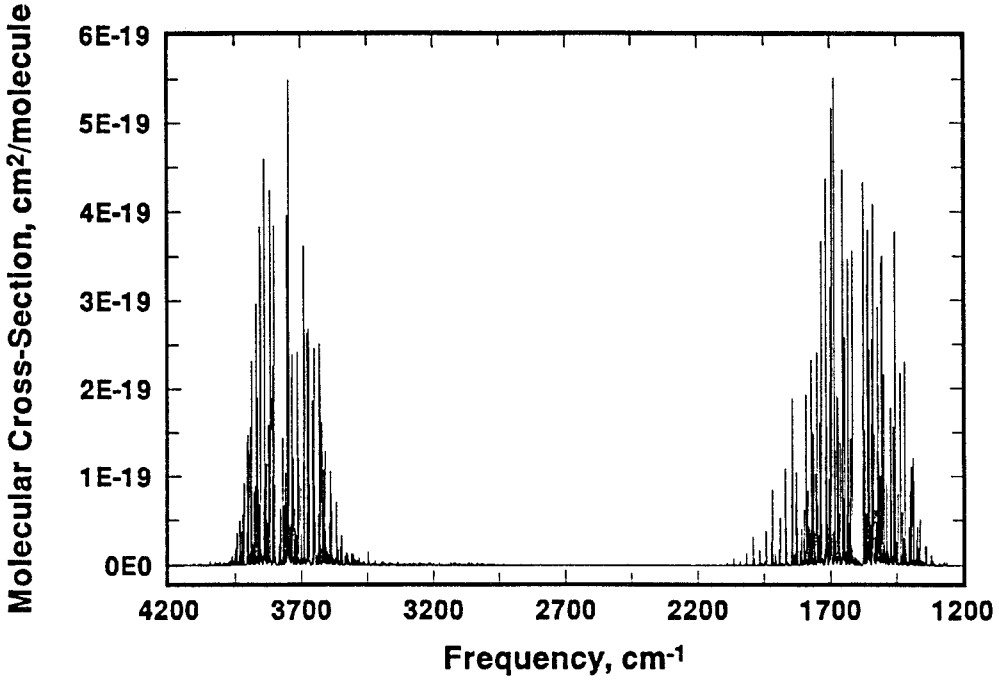

Figure 5.2 Portion of the water vapor absorption spectrum showing the H_2O mid-IR absorption bands at 1600 cm^{-1} and 3800 cm^{-1}.

Infrared detectors are characterized by their spectral response, speed of response, and their noise equivalent power (NEP), which is a measure of the minimum radiant power they can detect.[1] A more useful quantity in the comparison of detectors is their specific detectivity values, D*, which is the area and frequency normalized inverse of NEP, and can be interpreted as the SNR of the output of the detector when 1 W of radiant power is incident on a 1 cm^2 detector surface with a 1 Hz bandwidth. Figure 5.3 shows the D* values of the InSb and MCT infrared detectors used in this work.[2] Individual detectors will vary slightly from these curves, even for detectors that are nominally identical. The sensitivity of MCT detectors is dependent on the composition of the alloy in the semiconductor material,[3] hence MCT detectors designed for different applications can have significantly different response characteristics. Figure 5.4 displays a single beam spectrum obtained with each detector, the shape of which is due to the sensitivity of the detector, emissive properties of the glowbar source, transmission and reflection properties of the beamsplitter, and reflective properties of the mirrors. Note that the MCT single beam spectrum has a high H_2O signal indicating the position of these bands. The DTGS detector is sensitive to both mid-infrared H_2O bands, and does

not require cooling by liquid nitrogen. Therefore, it was conveniently employed to monitor the background water inside the spectrometer. Its main drawback is its low D* and relatively slow response compared with the liquid nitrogen cooled MCT or InSb detectors. The MCT detector is sensitive to frequencies between about 600 and 7000 cm^{-1}, with a peak D* of approximately 1 x 10^{10} cm $Hz^{1/2}$ W^{-1} at 850 cm^{-1} (11.8 μm). While the MCT detector is sensitive to both mid-infrared H_2O bands, Figure 5.4.b shows that the 1600 cm^{-1} frequency region is approximately 20% more sensitive than the 3800 cm^{-1} region. As shown in Figure 5.4.a the InSb detector is limited to measurements of the 3800 cm^{-1} H_2O band since the operating range is about 1800 to 8000 cm^{-1}, with a peak D* of approximately 1 x 10^{11} cm $Hz^{1/2}$ W^{-1} at 2000 cm^{-1} (5 μm).

When operated properly, the dominate noise source in an FTIR is signal-independent detector noise. Since a large D* implies a better SNR, an InSb detector operating at 3800 cm^{-1} (2.6 μm, D* is about 6 x 10^{10} cm $Hz^{1/2}$ W^{-1}) should be 10 times more sensitive than a MCT detector operating at 1600 cm^{-1} (6.2 μm, D* is about 6 x 10^{9} cm $Hz^{1/2}$ W^{-1}) assuming similar detector area and bandwidth. This was experimentally confirmed by measuring the RMS noise of the respective 100% lines. Using the Nicolet spectrometer at 1 cm^{-1} resolution the light had to be attenuated by a factor of 10-30 to avoid saturation of the InSb detector. Therefore, an InSb detector is favored for low light level applications (which was often the case for the measurements made using the 8m Axiom cell). The MCT detector could be used at higher light levels without saturation. In cases where throughput is high, i.e., a high level of light available at the detector, an MCT detector might outperform an InSb detector. The use of an optical band-pass filter solves the saturation problem for typical spectrometer light levels making the InSb detector the preferred detector.

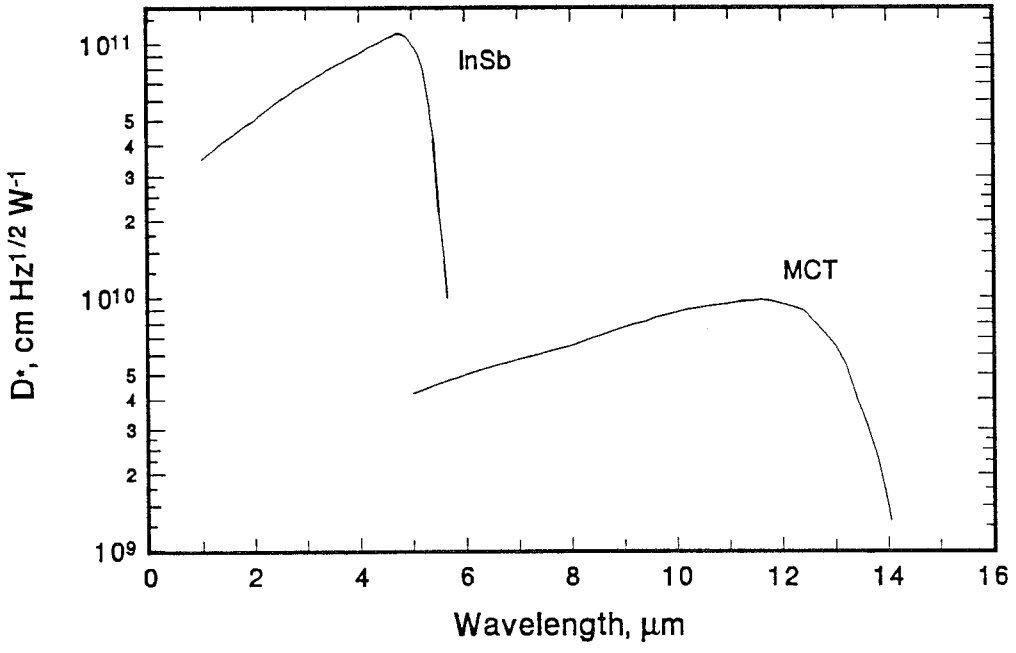

Figure 5.3 Spectral specific detectivity (D*) for the InSb and MCT detectors.

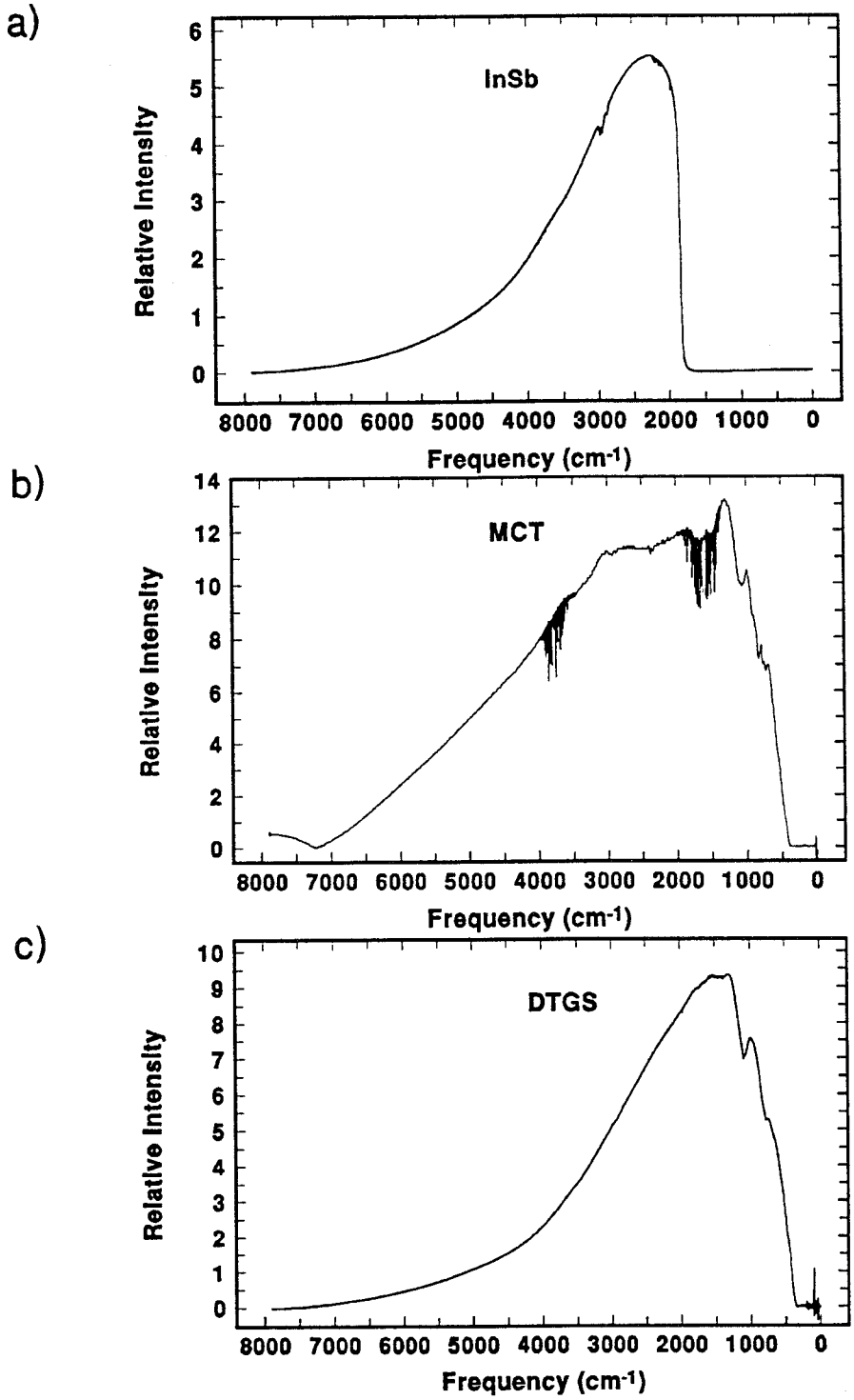

Figure 5.4 Single beam spectra for the InSb, MCT, and DTGS detectors.

5.3 OPTICAL BAND-PASS FILTER

By looking at the InSb single beam spectrum in Figure 5.4.a, the whole mid-infrared frequency region about 7899-1800 cm^{-1} is detected, but the region of

interest for H_2O determination is about 3910-3600 cm^{-1}. Therefore, the use of an optical band-pass filter that passes the region of interest will limit the light intensity on the detector to only those frequencies that carry useful information. The area under the InSb single beam spectrum is approximately 14 times greater than that between 3900-3600 cm^{-1}. Therefore, the light intensity in that region can be increased by one order in magnitude by using an optical band-pass filter. To avoid saturation, the light flux from the glowbar source had to be attenuated when using the InSb detector. Use of the filter allow an increase in the light intensity with no increase in noise (the dominate noise is signal-independent detector noise) improving the SNR. Figure 5.5 shows the single beam spectrum obtained using the optical band-pass filter and the InSb detector.

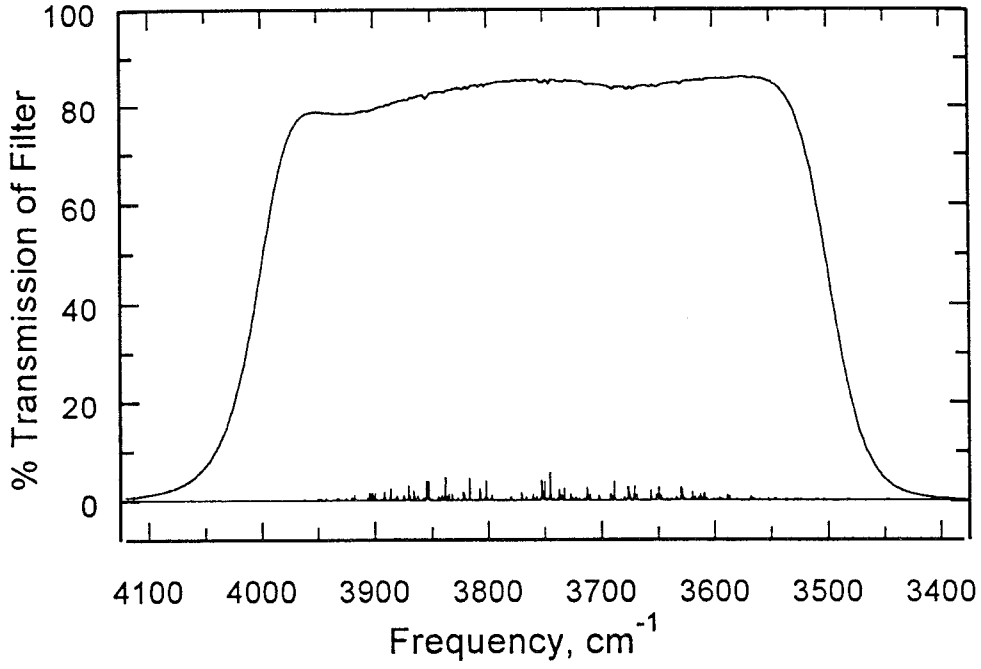

Figure 5.5 Percentage of transmission vs. frequency of the optical band-pass filter that passes only the water vapor absorption frequencies.

5.4 GAS CELL AND OPTIMUM PATHLENGTH

As discussed in Chapter 4 the walls of a gas cell can act as a source or sink of water. Hence, the ideal cell has a high pathlength to surface area. The 22 m White cell (See Figure 2.5) has a pathlength to surface area ratio of 60 m^{-1}, which apparently makes it more suitable for trace gas analysis than the 32 mm diameter Axiom cell (pathlength to surface area ratio = 10 m^{-1}), shown in figure 2.6. The 8 mm diameter Axiom cell has a pathlength to surface area ratio equal to 40 m^{-1}. The pathlength to surface area ratio is, however, only one factor in the determination of a cell usefulness.

The multi-pass cell design has a significant drawback for use in applications involving in-line monitoring of gases. The gas flow enters and exits the relatively large cell volume through small orifices ,thus it takes several cell volumes of gas flow to remove a reasonable amount of a given gas sample from the cell. The gas flow volume required is termed the exchange volume. An ideal cell will have a low exchange volume. In contrast to the White cell, the nearly laminar flow in the Axiom results in a complete exchange of the gas sample when the flow volume approaches the cell volume. Figure 5.6 shows that when a relative small amount of acetone is injected to a 10 m White cell (volume = 1.75 L) compared to a 4m Axiom cell (volume = 3.2 L) the residence time of the acetone in the cell is longer in the White cell than in the Axiom cell. Furthermore, the White cell available for this research could not be heated nor dried lower than about 150 ppb as explained in section 4.1. Hence, the Axiom cell was selected for incorporation into a prototype of a trace water determination instrument. A White cell with considerably improved design is now available from CIC Photonics (see section 7.2.4).[4]

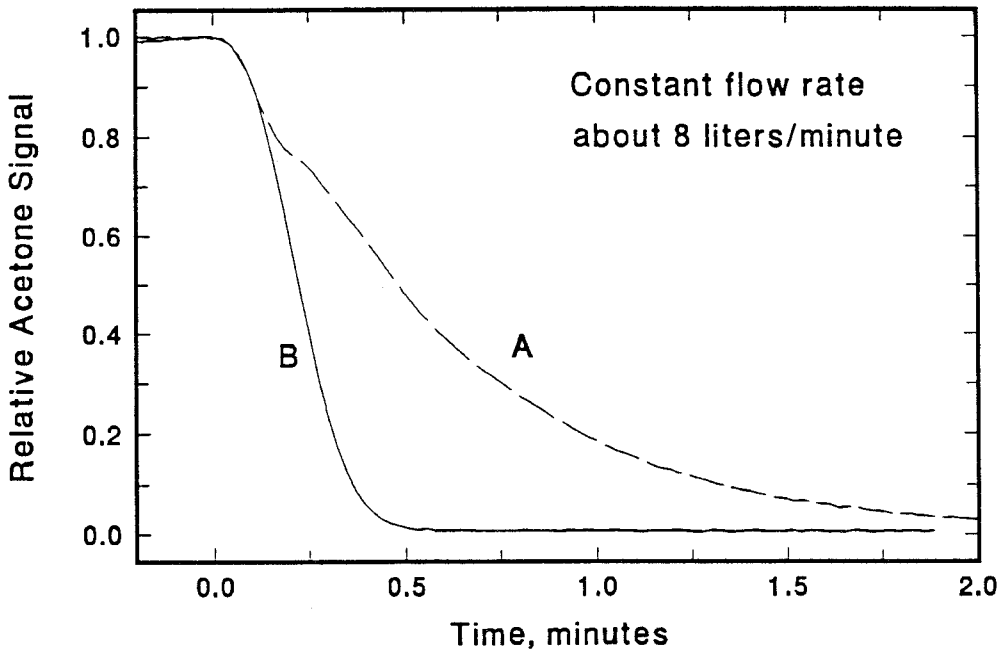

Figure 5.6 Plot of the relative acetone signal level vs. time for A) 10 m White cell and B) 4m Axiom cell. It can be seen that the time to decrease the acetone signal to zero is longer in the White cell than in the Axiom cell.

A SNR calculation as a function of the length of the cell can be performed to determine the optimum pathlength. The optimum SNR using the DTGS and InSb detectors for the background and cell H_2O concentration determination occurs at a gas cell length of 14.5 m.[5] That value is dependent on the noise levels in the DTGS and InSb detector, and on the transmission of the Axiom cell. The analysis assumes only signal-independent detector noise, small absorbances, and a univariate concentration estimate at the 3744.6 cm^{-1} H_2O absorption. However, the

ultimate FTIR system will be based on an evacuable and/or purged dual-beam FTIR system with one detector. The optimum pathlength in this single detector system will be different from that found to be optimum in the two detector system.

Optimization of the pathlength depends on the tradeoff between two factors, increase in absorbance and loss of light, as the pathlength increases. The signal or absorbance, S, is proportional to the cell length, L, and the noise, N, is dependent on only the InSb detector noise, σ_{InSb}, as shown in equation 5.1.

$$N \propto \sigma_{InSb}[I_B^{-2} + I_S^{-2}]^{1/2} \quad .....(5.1)$$

where I_B and I_S are the background and sample cell intensities that reach the detector, respectively. I_B and I_S are dependent on the initial intensity coming from the spectrometer source, I_i ,and any loss of light due to the transmittance of the gas cell. Two cases are now considered; first in a single channel evacuable FTIR system, the background and sample intensities are equal to $I_i T_o^{Lc/Lo}$, where L_c is the length of the gas cell, and T_o is the transmittance of the gas cell per unit length L_o. In a dual beam FTIR system the reference channel bypasses the gas cell so that the background intensity is equal to I_i. By applying equation 5.1 to both cases we obtain the following SNR proportionalities as shown in table 5.1.

Table 5.1 SNR proportionalities for a single channel and dual channel FTIR system.

Case	SNR proportional to
I. $I_B = I_S = I_i T_o^{Lc/Lo}$	$2^{-1/2} L T_o^{Lc/Lo}$
II. $I_B = I_i$ $I_S = I_i T_o^{Lc/Lo}$	$L[1 + T_o^{-2Lc/Lo}]^{-1/2}$

Assuming a transmittance value of 0.85 and 0.32 per meter for the 32 mm and 8 mm diameter Axiom gas cell, respectively, and considering case II, the maximum SNR is obtained at a pathlength of about 6.8 m in the 32 mm diameter cell and 1 m in the 8 mm diameter cell. These results are shown in Figure 5.7. Table 5.2 summarizes the optimal pathlength and the relative value of the SNR for each cell and spectrometer configuration considered in this dissertation. It should be noted that even though the White cell has three times more SNR than the 32 mm diameter Axiom cell, the decision to use a folded single-path cell instead of a multiple-path was due to considerations of equilibration time discussed above. The 32 mm diameter Axiom cell has seven times more SNR than the 8 mm diameter cell. Experimental results with both cells will be discussed in Chapter 6.

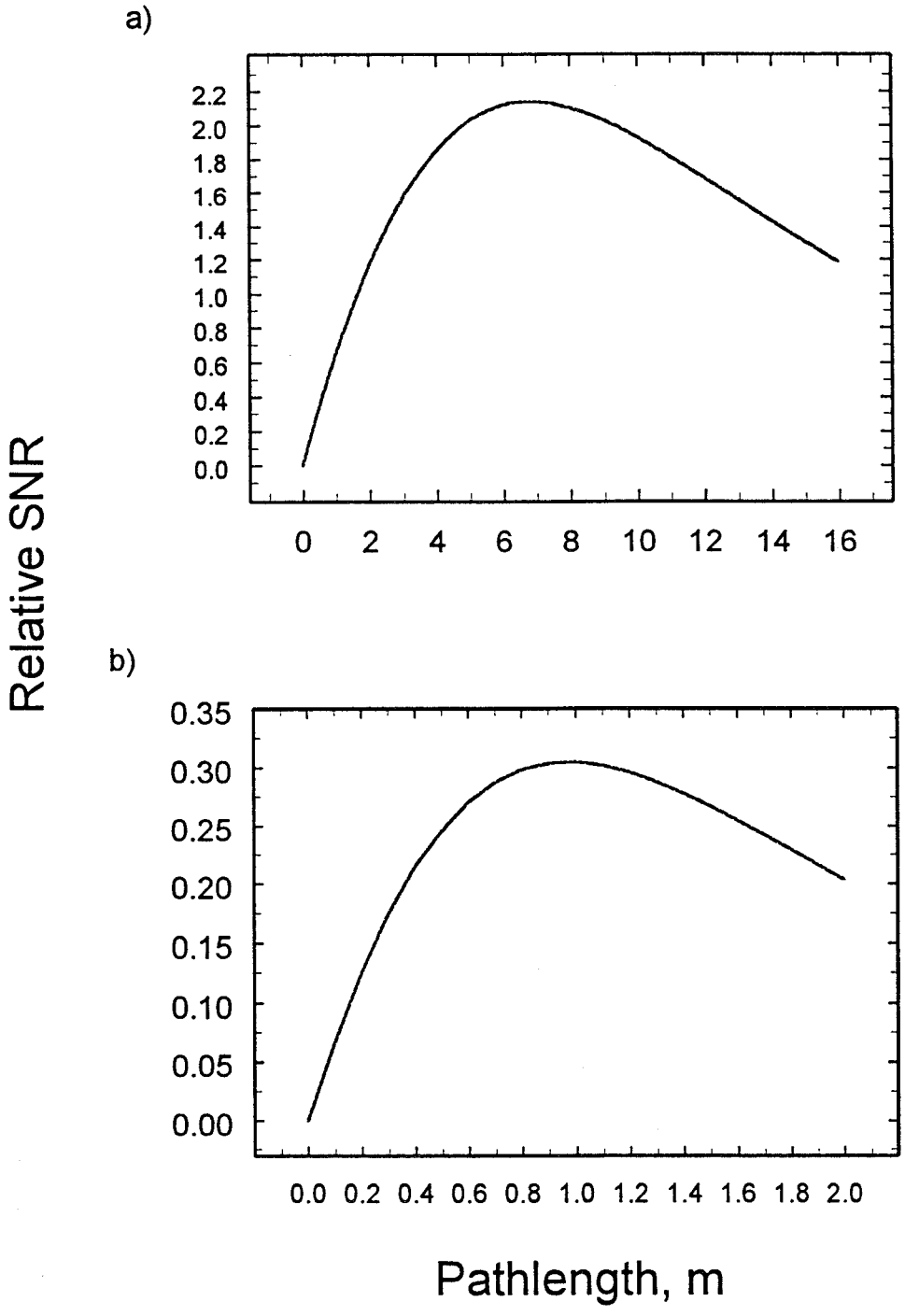

Figure 5.7 Plot of the relative SNR as a function of the Axiom cell pathlength according to case II in table 5.1. Plot a) is for T=0.85 (32 mm diameter cell, while plot b) is for T=0.32 (8 mm diameter cell).

Table 5.2 Optimal pathlength and relative SNR value for the three cell and spectrometer configuration considered in this dissertation.

Cell Type	T_o	L_o (m)	Case I Max. L(m) , rel. SNR	Case II Max. L(m) , rel. SNR
32 mm diam. Axiom cell	0.85	1	6.2 , 1.60	6.8 , 2.14
8 mm diam. Axiom cell	0.32	1	0.9 , 0.23	1 , 0.30
White cell	0.97	0.55	18 , 4.70	20.0 , 6.27

Even though a 14.5 m is the optimum length for maximum SNR using the Nicolet 800 two detector system,[5] a 32 mm diameter 8m pathlength Axiom cell was used in most of the optimization experiments. The time required to reach equilibrium with a new sample decreases significantly as surface area is decreased, hence shorter cells have been considered. Results with a 1m pathlength 8 mm diameter and 2 m 32 mm diameter Axiom cell will be discussed in chapter 6.

5.5 IMPROVEMENT OF CLS DATA ANALYSIS

When processing spectrochemical data the Classical Least Squares multivariate calibration method provides significant improvement in sensitivity when compared with univariate analysis, e.g., measurement of just one isolated peak height or area. The improvement derives from the use of multiple frequencies relating the reference spectrum to the sample spectrum. Haaland and Easterling showed improvements of factors of 5 to 7 when CLS was compared to univariate methods applied to gas phase analysis of CO, N_2O, and CO_2.[6] They also mathematically estimate the improvement in precision of the CLS method over the univariate method by comparing the standard deviation of the concentration estimates produced by the two methods using different baseline assumptions.[7]

The CLS concentration estimate that was used in this research across each H_2O absorption region is based on the following CLS model:

$$A_{si} = a + b\nu_i + kA_{ri} + e_{si} \quad .....(5.2)$$

where A_{si} and A_{ri} are the sample and reference absorbances at frequency i, respectively, k is the ratio of the sample to the reference concentrations, a and b are the offset and slope parameters used to model an assumed linear baseline in the sample absorption spectrum across each H_2O band, ν_i is the frequency at the ith point in the sample absorbance spectrum, and e_{si} is the absorbance error in the model. Note that the sample absorbance is related to the reference absorbance plus a linear baseline, with a,b, and k as the unknowns. To determine the least-squares estimates of k (since it is the only parameter containing concentration information), several assumptions about the spectral noise are made. It is assumed that the reference spectrum has no error, that the noise in the sample spectrum is uncorrelated, additive, zero-meaned, and normally distributed, and that the variance of the noise within the sample spectrum is a constant, σ_s^2. This last assumption is

true only in transmission spectra, but it is a good approximation for weak absorption spectra. Under these conditions the least squares estimates of k is obtained solving:[6]

$$\hat{k}_{CLS} = \frac{c_{11}c_{23} - c_{12}c_{13}}{c_{11}c_{22} - c_{12}^2} \quad .....(5.3)$$

where the various c_{ij}'s coefficients are combination sum of squares and cross products of spectral frequencies and absorbances over the n frequencies in the spectral region as follows:

$$c_{11} = \sum \nu_i^2 - (\sum \nu_i)^2 / n \quad .....(5.4)$$

$$c_{12} = \sum \nu_i A_{ri} - (\sum \nu_i)(\sum A_{ri}) / n \quad .....(5.5)$$

$$c_{13} = \sum \nu_i A_{si} - (\sum \nu_i)(\sum A_{si}) / n \quad .....(5.6)$$

$$c_{22} = \sum A_{ri}^2 - (\sum A_{ri})^2 / n \quad .....(5.7)$$

$$c_{23} = \sum A_{ri} A_{si} - (\sum A_{ri})(\sum A_{si}) / n \quad .....(5.8)$$

The variance of the CLS concentration estimate is:

$$Var(\hat{k})_{CLS} = \sigma_s^2 / c \quad .....(5.9)$$

where:

$$c = \frac{c_{11}c_{22} - c_{12}^2}{c_{11}} \quad .....(5.10)$$

The univariate concentration estimate can be calculated by taking the difference between the peak height of a chosen absorption peak and a nearby baseline in the sample spectrum, A_{sm}, relative to that of the same peak in the reference spectrum, A_{rm}. The concentration estimate in this case is:

$$\hat{k}_{uni} = \frac{A_{sm}}{A_{rm}} \quad .....(5.11)$$

The variance of the estimated k at a single frequency, is:

$$Var(\hat{k})_{Uni} = \sigma_s^2 / A_{rm}^2 \quad .....(5.12)$$

which is greater than $Var(\hat{k}_{CLS})$ since the denominator consists of the absorbance at only one isolated frequency. The improvement in precision of the CLS estimate relative to the conventional univariate analysis is obtained by taking the square root of the ratio of the variances in equations 5.12 and 5.9.

$$\sqrt{\frac{Var(\hat{k}_{Uni})}{Var(\hat{k}_{CLS})}} = \sqrt{\frac{c}{A_{rm}^2}} \quad .....(5.13)$$

In order to experimentally determine the improvement in precision of CLS analysis over univariate analysis, 40 consecutive spectral measurements collected using fixed time and aperture and a series of resolutions of a slowly varying sample of H_2O in N_2 were analyzed. The data collected at each resolution are similar to those in Figure 4.12. The goal is to determine the increase in SNR of the CLS method relative to univariate analysis. The SNR is calculated by taking the inverse of the standard error of estimates, SEE of the 40 consecutive spectra assuming a fixed signal level (constant concentration of water). Plots such as the one shown in Figure 4.5 give us a confirmation that we are measuring the noise level at each

resolution with proper cancellation of the H_2O absorption bands. The interferograms were processed using the boxcar apodization, no zero-filling, and spectral region 3788 to 3910 cm^{-1} without peak selection for the CLS analysis. The univariate results were obtained using an analogous calculation of the SEE of 40 repeated measurements but only at the 3837.87 cm^{-1} absorption band. Figure 5.8 confirms the increase in the SNR of the CLS method over the univariate analysis for a series of resolutions, where the improvement is 2-5 times depending of the resolution chosen.

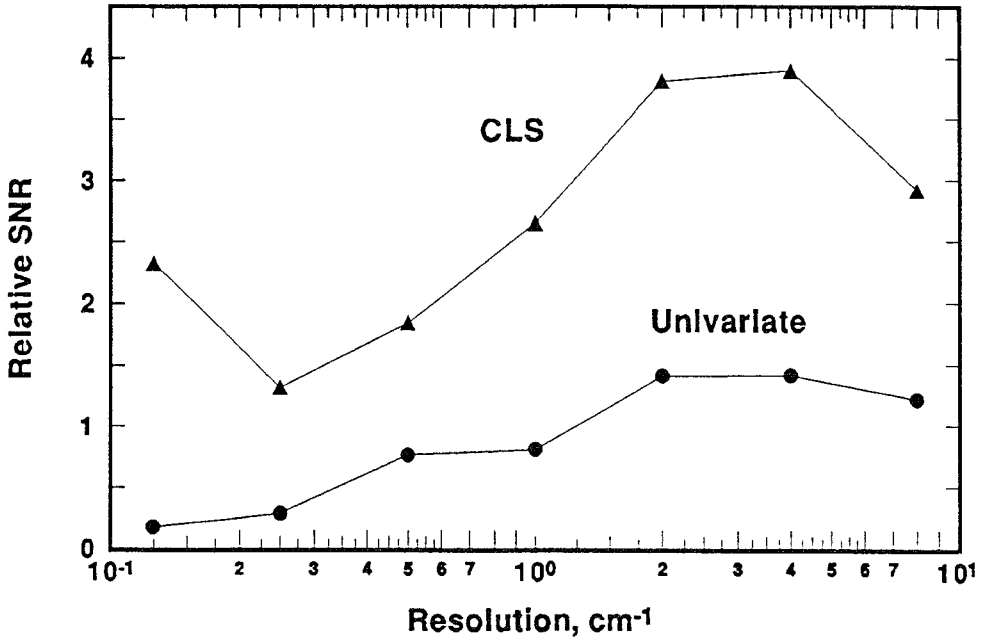

Figure 5.8 Experimental results for a fixed scan time showing the relative SNR of the CLS and univariate calculations as a function of spectral resolution.

5.6 SPECTRAL RESOLUTION

It was initially thought that high resolution should be used in the analysis to fully resolve the narrow gas phase H_2O spectral lines. However it was noted in section 1.2 that SNR is directly proportional to resolution, so that high resolution spectra are noisier than low resolution spectra. Another consideration is the detection of interfering species. Interference can be detected and avoided by the use of high resolution. The best situation is to identify the lowest resolution that still retains the required information, because this resolution will produce the highest SNR in a given measurement time. The experimental result in Figure 5.8 showed the dependence of SNR on resolution at fixed collection time and fixed aperture, which is small enough to be compatible with high resolution spectra. Maximizing the instrument throughput for each resolution further favors broad resolution measurements. Despite the 0.2 cm^{-1} H_2O line width, resolutions as low as 2 or 4 cm^{-1} produce spectra that give good analytical results. This is a significant result because a low-resolution spectrometer which is potentially smaller, more robust,

and cheaper, can be used with no sacrifice in performance. Figure 5.9 shows H_2O spectra measured with varying resolution. A resolution of 4 cm^{-1} does not allow us to clearly differentiate the peaks selected by the CLS routine and therefore does not allow us to recognize spectral interference. Thus, we have chosen to focus our work on resolution of 1 and 2 cm^{-1}, values that represent good compromise between instrumental complexity and the ability to recognize interferences.

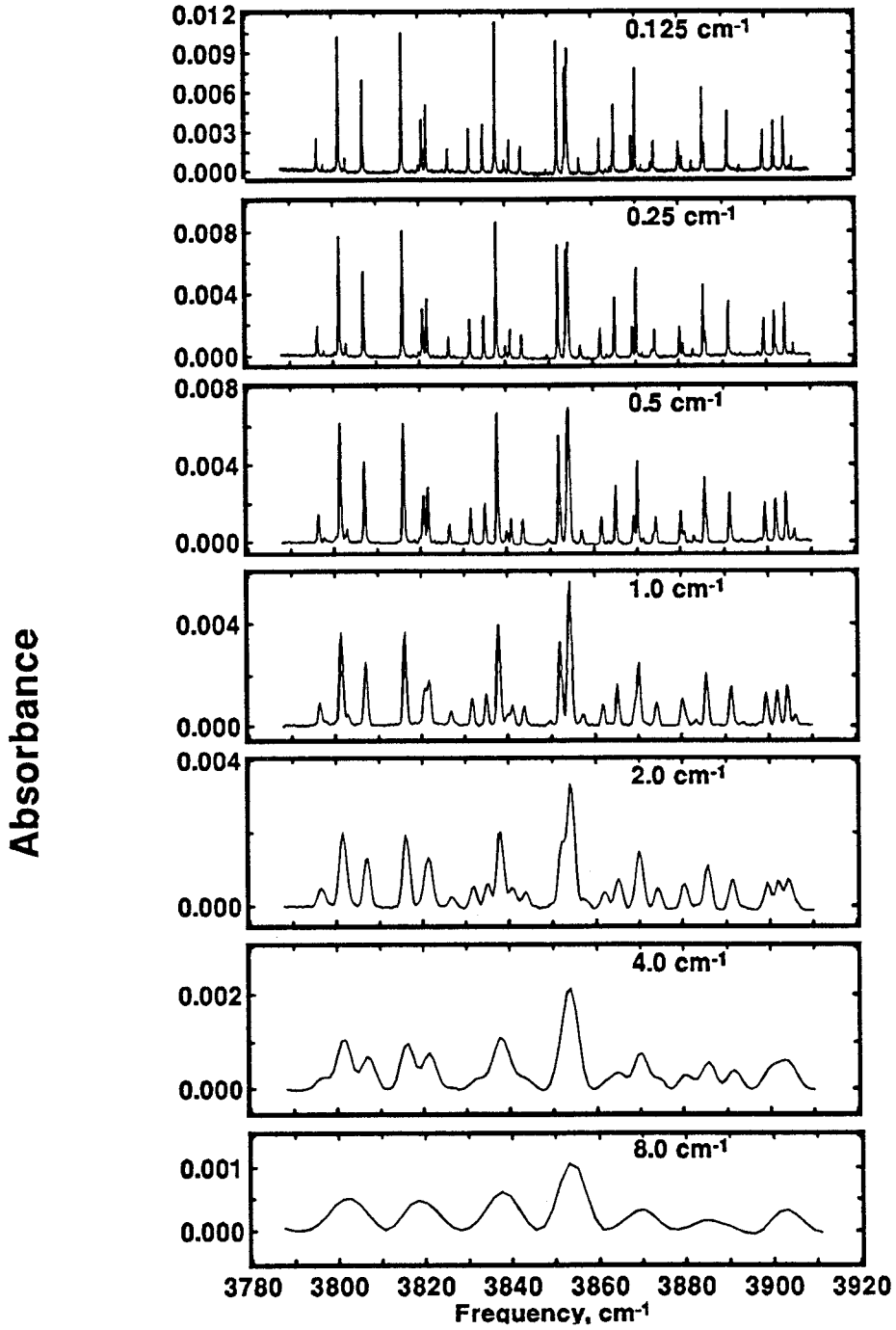

Figure 5.9 A series of H_2O absorption spectra at different spectral resolution.

5.7 REFERENCES

1. H. Levinstein, Anal Chem., 41, 81A (1969).
2. Staff report, "Optical Detectors across the Spectrum," Lasers and Optronics, p.19, Sep. 1992.
3. P. B. Rousch, and B. J. McGrattan, Amer. Labor., 21(12), p. 33 (1989).
4. The Ranger, CIC Photonics, Inc., 2715-D Broadbent Parkway N.E., Albuquerque, NM 87107.
5. B. R. Stallard, R. K. Rowe, L. H. Espinoza, M. J. Garcia, T. M. Niemczyk, and D. M. Haaland: "Trace Water Vapor Determination in Corrosive Gases by Infrared Spectroscopy", Report SAND 93-4026, Sandia National Laboratories, Albuquerque, NM, 1993.
6. D. M. Haaland and R. G. Easterling, Appl. Spectrosc., 34, 539 (1980).
7. D. M. Haaland and R. G. Easterling, Appl. Spectrosc., 36, 665 (1982).

CHAPTER 6

PROTOTYPE DEVELOPMENT

6.1 ENHANCED FTIR INSTRUMENT

The results obtained with the Nicolet 800 FTIR system presented in chapter 4 show that it is possible to determine low ppb levels of water vapor in gaseous samples using FTIR spectroscopy and classical least squares multivariate data analysis. A number of design improvements have been discussed in chapter 5 that should be incorporated into an optimized FTIR spectrometer for trace water determination in corrosive gases. Not only the choice of pathlength and collection time dictate the detection limits, other parameters such as beam path design, cell equilibration time, and spectral resolution must be also considered.

Two beam path designs, an evacuable single beam and purged dual-beam systems, were discussed in section 5.1. The most significant difference between the proposed enhanced purged dual-beam FTIR system and its predecessor (Nicolet 800) is the use of a single InSb detector, which greatly improves the SNR. This dual-beam design allows the measurement of the background H_2O and the sample H_2O. It was calculated from table 4.4 that the 2 σ detection limits for the determination of H_2O in N_2, HCl, and HBr, using only the InSb detector, are about 7, 17, and 10 ppb, respectively. However, the use of a 8 m pathlength and a 10 minute collection time makes this determination impractical for field use. Significant improvement in the SNR (by an order in magnitude) could be obtained with the use of an optical band-pass filter that limits the light incident on the detector to only the frequencies of interest. This fact allows the use of a shorter cell and less collection time that give up some sensitivity in order to perform more practical measurements. Table 6.1 shows a summary of improvement changes and trade offs that can be obtained in the prototype FTIR system.

Table 6.1 Summary of improvement changes in SNR and trade offs expected in the prototype FTIR system.

Improvement	Change in SNR	Comments
Dual Beam, InSb detector	1 x	allows H_2O background measurement
Optical band-pass filter	10 x	limits frequencies of interest
Low resolution	1 x	reduces FTIR cost
Compact, well sealed FTIR	1 x	decreases purged time
1 minute collection time	$1/\sqrt{10}$ x	fast collection time
2 m pathlength	1/4 x	fast equilibration time
Total Change SNR	0.8 x	

The data in table 6.1 show that even using a short absorption path and fast measurement time, low ppb detection limits can be achieved. Results with a purged system accessory connected to the Nicolet 800 spectrometer will be first presented. An evacuable FTIR system from Midac Corporation was also tested. The ultimate FTIR system will be a compact, well-sealed spectrometer but, alternatively, an accessory for existing FTIR spectrometers can be made available.

6.2 DUAL BEAM ACCESSORY PROTOTYPE

A dual beam prototype accessory for the infrared determination of trace H_2O levels in corrosive gases has been built in collaboration with Axiom Analytical. A detailed schematic is shown in Figure 6.1. The accessory consists of two beam paths, that are alternatively selected by two 2" movable plane gold mirrors, and a single-pass folded Axiom gas cell similar as the one shown in Figure 2.6. The accessory was attached to the Nicolet 800 FTIR using Axiom tubing as shown in Figure 6.2. Two different gas cells with different diameters and length tubing were tested to determine the best configuration. In this case "best" is a trade off between fast equilibration response at different H_2O concentrations and low detection limits.

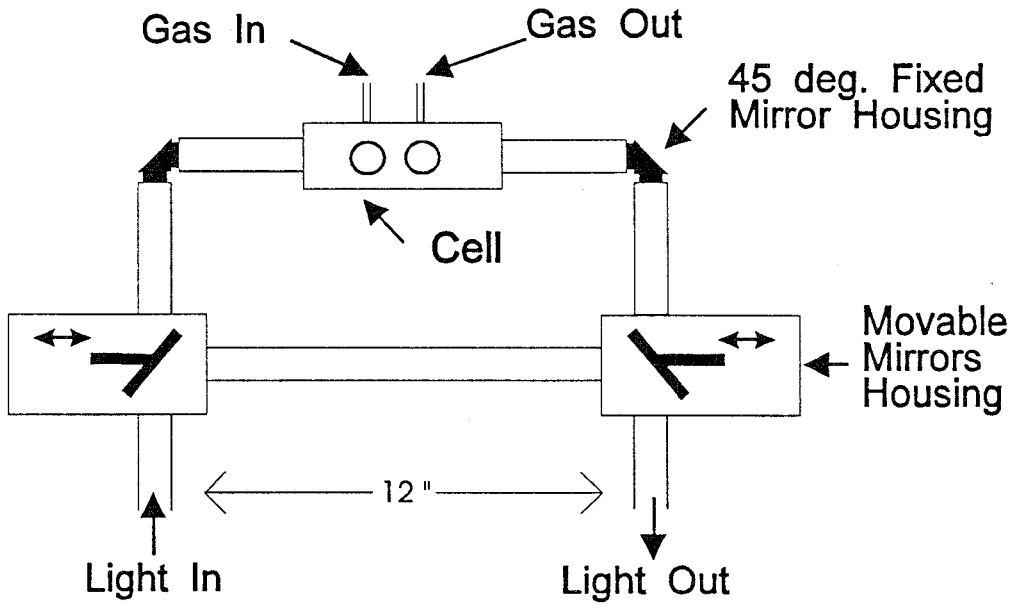

Figure 6.1 Schematic of the dual-beam accessory. Note the two movable mirrors to select whether the reference or cell channel.

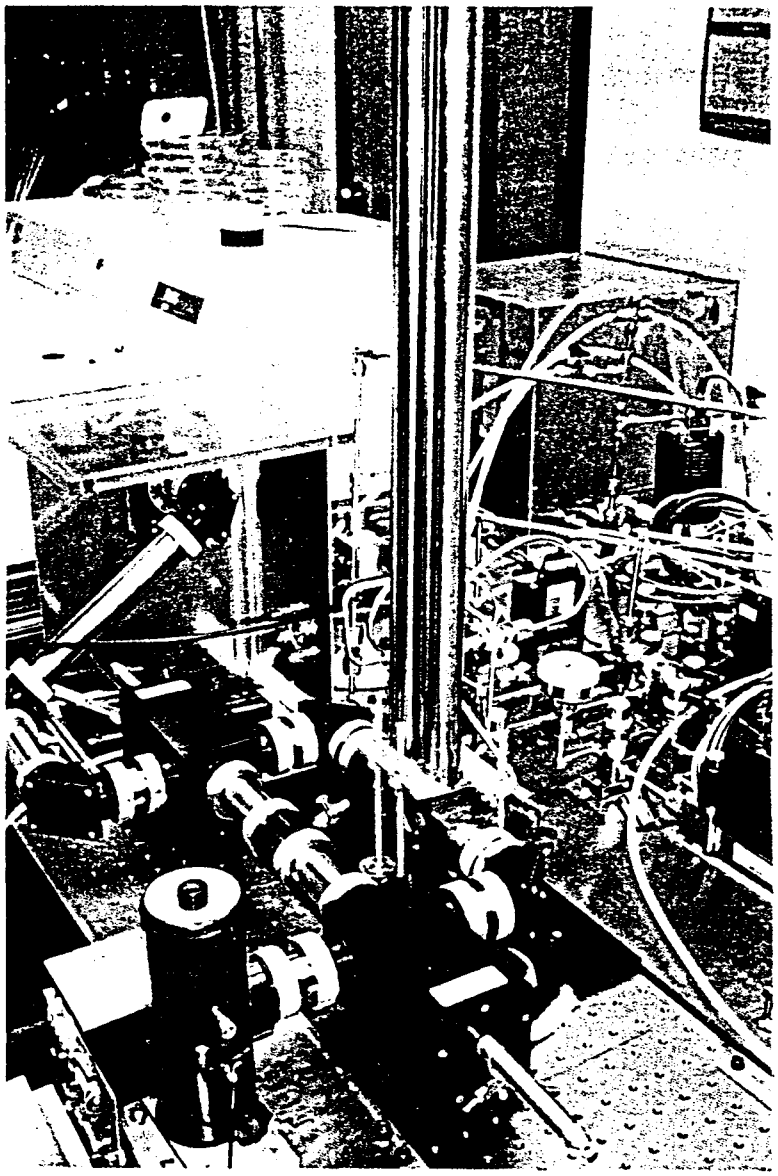

Figure 6.2 Photo of a 32 mm diameter, 2 m Axiom cell.

The optimum pathlength for maximum SNR was discussed in section 5.4. For an 8 mm diameter Axiom gas cell the optimal pathlength under case II is 1 m (see Table 5.2). The cell is shown in Figure 6.3. Even though a 6.8 m length gives maximum SNR for a 32 mm diameter Axiom cell, a 2 m cell was used as showed in Figure 6.2. Both cells give up some sensitivity in favor of coming to equilibrium rapidly. The loss in sensitivity is recovered by incorporating an optical band-pass filter into the optical system that limits the spectral range to the 3600-3910 cm^{-1} H_2O frequency range and improves the SNR.

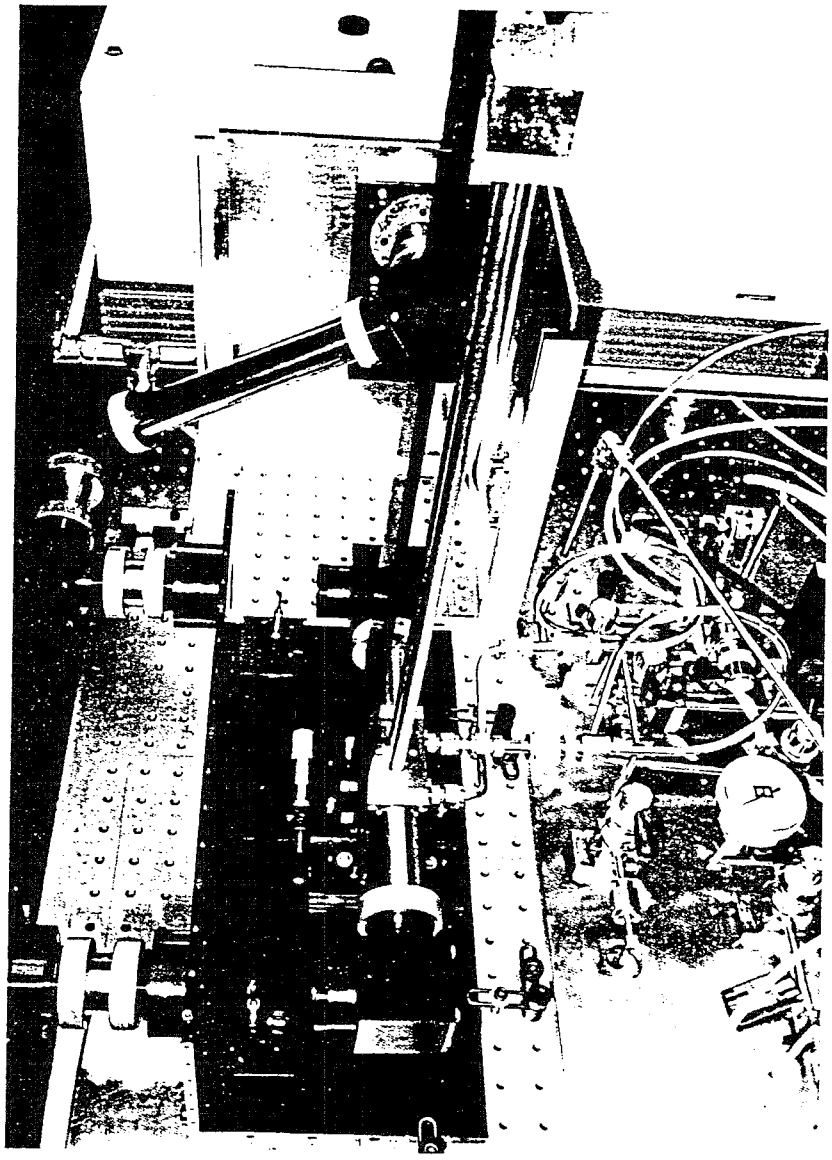

Figure 6.3 Photo of a 8 mm diameter, 1 m Axiom cell.

It was noted in chapter 4 that the InSb detector saturates at relatively low light levels. Experiments carried out without the optical band-pass filter, but using an 8 m cell, avoided the saturation problem due to the low transmittance (about 5 %) of the 8 m cell. The use of a band-pass filter in a smaller cell (8 or 32 mm diameter) with a higher transmittance than the 8m cell, avoids the InSb saturation problem.

An experiment was performed in order to test the linearity of the response of the InSb detector using the dual beam accessory and the optical filter with the light source from the Nicolet 800 spectrometer. The light was attenuated by using

blocking screens and maintaining the InSb preamplifier at its minimum value. Figure 6.4 shows the response of the InSb detector (peak-to-peak voltage in the interferogram signal) to varying light intensity reaching the detector with no cell. It can be seen that the InSb detector does not saturate under these conditions.

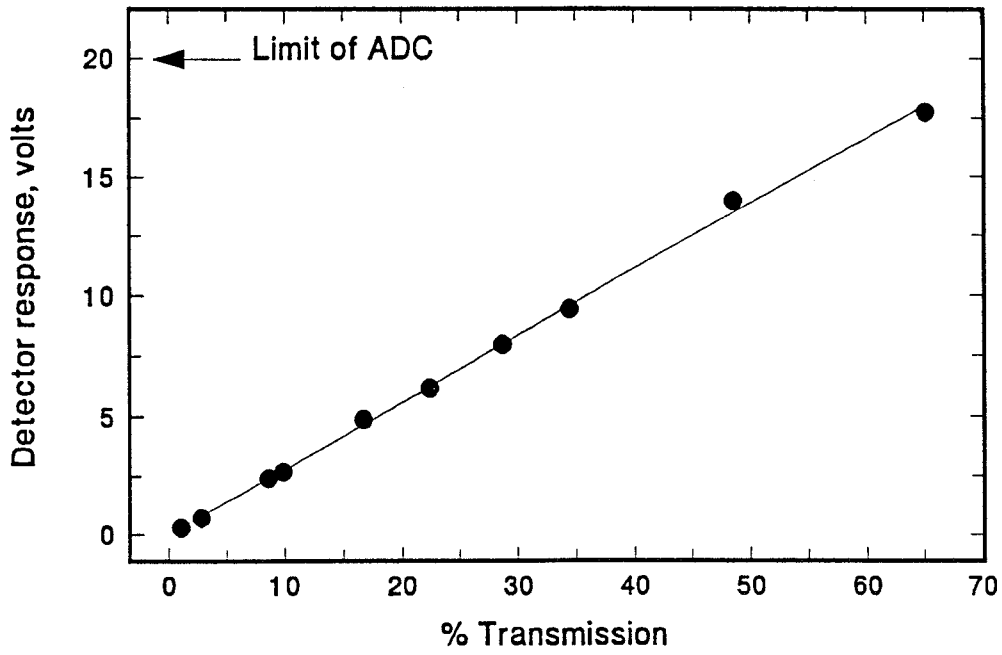

Figure 6.4 InSb detector linearity

6.2.1 H_2O Calibration

A H_2O calibration in N_2 was performed using the Nicolet 800 FTIR spectrometer attached to the dual beam accessory with a 32 mm diameter, 2m Axiom cell. Purging the enclosed spectrometer for about two weeks was still necessary to bring down the background H_2O level to less than 1 ppm. Figure 6.5 shows the calibration curve of the H_2O concentration determined spectroscopically using CLS data analysis as described earlier, versus the H_2O concentration measured by the reference method (permeation tube). Each point in the calibration curve is the total H_2O concentration measured in the sample path minus the background H_2O measured in the reference path. There was a slight difference in the cell and reference pathlengths. It is possible to design an instrument where both paths are identical in length so that the absorption spectrum of H_2O in the gas cell may be derived from the ratio of the sample and reference spectra.

The data in Figure 6.5 were collected using one minute scanning time at 2 cm^{-1} spectral resolution in the sample channel, and then the moving mirrors were switched to the reference channel for another one minute collection. It was observed experimentally that the drift using a one minute collection time is about 1 ppb after conditioning the cell, thus the error due to the background drift is negligible. The inverse of the slope of the linear fit in the calibration curve is about 532 ppb/arbitrary CLS unit, that converted to a 8m cell gives 133 ppb/ arbitrary CLS unit, which is a 20 % over the values found in section 4.2. Those calibration results

may differ partly because of a few percent error in the pathlengths, and highly due to the reliability of the reference methods (see section 4.2.1). However, the time required to equilibrate the system using the 2m cell is considerably less than that required when using the 8 m cell. Each calibration point could be performed at about 0.5-2 hour with the usual procedure of heating and purging the cell and letting the cell equilibrate to measure a specific H_2O concentration.

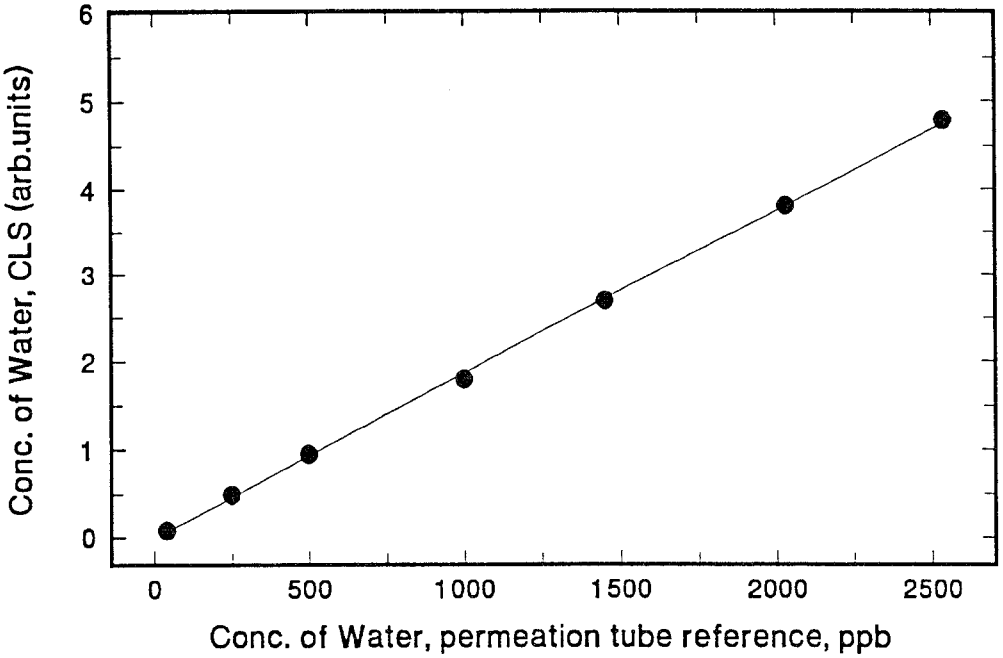

Figure 6.5 Measured H_2O concentration in N_2 vs. the reference values from the permeation tube (2 m Axiom cell). The solid line is a linear regression.

6.2.2 Detection Limits

To determine the detection limits using the dual beam accessory with the 32 mm diameter 2m cell, 54 consecutive spectra were sequentially collected using the band-pass filter at a low constant level of H_2O concentration in N_2. One minute spectral collections were used. The experimental data showing the precision of this determination is presented in Figure 6.6. The solid line is a second order polynomial fit to account for the small drift in the H_2O determination. The SEE is reported to be 6.1 ppb using the reference channel data and 6.4 ppb using the cell channel data. Pooling both results the estimated two sigma detection limit is $2\sqrt{(6.1)^2+(6.4)^2}=18$ ppb. Repeating the same experiment but now not using the optical band-pass filter the SEE is reported to be about 25 ppb using the reference channel and 31 ppb using the cell channel. Thus, a factor of 4-5 times improvement in precision is achieved by using the optical band-pass filter. Note that the use of an optical filter avoids saturating the InSb detector but the light intensity could not be increased to see the theoretical ten times improvement in SNR. Obviously the detection limits could be reduced to 10 ppb using a longer collection time. The same experiment using the 8 mm diameter 1m cell, with the optical band-pass filter was carried out. A 126 ppb detection limit was achieved. The higher detection limit

is caused by less transmittance and less pathlength of the cell as expected by the SNR values in table 5.2.

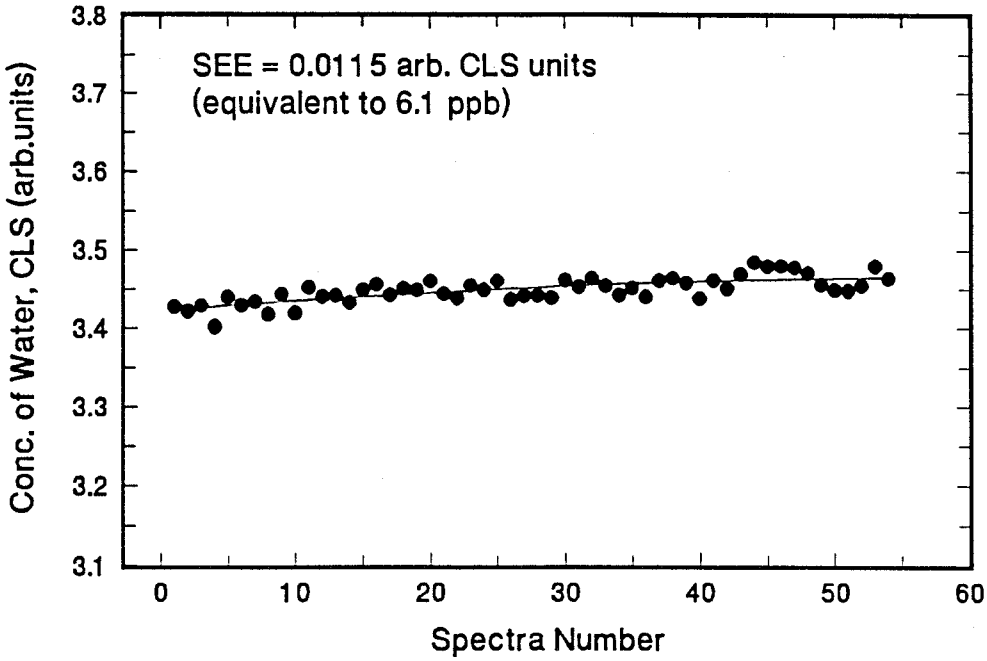

Figure 6.6 Experimental data showing the precision of the measurement of the background H_2O plus cell concentration ion N_2 using an optical filter, 2 m Axiom cell, InSb detector and one minute collection time.

6.3 EVACUABLE MIDAC FTIR SPECTROMETER

P. B. Henderson and S. Werschke tested an evacuable FTIR system (Midac Corporation) and demonstrated a detection limit of less than 10 ppb in HCl and other gases.[1] The spectrometer features a sealed optical bench that can be evacuable to about 10^{-6} torr. By evacuating the spectrometer to 1 x 10^{-6} torr less than 1 ppb of H_2O is present in the background, as it was calculated in section 5.1.1. The system included also a sensitive InSb detector with an optical band-pass filter, and a linear-flow 4 m Axiom gas cell.

We have also tested the Midac evacuable FTIR system in our facility. We were able to obtain pressures of about 5 x 10^{-6} torr in about 48 hours of pumping with an 80 liter/minute mechanically-backed turbo pump. Pressures of about 1 x 10^{-6} torr are obtained after 3-4 days of pumping.

An H_2O calibration in N_2 was performed using the Midac FTIR spectrometer attached to a 32 mm diameter, 4m Axiom gas cell as shown in Figure 6.7. Figure 6.8 shows the calibration curve of the H_2O concentration, determined spectroscopically using the CLS data analysis as described earlier, versus the H_2O concentration measured by the reference method, the permeation tube. Each calibration point on the curve was calculated from the standard H_2O concentration of 1942 ppb (See Figure 6.9). This concentration was determined using the permeation tube. When using the vacuum spectrometer the contribution to the

water spectral features due to the background H_2O are considered negligible since the spectrometer pressure was maintained below 5 x 10^{-5} torr.

Consecutive spectra were collected using 2 cm^{-1} resolution and one minute collection time to determine the detection limits. No optical band-pass filter was used in this measurement. A graph similar to that in Figure 6.6 yielded an estimated SEE value of 46 ppb. However, here was some evidence of misalignment in the Midac spectrometer which might have occurred during shipping. The misalignment could not be corrected due to the ruggedness of the system. However, by using an optical band-pass filter and proper spectrometer alignment an improvement in SNR and therefore low ppb detection limit is expected.

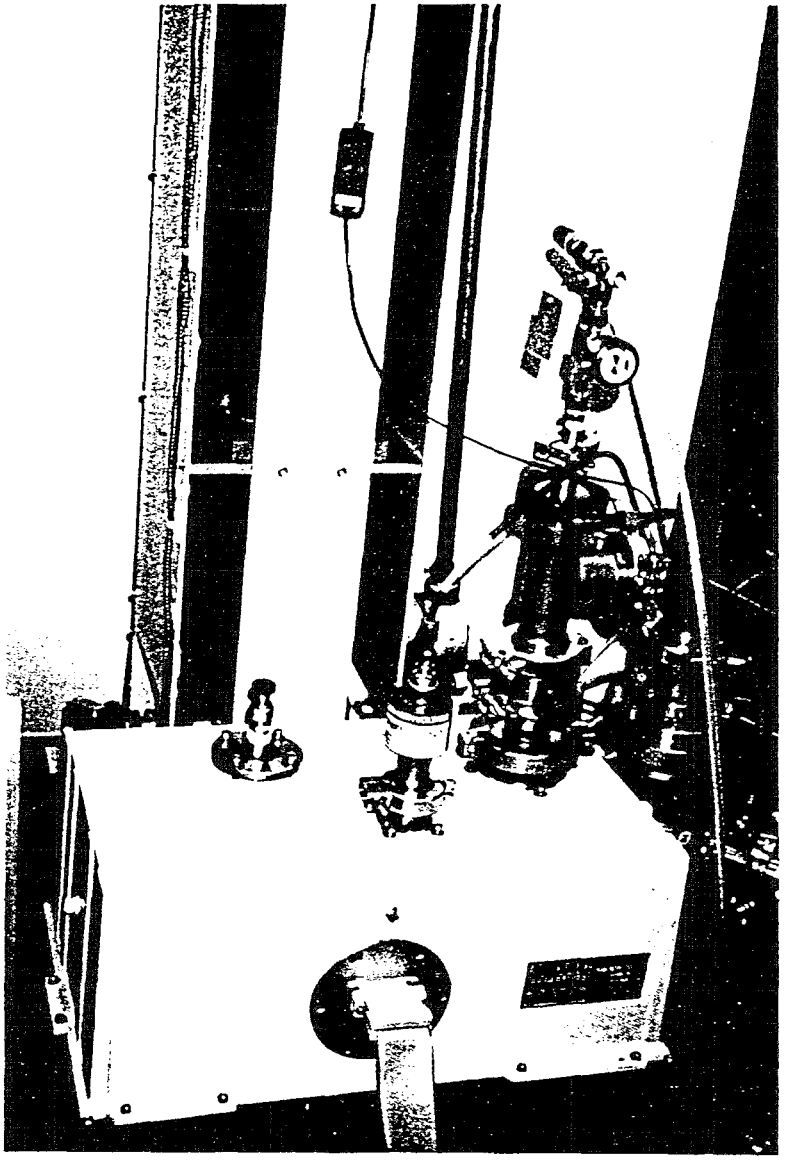

Figure 6.7 Photo of the evacuable Midac FTIR spectrometer.

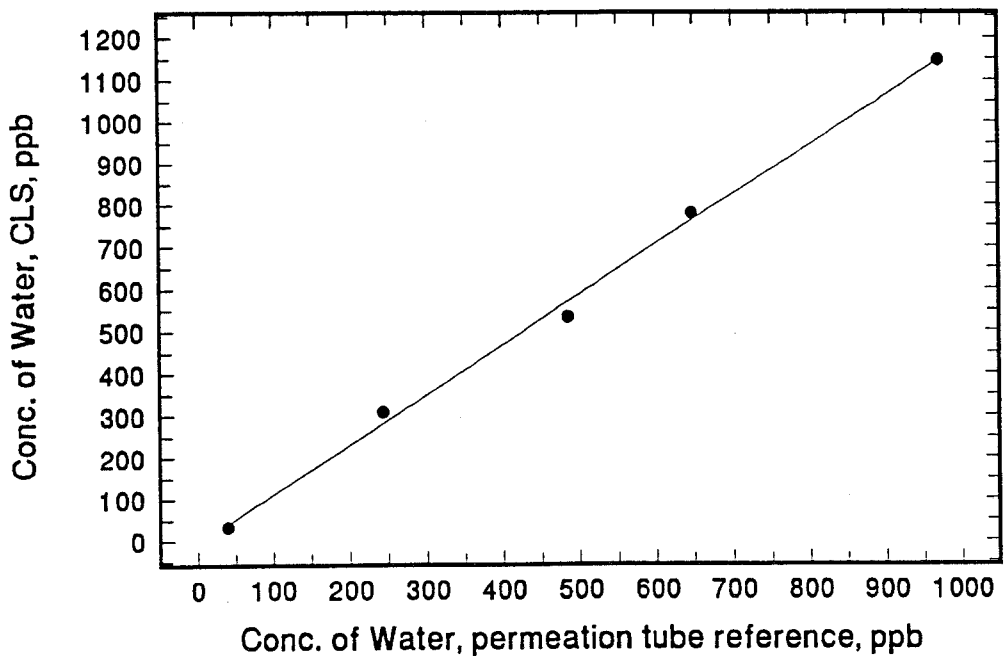

Figure 6.8 Measured H_2O concentration in N_2 vs. the reference values from the permeation tube. Data were collected using a 4 m pathlength Axiom cell and an evacuable Midac spectrometer. The solid line is a linear regression.

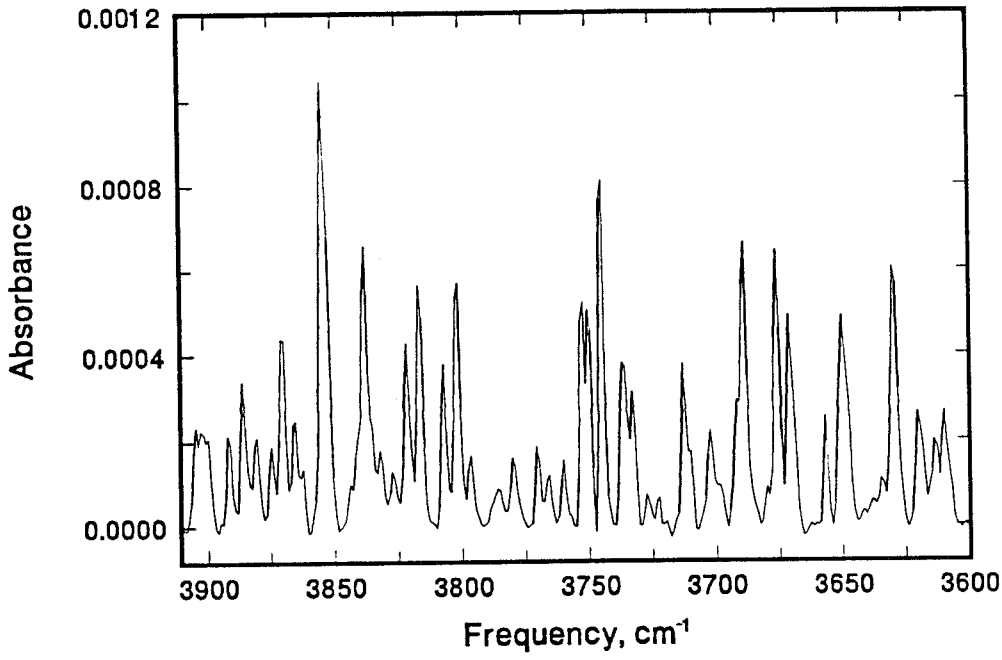

Figure 6.9 Spectrum of 1942 ppb of water vapor. The spectrum was collected at 2 cm^{-1} spectral resolution with the evacuable Midac spectrometer.

6.4 DUAL-BEAM OR EVACUABLE FTIR SYSTEM

Both FTIR system configurations, purged or evacuated, use an optical band-pass filter to limit the light intensity to the H_2O frequency of interest. An experiment was performed with the Midac FTIR optical bench without any attached gas cell . The goal was to compared the noise level or SNR, of the Midac system with and without the optical filter. In both cases, with and without the filter, the detector preamplifier was adjusted so as to take advantage of the ADC range, but avoids saturation. Consecutive 1 minute scans were recorded at 2 cm^{-1} resolution with and without the filter to determine the RMS noise level of the Midac FTIR system. The RMS noise, shown in table 6.2, was determined by examining a 100% line plot. To assure proper cancellation of the H_2O bands, the experiment was performed at a low and stable concentration of H_2O in N_2, so that if the data in Table 6.2 were plotted, the RMS noise of the 100% lines would show the expected dependence of $(\#\ time)^{-1/2}$ similar to that shown in Figure 4.5. From the data in table 6.2 it can be concluded that the improvement in SNR achieved by using the optical filter is a factor of 5 as it was seen with the 2 m cell attached to the Nicolet FTIR.. This improvement in SNR by using the optical filter was confirmed by estimating the precision of 54 consecutive one minute 2 cm^{-1} resolution scans. The SEE of the data using no filter is about 40 ppb compared with about 9 ppb using the filter. It must be noted that the specific improvement by using the optical filter depends on the available light intensity in the spectrometer. Ideally a ten times improvement is reachable if the intensity of the light could be increased by an order of magnitude without saturating the InSb detector.

Table 6.2 RMS noise measured without and with the optical filter using the Midac FTIR spectrometer.

Scanning Time (Minutes)	RMS Noise No Filter, x 10^{-5}	RMS Noise With Filter, x 10^{-5}
1	13.56	2.74
2	9.95	2.11
3	8.15	1.71
4	7.46	1.53
5	6.76	1.34
6	6.09	1.18
7	5.18	1.04
8	5.12	0.96
9	4.75	0.98
10	--	0.95

Reducing the background H_2O to a low and stable concentration is the key issue in a purged system. To measure low ppb levels of H_2O vapor in the gas cell is difficult especially when the background H_2O is 10-100 times the H_2O concentration in the gas cell. A small, rugged, sealed spectrometer, such as the Midac, has less

internal volume, less internal surface area, and far less "leaks" to the ambient atmosphere than does a spectrometer such as the Nicolet 800. Thus, purging the Midac should be more efficient than purging the Nicolet. As with the Nicolet we purged the Midac with dried N_2 that was passed through a molecular sieve dryer to provide a N_2 flow with about 100 ppb of H_2O. Figure 6.10 shows the drydown curve, i.e., the H_2O background concentration versus time, for the Midac spectrometer. The spectrum of about 2 ppm of H_2O, shown in Figure 6.9, was used as the standard. It can be seen that only 24 hours are required to achieve a relatively stable background H_2O level of less than 1 ppm. This value compares to Figure 2.4, where 2 weeks were required to obtain the same background H_2O concentration level using the Nicolet 800 system.

Both FTIR system configurations, purged or evacuated, have been shown to be capable of determining H_2O vapor with a precision of about 10-20 ppb when using an optical band-pass filter, classical least squares multivariate calibration, and 1 minute collection time. This statement is based on our characterization of the purged system, and the work of Henderson and Werschke using an evacuable system. We believe that the ultimate user will decide which configuration is more suitable for his application. Nevertheless, there are similarities, advantages and disadvantages of both configurations

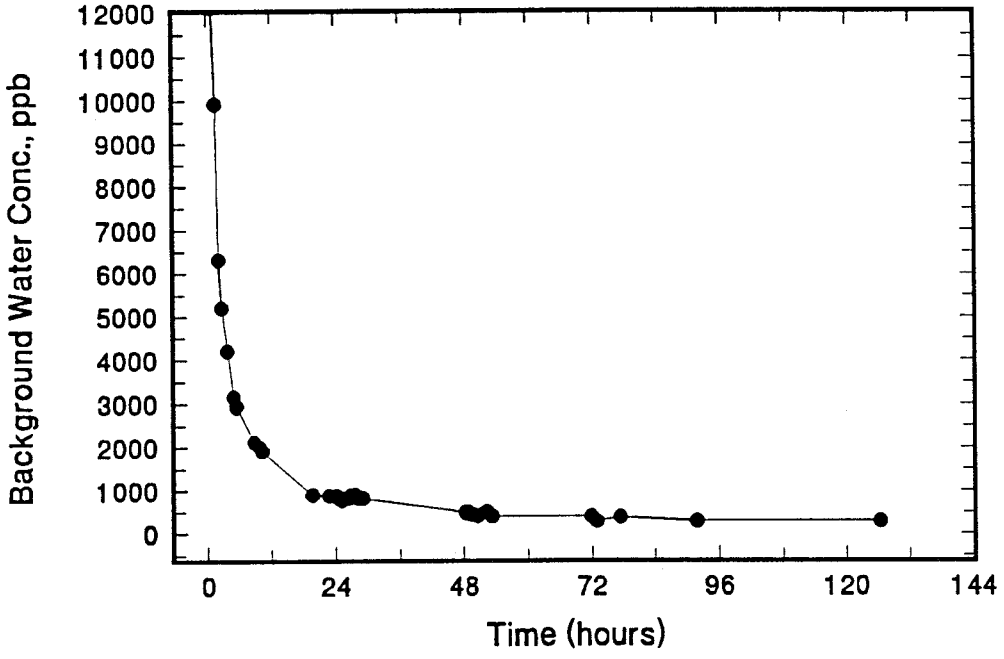

Figure 6.10 Drydown characteristics of the Midac spectrometer.

The main advantage of the evacuable FTIR system is that the background water level is reduced to a negligible level, hence the water level in the sample is the result of a single measurement. The disadvantages of using an evacuable system involve maintaining and monitoring the vacuum. Furthermore, small leaks may establish gradients of water vapor concentration throughout the instrument that

are not adequately monitored by a pressure gauge near the pump. Finally, the cost of a vacuum system will be higher than a purged system since it adds complexity to the system.

6.5 CONCLUSIONS

A FTIR prototype accessory system has been built and tested for the infrared determination of trace levels of H_2O vapor in corrosive gases. The detection limit of the system is about 20 ppb using CLS data analysis, 1 minute collection time, and an optical band-pass filter. The accessory consists of a dual beam path design with movable mirrors. The cell is a single folded path, 2m pathlength, linear flow cell manufactured by Axiom Analytical. The advantage offered by this shorter cell is that it is easier to dry out and stabilize. However, if improved sensitivity is necessary either or both the length of the gas cell or the collection time can be increased. Longer data collections increase the measurement time. Longer cells require more time to reach equilibrium. Thus, increased sensitivity comes with a price.

A complete FTIR system is also currently available from Midac Corporation. The system consists of an evacuable and/or dual-beam bench with a 4 m Axiom gas cell and comes equipped with the software necessary to perform an auto background correction (chapter 3) and CLS data analysis. The user will ultimately decide which system is more suitable for his/her application. We propose, when the cost is justified, that the ultimate instrument should have both the capabilities to operate using dual-beam and at vacuum. Such a system offers the flexibility to choose the operating mode on site, or change as experimental conditions dictate.

6.6 REFERENCES

1. P. B. Henderson and S. Werschke, "An optimized FTIR spectrometer for the determination of moisture in corrosive gases," 1996 Pittsburgh Conference, paper No. 308, Chicago, IL (1996).

Intentionally Left Blank

CHAPTER 7

RESEARCH SUMMARY AND FUTURE STUDIES

7.1 RESEARCH SUMMARY

FTIR spectroscopy combined with Classical Least Squares multivariate calibration has been shown to be an appropriate method for determining the trace water content in semiconductor gases. CLS data analysis has been shown to lower the detection limits relative to a univariate data analysis, and should be more reliable if a large suite of outlier diagnostic tools can be used to detect situations, e.g., an interference, where the accuracy of the determination might be suspect. The major challenges encounter when performing a H_2O calibration or estimate of detection limits in semiconductor gases have been addressed and experimental, as well as data analysis procedures, have been applied to successfully make the determinations.

A prototype dual-beam system has been built and tested. The detection limit of the system is about 20 ppb using 2 cm^{-1} spectral resolution, a one meter cell, and an optical band-pass filter. This performance is better than any commercial instrument capable of a quantitative determination of H_2O vapor in corrosive gases. Other optical techniques are currently being investigated and may ultimately be shown to have a better detection limit than does infrared spectroscopy. However, the low cost, simplicity, and wide acceptance of infrared spectroscopy will insure its future use within the scientific community.

An FTIR accessory and a complete FTIR system based on the concepts developed in the research discussed here are now commercially available from Axiom Analytical and Midac Corporation, respectively. The accessory consists of a dual-beam single-pass folded Axiom cell with an InSb detector. It can be attached to any existing FTIR spectrometer. The software necessary to perform an auto background correction and CLS data analysis must be added to the system. The pathlength in the cell is user dependent but we recommend the use of a 2 m or 4 m length due to equilibration issues discussed above.

A complete FTIR system is manufactured by Midac Corporation. It consists of a small ruggedized evacuable spectrometer integrated with a suitable cell. The cell is either a dual beam or single beam folded Axiom cell coupled to an InSb detector. The evacuable FTIR system operates at pressure of at least 10^{-5} torr (preferably 10^{-6} torr) so that the H_2O background is reduced to a negligible level. This is the main advantage of the evacuable system, but the set-up cost, maintenance and monitoring of the vacuum are the main disadvantages.

The key issue for successful operation of a dual-beam non evacuated FTIR system is to have an excellent and stable purge. We have demonstrated that the H_2O background level in the Midac spectrometer can be reduced to less than 1 ppm in about 24 hours. The ultimate instrument will be, when the cost is justified, one

that uses evacuation to reduce the H_2O background and a dual-beam design to monitor the background.

7.2 FUTURE STUDIES

7.2.1 Effect of hydrogen bonding in the HCl-H_2O calibration

We have assumed during our instrument development that the calibrations for low levels of water vapor in the three gases studied (N_2, HCl, and HBr) are identical. However, there are some indications in the literature that suggest that hydrogen bonding in an HCl-H_2O sample may cause decrease peak intensities, peak shifts, and peak broadening, when compared to the N_2-H_2O sample. Pivonka[1] reported no observable difference in the molar absorption coefficient, nor any band broadening or frequency shifts, between the two sample mixtures when measured at 2 cm^{-1} resolution in a high H_2O concentration sample (about 25 ppm). However, he reported a slight absorbance attenuation and band broadening for H_2O in the HCl versus N_2 matrix at 0.5 cm^{-1} resolution. Miyasaki and coworkers[2] observed a H_2O peak height reduction of 18-33 % in HCl depending on the specific absorption peak, compared with those in N_2. They also reported a 50% bandwidth broadening in the HCl matrix in the 1653 cm^{-1} water absorption band when measured at 0.25 cm^{-1} resolution in a 10 ppm H_2O sample. Figure 7.1 shows their H_2O calibration in N_2 and HCl matrices at 2 cm^{-1} resolution measuring the peak height absorbances at 3854 cm^{-1}. Note that by diminishing the H_2O concentration in the matrices the difference in peak intensities get smaller in both matrices. Inman and McAndrew[3] reported no shift in the H_2O absorption frequency in the HCl matrix compared to the N_2 matrix, but showed the pressure broadening coefficient of H_2O in HCl is approximately three times its value in N_2.

The impact of the H_2O-HCl interaction is a change in the calibration for the amount of water present in the sample. As shown in Figure 7.1 there is about a 30% difference in the slopes of the calibrations for water in HCl versus water in nitrogen. If, as done in our work, the determination of water in HC is based on a calibration performed in N_2, an error will result. The error, however is small in the region of water concentration less than 400 ppb, the region of concern in the microelectronics industry.

The differences in calibration, hence the amount of error, is dependent upon the experimental conditions, i.e., choice of water bands, cell pressure, spectral resolution, etc. The differences in calibration for water in N_2 versus water in HCl or HBr should be carefully characterized. It will require, however, the use of a vacuum spectrometer. If, as was the use for almost all of our work, a purged system used, it will be almost impossible to study the changes due to hydrogen bonding in a sample of low water concentration due to the presence of the large (and unperturbed) background signal.

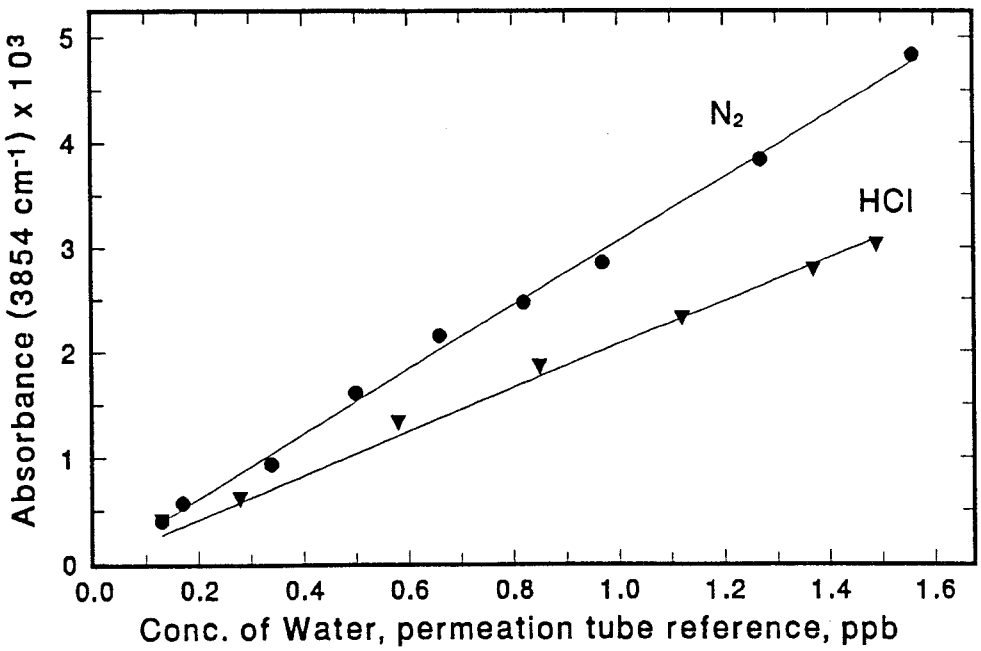

Figure 7.1 Calibrations of H_2O in N_2 and in HCl matrices[2].

7.2.2 Background Modulation

The FTIR accessory described in section 6.2 uses a dual-beam path channel to separately measure the background and sample H_2O concentrations. These measurements are made by moving the mirrors as shown in Figure 6.1 and collecting a spectrum from each channel. For this approach to be successful the drift in the H_2O background concentration needs to be small relative to the desired precision of the determination.

An improvement to the dual-beam approach is to use beamsplitters in place of the moveable mirrors and modulate the bypass beam. As shown in Figure 7.2, the light coming from the FTIR spectrometer will be directed to the FTIR accessory through an optical band-pass filter, and then split into two equal portions by a beamsplitter. One beam is directed into the sample gas cell. The other beam bypasses the cell. A modulator, mechanical or electro-optical, chops the bypass beam at a certain frequency f. The two beams will be recombined by a second beamsplitter and will be directed to the detector. The optimum design would have the pathlengths (external to the sample cell) identical. By using this modulation technique, both measurements (sample and background) will be acquired simultaneously, which will eliminate the error due to the background drift.[4]

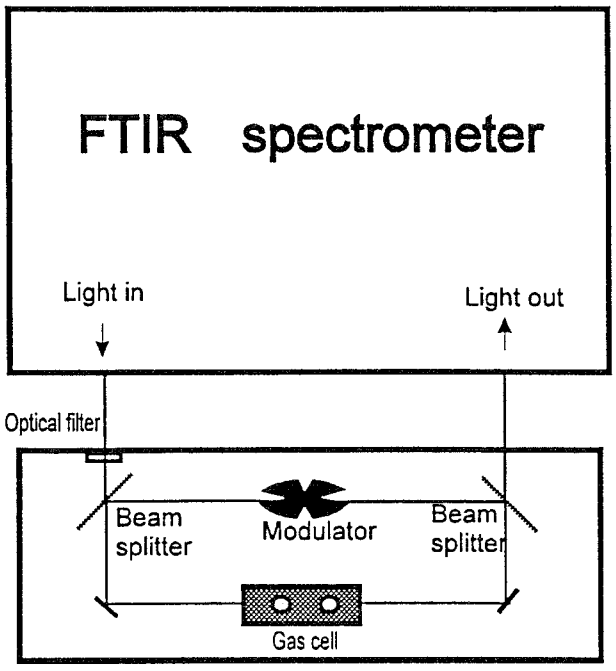

Figure 7.2 Schematic of a dual-path FTIR accessory where the reference beam is modulated.

7.2.3 Multicomponent CLS analysis

Impurities other than H_2O in semiconductor corrosive gases include N_2, O_2, CO_2, CO, CH_4, and some metals such as Fe, Cr, Ni, etc. Usually the analysis methods quantify these impurities contents are gas chromatography, ICP/MS, and FTIR spectroscopy. It has been emphasized that CLS multivariate calibration is highly suited to the analysis of gas phase infrared spectra. We have focused only to the determination of H_2O, but other impurities, such as CO, CO_2, CH_4, and even HCl in HBr or viceversa could be quantitatively be determined by infrared spectroscopy and CLS multivariate analysis. For monitoring HCl purity, for example, the approach would be to use a pure component spectrum for each of the five gases (H_2O, HBr, CO, CO_2, and CH_4) in a five component CLS model. A multicomponent CLS model should have better precision when compared to a single component CLS model. In section 4.2.2 only five H_2O bands were used to determine the detection limit of H_2O in HCl due to the potential presence of interfering species such as CO_2 and CH_4. By including these species in the CLS model we can include more frequencies in the calibration and therefore improve the detection limits of the determinations. A more rigorous analysis on how many frequencies should be used in the calibration needs to be carried out.

FTIR spectroscopy coupled with CLS multivariate data analysis can be applied successfully for the determination of gaseous impurities in gas samples with

improved detection limits. The exact performance for each impurity must be determined experimentally as it was done with trace water vapor.

7.2.4 Use of a multiple-pass folded gas cell

A method of enhancing the sensitivity in the measurement of gas phase spectra is the use of a very long pathlength. There are two basic gas cells long path designs that differ on how many times the infrared beam pass through the gas sample. These are the single-pass and multiple-pass gas cell designs. Single-pass gas cells, like the Axiom gas cell, allow the beam to pass through the gas only once. They are made of nickel-coated brass tubes. That function as gas cell and lightpipe. They are generally used as process gas cells. Multiple-pass gas cells are based on the White cell design, where multiple reflections using a three mirror arrangement direct the beam back and forth through the sample. They are commonly made of borosilicate glass to preserve chemical inertness. They are generally used in laboratory analysis.

The reasons for choosing the single-pass, folded Axiom gas cell in our prototype development centered mostly on the time required for the cell to come to equilibrium with a new sample (see section 5.4). The glass-made White cell that we tested could not be heated nor dried lower than 150 ppb. However, there are now heatable cells available constructed of aluminium with specialty coatings. The main concern with adjustable multiple-pass cells is maintenance of good alignment during heating/cooling cycles. Fixed pathlength cells are now available that according to specifications, maintain alignment during heating/cooling cycles.

CIC Photonics has introduced a multiple-pass, heatable, 10 m fixed pathlength gas cell for high sensitivity gas analysis. The cell material is made of nickel-plated stainless steel. It has been designed specifically to be low volume (1.7 liters) and minimum surface-to-volume ratio[5]. This cell could be an attractive alternative to the long single-pass design used in our measurements. The small volume, low surface area might make equilibration times fast and the 10 m pathlength might improve sensitivity. The performance of the cell will have to be proven experimentally.

7.3 REFERENCES

1. D. E. Pivonka, Appl. Spectrosc., 45, 597 (1991).
2. K. Miyasaki, Y. Ogawara, and T. Kimura, Bull. Chem. Soc. Jpn., 66, 969-971 (1993).
3. R. S. Inman and J. J. McAndrew, Anal. Chem., 66, 2471 (1994).
4. R. K. Rowe and B. R. Stallard, Apparatus & Method for Background's Compensated Fourier Transform Spectrometry, submitted for patent application, Sept. 1994.
5. The Ranger, CIC Photonics, Inc., 2715-D Broadbent Parkway N.E., Albuquerque, NM 87107.

DISTRIBUTION:

1 T. M. Niemczyk
Department of Chemistry
University of New Mexico
Albuquerque, New Mexico 87106

10	MS	0980	B. R. Stallard, 5725
1		1411	M. J. Garcia, 1823
1		0970	J. R. Kelsey, 5700
1		1411	J. M. Phillips, 1823
1		0343	M. J. Kelly, 1824
1		0874	R. S. Blewer, 1305
1		9018	Central Technical Files, 8940-2
5		0899	Technical Library, 4916
2		0619	Review & Approval Desk for DOE/OSTI, 12690
1		1380	Technology Transfer, 4212